THESIS

COMPUTATIONAL FLUID DYNAMICS MODELS OF RIO GRANDE BENDS FITTED WITH ROCK VANES OR BENDWAY WEIRS

Submitted by

Seth Siefken

Department of Civil and Environmental Engineering

In partial fulfillment of the requirements

For the Degree of Master of Science

Colorado State University

Fort Collins, Colorado

Summer 2019

Master's Committee:

Advisor: Robert Ettema

Christopher Thornton
Daniel McGrath

ABSTRACT

COMPUTATIONAL FLUID DYNAMICS MODELS OF RIO GRANDE BENDS FITTED WITH ROCK VANES OR BENDWAY WEIRS

Rock vanes (also known as stream barbs) and bendway weirs are two types of transverse rock structures used to modify the flow field in river bends. This study examines the effectiveness of the two types of structures at reducing velocity along the outer bank of river bends to protect the bank from erosion. A numerical model using the commercially available FLOW-3D software was used to evaluate the effect of various rock vane and bendway weir configurations on the flow field through two river bends typical of the Middle Rio Grande. The model was calibrated and validated using data from a previous physical model study of rock vanes. 33 different rock vane configurations were tested in the numerical model to evaluate the effect of altering planform angle, crest slope, projected length, and structure spacing. In addition, 14 different bendway weir configurations were tested to provide a comparison of the relative performance of bendway weirs and rock vanes.

The numerical modeling results indicate that rock vanes are more effective at reducing the velocity along the outer bank of a bend than bendway weirs. Modelling showed that the completely submerged crest of bendway weirs allows a substantial amount of flow to pass over the crest, limiting their effectiveness in reducing velocity along the bank. In contrast, rock vanes, with a sloped crest intersecting the waterline at the design flow rate, directed more flow around the tip of the structure rather than over the crest and were much more effective at reducing

velocity along the bank. Based on the modeling results, it is recommended that bendway weirs not be installed for the purpose of erosion protection along riverbanks.

The reduction in velocity along the bank produced by the various rock vane configurations varied considerably with the geometry of the configuration. Based on the results, the following conclusions are made regarding rock vane geometry: (1) Rock vanes should be installed at a planform angle between 45° and 90° to the river bank. (2) There exists an optimal projected length of rock vane, which lies in the neighborhood of 1/5 to 1/3 of the channel top-width. (3) Rock vanes with a 10% crest slope perform well, although decreasing the crest slope will decrease the velocity along the outer bank and vice versa. (4) Decreasing the spacing of rock vanes decreases the velocity along the outer bank, up to a limit.

A design equation was developed to predict the velocity reduction along the bank of a river bend produced by a given configuration of rock vanes, based on the geometry of the rock vanes and the river channel. The equation provided good predictions for the range of configurations tested, having a coefficient of determination $r^2 = 0.83$ and predicting the velocity reduction along the outer bank to within 15 percentage points for all of the tested configurations.

ACKNOWLEDGEMENTS

First and foremost I thank my advisor, Dr. Robert Ettema for his guidance and encouragement throughout my time at CSU. It has been a true pleasure to work with him and his direction was indispensable to the completion of this project. I also thank my other committee members, Dr. Christopher Thornton and Dr. Daniel McGrath for contributing their time and expertise.

I express my special thanks to Dr. Shin for teaching me FLOW-3D and walking me through every step for setting up and analyzing bendway weir models. The hours of time he devoted to teaching me were a tremendous help.

I thank all of my colleagues at the Engineering Research Center for their support and advice, especially Taylor Hogan and Mason Garfield. I also thank my colleagues at the Wyoming-Montana Water Science Center for their encouragement and willingness to accommodate my graduate school schedule.

Finally, I thank my mom for her support throughout my time in graduate school and my dad, whose frequent fishing trips with me a child are no doubt responsible for my choice to study hydraulic engineering.

TABLE OF CONTENTS

LIST OF TABLES

LIST OF FIGURES

CHAPTER 1. INTRODUCTION

The U.S. Bureau of Reclamation (USBR) has attempted to stabilize the Middle Rio Grande in order to protect infrastructure and farmland from lateral movement of the river. As part of this effort, Colorado State University (CSU) has been contracted to study the effectiveness of various transverse structures for erosion protection along river bends. These riprap structures, herein called bendway weirs and rock vanes, are shown in Figure 1. The purpose of these structures is to retard flow along the outer bank of a bend, thereby decreasing flow velocity along the outer bank, reducing bank erosion, and aligning the channel's thalweg toward the channel's center.

Channel stabilization activities are not straightforward, as rivers are inherently dynamic systems, continually shifting their channels in response to changes in water and sediment supply. Until recently, the channel of the Middle Rio Grande was aggrading, a trend which began some 11,000 years ago (Richard 2001). The aggradation of the river presented problems for human development, so the U.S. Army Corps of Engineers constructed Cochiti Dam to provide sediment detention and water storage. Following closure of the dam in 1973, the channel began to degrade and increase in sinuosity (Richard 2001). These geomorphic changes have led to increased lateral migration of river bends due to bank erosion.

Research at CSU has produced the first systematic, quantitative design guideline for transverse structures, included in *Bank Stabilization Design Guidelines* (Baird et al. 2015). However, this design approach has several limitations. The regression equation used in the design method is based on a channel with a trapezoidal cross-section, which does not take into account the effect of natural channel topography. In addition, the regression equation has no

explicit parameter to account for the crest slope of rock vanes, and little investigation has been made into the effect of crest slope on rock vane performance.

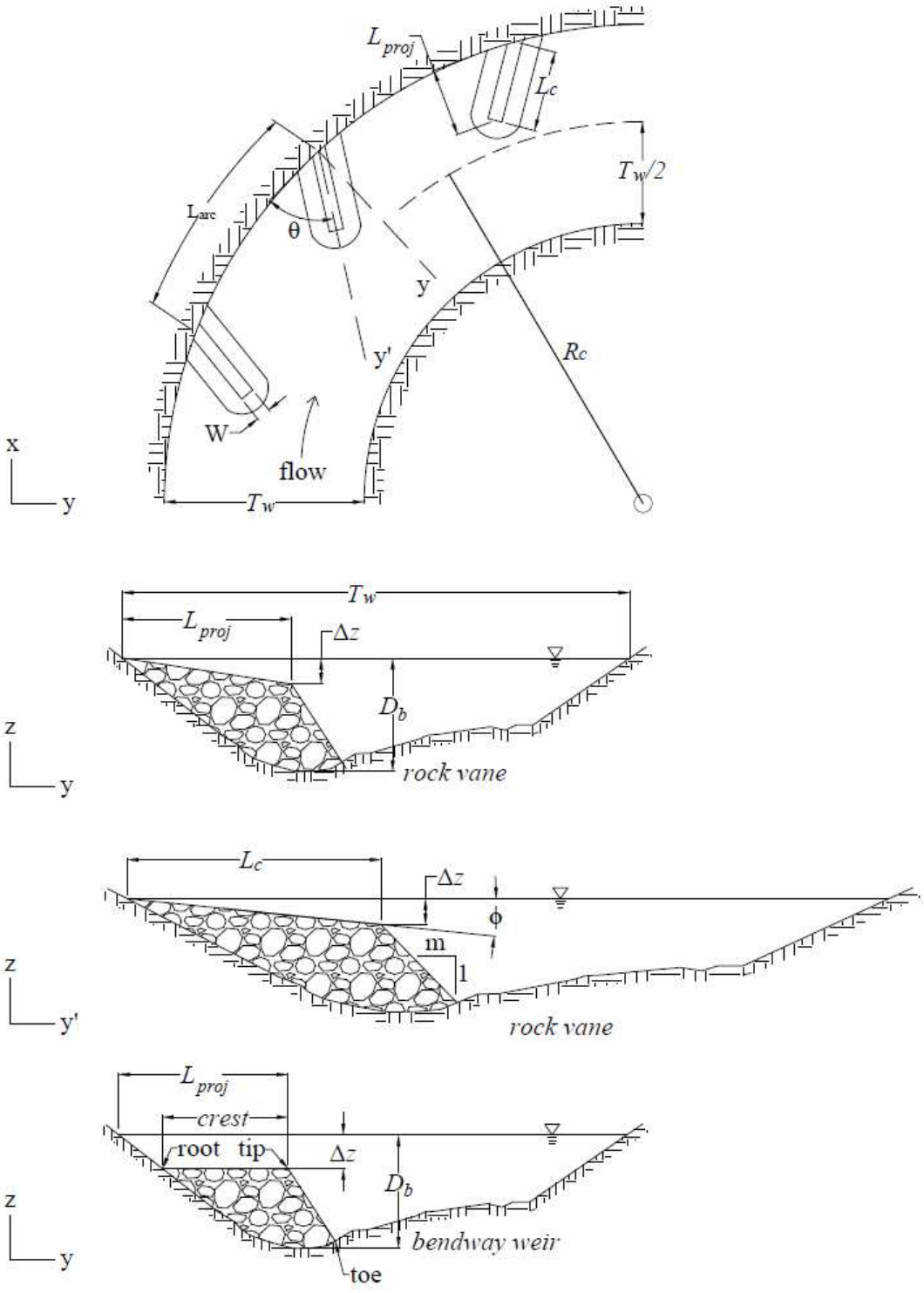

Figure 1. Geometric parameters of bendway weirs and rock vanes

Objectives

This study focused on the flow-altering performance of rock vanes and bendway weirs placed along the outer bank of two bends representative of the Rio Grande. To this end, the three-dimensional numerical model FLOW-3D was used to address the following sequence of specific objectives:

1. Construct, calibrate, and validate Computation Fluid Dynamic (CFD) models of rock vanes and bendway weirs placed in a river bend;
2. Use the models to determine the effects on the bend flow field of varying the spacing and geometric form of rock vanes and bendway weirs;
3. Illuminate the three-dimensional flow field around rock vanes and bendway weirs, and show how the flow field varies between the two types of structures; and,
4. Use the model results to provide design recommendations on the use of rock vanes and bendway weirs.

The flow-altering performance was pertinent to the use of configurations of rock vanes and bendway weirs to manage bends along the Middle Rio Grande.

CHAPTER 2. BACKGROUND

Rock vanes and bendway weirs are commonly used for channel control or management. This chapter briefly describes their use and current information regarding their design.

Rock Vane Geometry

Rock vanes (also known as barbs and point dykes) are riprap structures that extend out from the riverbank with their crest sloping down toward the center of the channel, as Figure 2 shows. The sloped crest increases the area of flow blocked as the water level increases, providing a progressive hydraulic effect as discharge increases (NRCS 2005). Well-designed rock vanes should provide sufficient velocity reduction along the outer bank of a bend to prevent erosion, usually at a lower cost and with less environmental impact than a riprap revetment (Baird et al. 2015).

Figure 2. Installation of rock vanes (NRCS 2007)

The terminology used in the literature to describe the geometric parameters of rock vanes is somewhat muddled. The following definitions are adopted in this study for the parameters shown in Figure 1:

T_w = average top-width of channel in the bend at the design flowrate before the installation of structures

R_c = radius of curvature of channel bend centerline

L_c = length of the structure crest, measured as the distance along the structure crest from the waterline at the design flowrate to the tip of the crest

L_{proj} = projected length of the structure, defined as the shortest distance from the tip of the structure crest to the waterline along the outer bank

L_{arc} = arc length along the bank between the centerline of adjacent structures

Δz = elevation difference between the baseline water surface and structure crest at the tip

D_b = average thalweg depth in bend before the installation of structures

θ = structure planform angle measured from the bank on the upstream side of the structure to the structure crest

$tan\phi$ = slope of the structure crest; $tan\phi = 0$ for bendway weirs

m = slope of the structure toe, given as mH:1V

W = width of structure crest

Previous studies have defined the projected length as $L_{proj} = L_c \sin\theta$. However, for structures installed at small angles to the bank in channels with a small radius of curvature, this definition results in projected lengths which are much greater than the distance from the outer bank to the tip of the structure, as illustrated in Figure 3. For such structures, it is better to use Equation 1, which computes the exact distance from the outer bank to the tip of a the structure crest for a channel of constant top-width and radius of curvature.

$$L_{proj} = R_c + \frac{T_w}{2} - \sqrt{L_c^2 + \left(R_c + \frac{T_w}{2}\right)^2 - 2L_c\left(R_c + \frac{T_w}{2}\right)\sin\theta} \quad (1)$$

Equation 1 simplifies to $L_{proj} = L_c sin\theta$ for $\theta = 90°$ or for R_c approaching infinity, which provides a very good approximation for rock vanes installed at angles greater than $\theta = 60°$.

When laying out rock vanes, it is useful to be able to calculate the crest length required for a given projected length. Manipulating Equation 1 to solve for crest length as a function of projected length, planform angle, top-width, and radius of curvature leads to Equation 2:

$$L_c = \left(R_c + \frac{T_w}{2}\right) sin\theta - \sqrt{L_{proj}^2 - 2L_{proj}\left(R_c + \frac{T_w}{2}\right) + \left(R_c + \frac{T_w}{2}\right)^2 \sin^2\theta} \qquad (2)$$

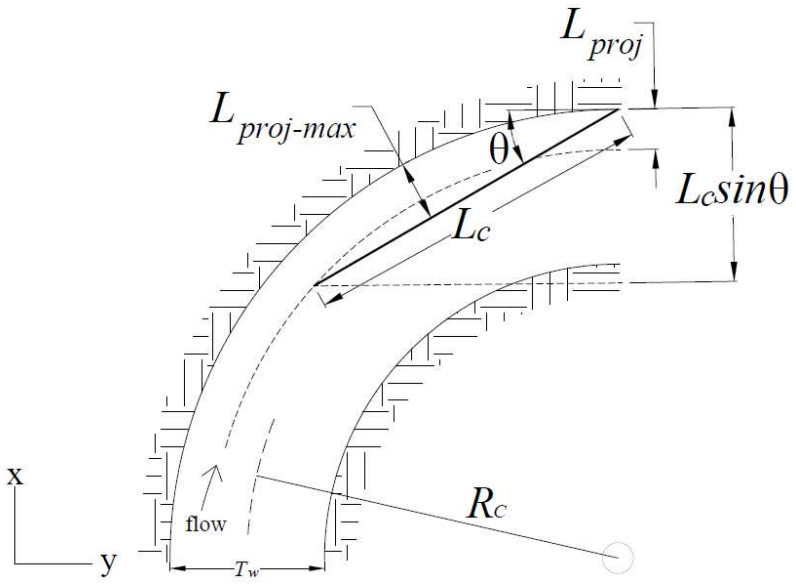

Figure 3. Illustration of the effect of curvature on the projected length of rock vanes

It is assumed throughout this study that the crest of a rock vane intersects the bank at the elevation of the design water surface, as illustrated in Figure 1. The submergence of the vane tip, Δz, can then be related to the crest length and slope of the vane, $tan\phi$, by the equation:

$$\Delta z = L_c tan\phi \qquad (3)$$

It is also useful to consider the area of flow blocked by rock vane or bendway weir structure. The flow blockage is defined as follows:

A^* = percentage of baseline cross-sectional flow area blocked by structure, computed using Equation 4.

$$A^* = \frac{A_{structure}}{A_{flow}} \tag{4}$$

Here, A_{flow} is taken as the baseline area of flow before the installation of structures at a cross-section perpendicular to the direction of flow located at the root of the structure. The area of the structure, $A_{structure}$, is determined by projecting the structure onto the cross-section perpendicular to the flow direction, as shown in Figure 4.

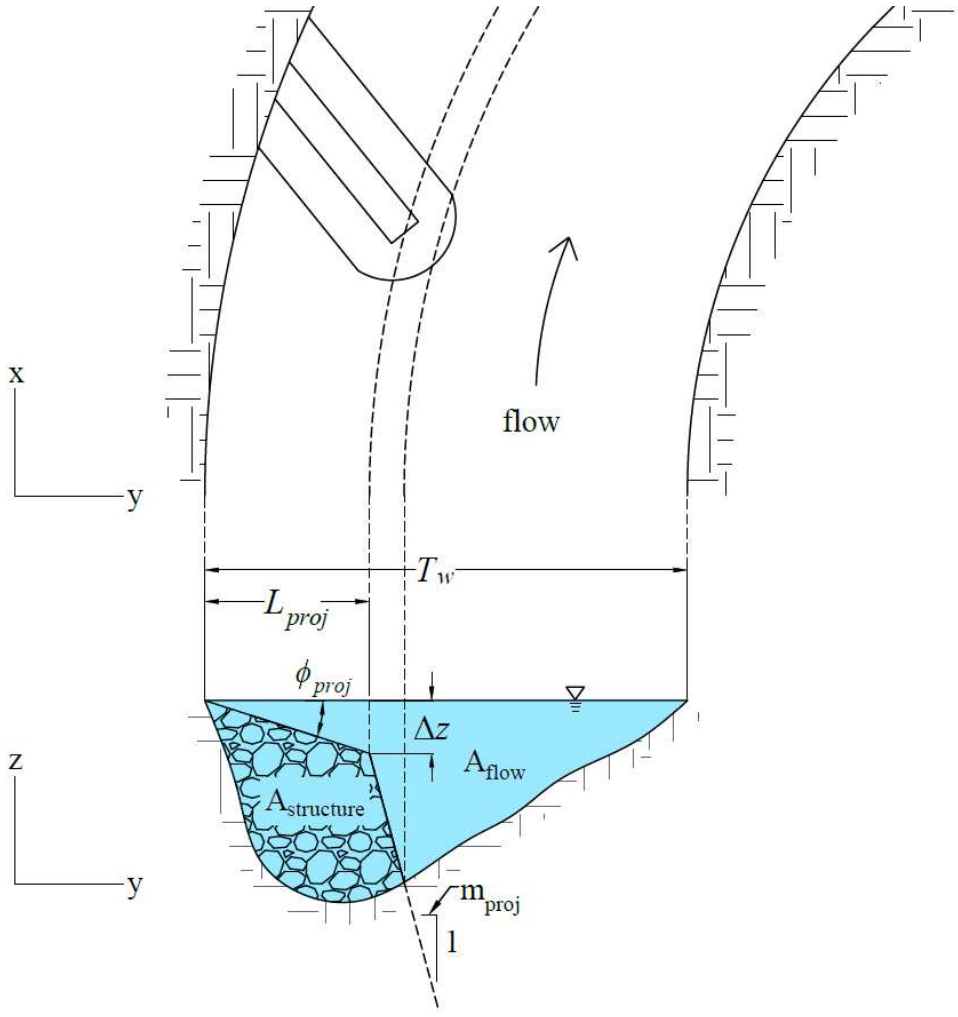

Figure 4. Projection of a structure onto a perpendicular cross-section

The projection results in a projected toe slope (m_{proj}H:1V) that is steeper than the toe slope of the installed structure and a projected crest slope of rock vanes ($tan\phi_{proj}$) steeper than the installed crest slope. For an exact projection, the crest and toe slopes would vary slightly along the structure, but the variation is small enough to disregard for practical calculations. The mean projected crest slope can simply be computed by dividing the projected length by the tip submergence:

$$\tan(\phi_{proj}) = \frac{L_{proj}}{\Delta z} \tag{5}$$

Because the area blocked under the toe of the structure is usually small compared to the area blocked under the crest, the projected toe slope can be satisfactorily approximated as:

$$m_{proj} \approx m * sin\theta \tag{6}$$

Appendix A provides a complete derivation of the equations for projected length and area.

Existing Rock Vane Design Guidelines

The geometric design of rock vanes is primarily concerned with determining vane length, spacing, and planform angle. Table 1 summarizes eight different sets of geometric design criteria proposed in the literature. While these criteria provide the designer with generally acceptable ranges of geometric parameters, they are largely anecdotal (Thornton et al. 2016).

The Washington State Department of Transportation (WSDOT) design was tested in a live-bed laboratory flume and found to provide good performance (Papanicolaou et al. 2004). The other design guides appear to be based primarily on field experience. Case studies are cited in several design guides but it appears little comparative testing of designs has been done.

The geometric design parameters vary greatly from one guide to another, with recommended planform angle ranging from < 20° (NRCS 2007) to 80° (NRCS 2009, NRCS 2010) and recommended crest slope ranging from 0% (NRCS 2009) to 20% (NRCS 2007). The

design guides are in agreement that rock vanes should be oriented upstream ($\theta < 90°$), as this orientation will direct flow away from the outer bank at low flows (NRCS 2007).

Table 1. Summary of various design guidelines for vanes

	Length		Length Type	Spacing		θ		Crest slope	
Source	min	max		min	max	min	max	min	max
WSDOT (2017)	$T_w/3$		Projected	$4L_{proj}$		50°		10%	
NRCS (2013)	Length based on designed thalweg location, not to exceed $T_w/3$		Crest	Line from DS structure tip, parallel to bank tangent at tie-in, to intersection of US bank		20°	30°	5%	8%
NRCS (2010)	$T_w/10$	$0.35T_w$	Crest, but called effective length	Flow direction analysis		50°	80°	3%	10%
NRCS (2009)	Must cross thalweg, dependent upon horizontal angle, not to exceed baseflow $T_w/2$		Crest	$4L_c$	$5L_c$	50°	80°	0%	n/a
NRCS (2007)	$T_w/10$	$T_w/4$	Projected	$4L_{proj}$	$5L_{proj}$	<20°	45°	20%	
NRCS (2005)	Must cross thalweg, dependent upon horizontal angle, not to exceed $T_w/3$		Crest	Line from DS structure tip, parallel to bank tangent at tie-in, to intersection of US bank		20°	30°	5%	8%
Johnson et al. (2001)	$T_w/4$	$T_w/3$	Projected	n/a	n/a	20°	30°	n/a	n/a
Maryland (2000)	n/a	$T_w/3$	Projected	$5T_w$	$7T_w$	20°	30°	3%	7%

The large variation in recommended parameter values between design guides leaves the design engineer with a great deal of uncertainty. Additionally, any purely geometric design method is limited by its failure to account for the approach velocity in the bend, an important parameter when attempting to prevent erosion along the outer bank (Baird et al. 2015).

Baird et al. (2015) describe an alternative design method using regression equations to predict velocity reduction along the outer bank of a bend. The design equation (Equation 7) uses six dimensionless terms to describe the geometric configuration of the rock vanes, with regression coefficients determined by physical model experiments. The Maximum Velocity Ratio (MVR) represents the ratio of the maximum velocity at a given location in the channel (inner bank, center, or outer bank) after vane installation to the bend-averaged velocity before vane installation. Likewise, the Average Velocity Ratio (AVR) is the ratio of the average velocity in a region of the channel after vane installation to the bend-averaged velocity before vane installation. The regression equation allows the designer to compute the outer bank velocity reduction produced by a particular vane configuration in a particular bend, providing a quantitative design method that takes into account the approach velocity as well as the geometry of the vanes and the river bend.

$$MVR, AVR = a_1 + a_2(A^*)^{a_3}\left(\frac{L_{arc}}{T_w}\right)^{a_4}\left(\frac{R_c}{T_w}\right)^{a_5}\left(\frac{L_{proj}}{T_w}\right)^{a_6}\left(\frac{D_b}{D_b - \Delta z}\right)^{a_7}\left(\frac{2\theta}{\pi}\right)^{a_8} \quad (7)$$

where:

A^* = percentage of baseline cross-sectional area blocked by structure;

L_{proj} = projected length of structure into channel [L];

L_{arc} = arc length between centerline of structures [L];

R_c = radius of curvature of channel bend centerline [L];

T_w = averaged top-width of channel measured at baseline in bend [L];

D_b = averaged maximum cross-section baseline flow depth in bend [L];

Δz = elevation difference between water surface and structure crest at the tip [L];

θ = structure plan angle [radians];

$a_1 \ldots, a_8$ = regression coefficients.

Whereas the regression equation allows the designer to estimate velocity reductions for various values for vane length, spacing, height, and planform angle, it does not include an explicit term for the vane crest slope. The literature suggests various values of crest slope. For example, NRCS (2007) states that a 20% slope is common, NRCS (2013) recommends a slope from 5% to 8%, Baird et al. (2015) recommends a slope range of 2% to 8%, and Jamieson et al. (2011) simply recommends a slope less than 50%. Such varied recommendations leave the designer with a great deal of uncertainty when trying to select a single value of slope for a particular installation.

Existing Bendway Weir Design Guidelines

Bendway weir geometric parameters are defined in the same manner as those for rock vanes, as shown in Figure 1. Bendway weirs are distinguished from rock vanes by their flat crest, which is designed to be submerged at the design flow. As such, the crest of a bendway weir intersects the bank below the elevation of the design water surface, unlike rock vanes which intersect the bank at the design water surface.

While originally developed as a structure to improve navigation, bendway weirs also have potential to mitigate erosion also the outer bank (Biedenham et al. 1997). Table 2 summarizes existing design guidance for bendway weirs from NCHRP Report 544 (McCullah and Gray 2005), Hydraulic Engineering Circular (HEC) 23 (Lagasse et al. 2009), and Julien and

Duncan (2003). The recommended design values vary considerably from one guide to another, with recommend length ranging from $T_w/10$ to $T_w/2$ and spacing from $1.5L_c$ to $5L_c$.

Table 2. Summary of existing design guidelines for bendway weirs (after Scurlock et al. 2014b). Height is given in terms of hydraulic depth (D) or bank full depth (BF)

	Length		Length Type	Spacing		θ		Height	
Source	min	max		min	max	min	max	min	max
NCHRP 544 (2005)	$T_w/3$	$T_w/2$	crest	$1.5L_c$		70°	80°	$D/2$	D
HEC 23 (2009)	$T_w/10$*	$T_w/3$	crest	$4L_c$	$5L_c$	60°	80°	0.3BF	0.5BF
Julien and Duncan (2003)	case-by-case		N/A	$2L$	$3L$	60°		Max permitting navigation	

*HEC 23 further recommends that the crest be long enough to cross the thalweg

As with rock vanes, purely geometric design criteria for bendway weirs are limited by their failure to consider the approach velocity of flow in the bend (Baird et al. 2015). Several investigators have attempted to overcome this shortfall with regression equations in the same form as that presented for rock vanes (Equation 7). Scurlock et al. (2012a) created a regression equation based on physical model studies at CSU and Shin et al. (2018) created a similar equation based on a numerical model study. However, neither of these equations has been adopted in an official design guide.

CSU Physical Model Studies

CSU has been investigating transverse structures since 2001 under contracts with the Bureau of Reclamation. The initial work consisted of physical model experiments on an S-curve bend with a trapezoidal cross-section (Figure 5) representative of bend geometry on the Middle Rio Grande. Heintz (2002) used the physical model to analyze the how placement of bendway

weirs in a river bend affects flow velocity along the inner and outer banks for various configurations of weir spacing. Darrow (2004) examined the how bank velocities change with varying weir lengths and planform angles. Schmidt (2005) used the trapezoidal model to examine the relationship between structure crest slope and bank velocities. Schmidt only investigated two values of crest slope, $\phi = 0°$ ($\tan\phi = 0\%$) and $\phi = 10°$ ($\tan\phi = 17.6\%$) and found that both could provide acceptable performance.

Figure 5. Trapezoidal physical model

In 2006, the physical model was modified to include topography representative of the native channel topography of the Middle Rio Grande (Walker et al. 2009). Figure 6 shows the plan view layout of the channel after the addition of native topography and Figure 7 shows construction of the native topography on top of the existing trapezoidal channel. The native

topography channel was used to test many different configurations of bendway weirs (Scurlock et al. 2014b) and rock vanes (Thornton et al. 2016).

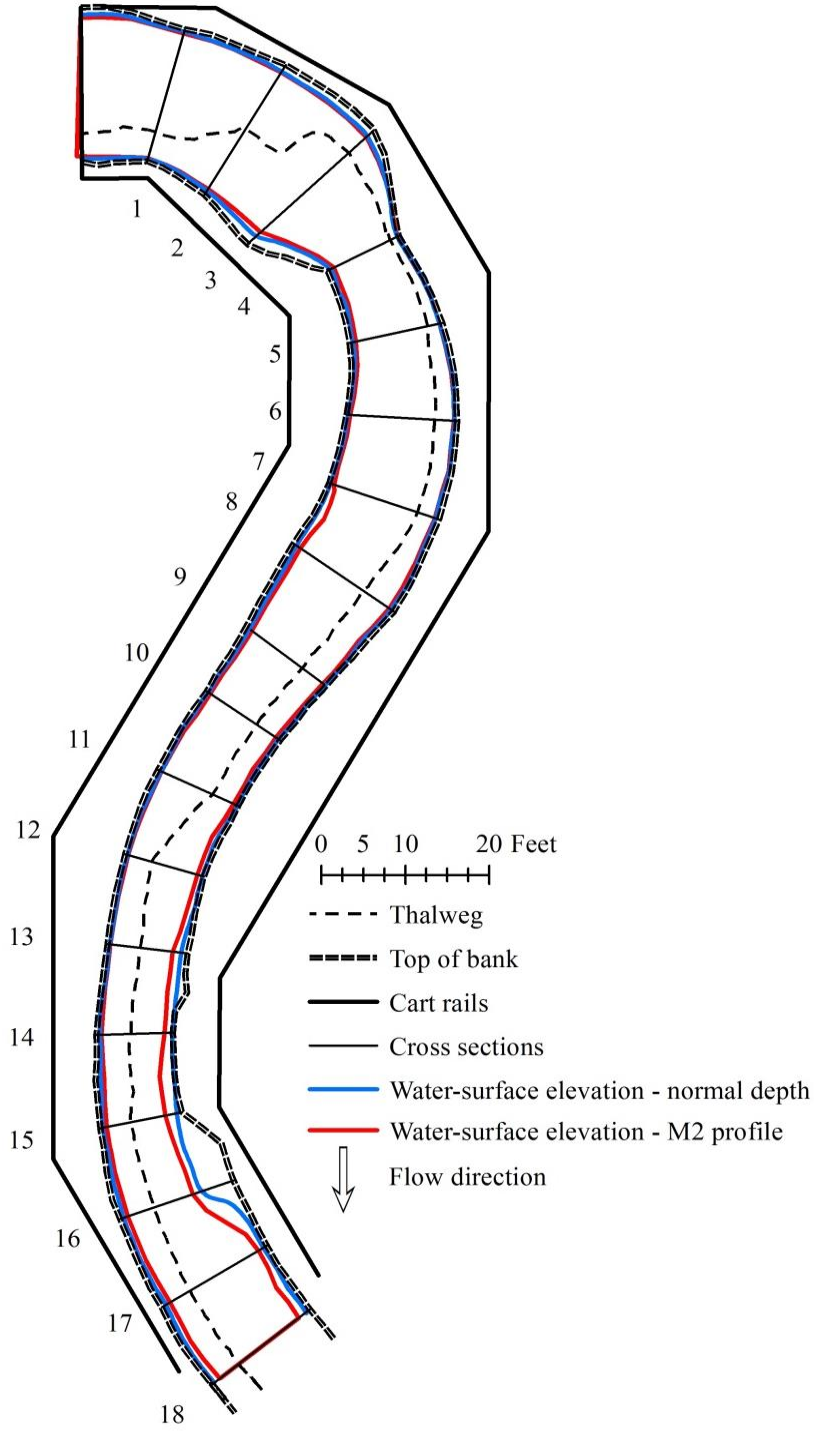

Figure 6. Plan view layout of the S-Curve physical model after the addition of the natural topography (Thortnon et al. 2016)

Figure 7. Construction of the native topography channel

Three different rock vane configurations were tested in the physical model by Thornton et al. (2016), designated V01, V02, and V07. The V01 and V07 structures were located in the downstream bend of the S-curve, while the V02 structures were located in the upstream bend. Table 3 describes the geometry of each configuration. For each test, velocity was measured at approximately 2,500 points, providing an extremely detailed dataset of the velocity field around the rock vanes. Figure 8 shows the layout of structures in the V01 configuration and the location of data collection points.

Table 3. Rock vane configurations tested by Thornton et al. (2016). Crest slopes are from unpublished spreadsheets.

Configuration	Length (ft)	Height (ft)	Top-width (ft)	Spacing (ft)	θ	Crest Slope
V01	variable	variable	1.0	9.30	85º	10%
V02	variable	variable	1.0	9.30	60º	10%
V07	$T_w/6$	variable	1.0	2.69L - 4.79L	variable	8%

The physical model tests indicated that all three of the vane configurations shifted conveyance toward the center of the channel and away from the outer bank, although the V07

configuration appeared to provide less protection of the outer bank than the other configurations. The decreased protection from V07 was attributed to flow separation at the vane tip directing higher velocity flow to the outer bank (Thornton et al. 2016).

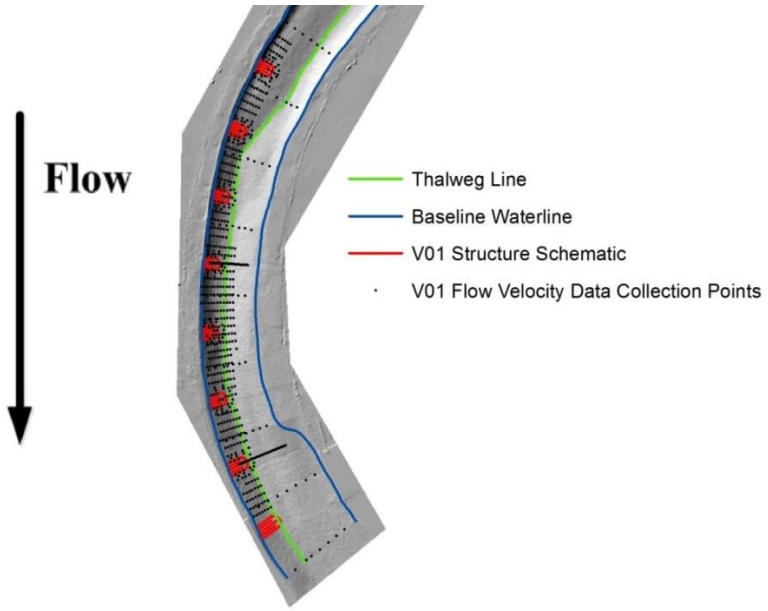

Figure 8: V01 constructed configuration (Thornton et al. 2016)

Numerical Models

Many investigators have used numerical models to examine the flow fields around transverse structures. Scott et al. (2001) used both two and three-dimensional numerical models to evaluate flow around bendway weirs in the Mississippi River. The 3D model using the CCHE3D code effectively captured the helical flow in the bend and effect of the bendway weirs in disrupting the helical flow. The 2D model with the CCHE2D code was found to be useful for modelling general flow characteristics in the bend, but did not adequately capture the redistribution of flow in the bend.

Jamieson et al. (2009) used a numerical model to assess design alternatives of rock vanes for channel stabilization on an urban stream in Ottawa. The model indicated that rock vanes

reduced velocities along the outer bank while generating complex, three-dimensional velocity fields around each structure. Field monitoring of the rock vanes after installation indicated that outer bank velocity was successfully reduced, as the model predicted (Jamieson et al. 2013).

Toniolo and Duvoy (2010) used the 2D numerical model CCHE2D to evaluate the flow field around rock vanes. The model was able to reproduce the flow fields observed around a rock vane in a laboratory flume and around vanes in one of two field installations in the study. However, the numerical model could not accurately reproduce the flow field around the second field installation, likely because the two dimensional model could not include the vertical velocity component of the helical flow in river bends.

Sotiropolous and Diplas (2014) used their Virtual Stream Lab 3D model to determine the optimum angle and spacing of rock vanes for bends with varying degrees of sinuosity. The velocity field around a single rock vane computed by the numerical model was found to be in good agreement with that observed from a laboratory flume experiment. Based on the model results, it was recommended that rock vanes be installed in a series of at least two structures and that structure spacing should be decreased for more sinuous channels.

Papanicolaou et al. (2018) used a CFD model to examine the turbulence structures formed around submerged rock barbs (similar structures to rock vanes). The study described four distinct vortices, the most prominent of which is the “primary vortex” which forms upstream of the barb, wraps around the barb tip, and extends downstream. The length scale of the primary vortex was found to be of the same order as the barb height.

CSU Numerical Model Studies

CSU's study of transverse structures has included considerable numerical modelling. Kasper (2005) created a 1D HEC-RAS model of bendway weirs in the trapezoidal channel physical model. Results from the calibrated HEC-RAS model closely matched the cross-sectional average flow depths observed in the physical model, differing by only 3% and 1% for the two bends. The model had much greater deviation from physical observations for energy loss, with differences of 60% and 7% for the two bends.

Sclafani (2012) developed a method for computing maximum velocity and shear stress in a bend fitted with bendway weirs using a 1D HEC-RAS model. Flow depth from the HEC-RAS model differed by 2.52% to 3.57% from the physical model while velocities differed by 4.1% to 32.6%. It was noted that observed flow fields around bendway weirs are characteristically three-dimensional, presenting a fundamental dilemma for the application of one-dimensional models.

More recent work has utilized 3D numerical models. Scurlock et al. (2014a) created a numerical model of the native topography channel physical model using FLOW-3D. Channel topography was created from a LiDAR scan of the native topography physical model. The LiDAR points were used to create a ground surface in AutoCAD Civil3D, which was then modified to extend the channel upstream to provide a straight reach for development of uniform flow above the S-curve bend, as shown in Figure 9. The model used a single mesh element to represent the entire flow domain with a cell size of 0.1875 ft x 0.1875 ft x 0.0625 ft. The RNG k-ε model was selected as the turbulence model, with the maximum turbulent mixing length set to 0.09 ft.

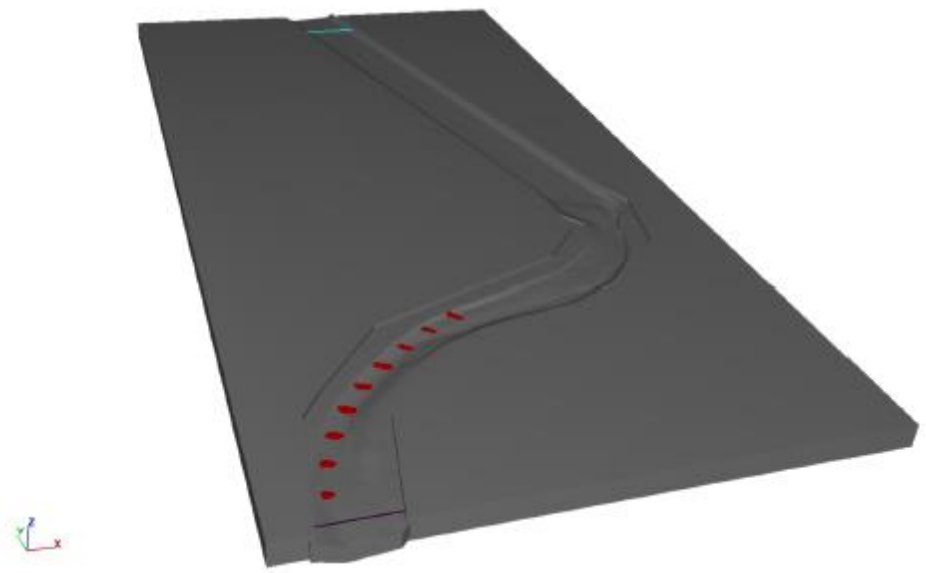

Figure 9. Channel geometry (gray) and installed structures (red) from Scurlock et al. (2014a).

The model was first calibrated for a baseline configuration without instream structures. Calibration determined the optimal roughness of the channel to be 0.07 ft. Additionally, calibration work determined that the model flow rate should be set to 11.5 ft^3/s rather than 12.0 ft^3/s as measured in the physical model. The flow reduction accounted for fluid loss in the physical model, which had developed considerable leakage with age. The calibrated baseline model had a Mean Absolute Percent Difference (MAPD) compared to the physical model of 3.78% for flow depth and 11.67% for velocity at 60% of the flow depth.

Additional calibration work determined the optimum roughness of bendway weir and spur-dike structures based on the physical model data. Optimal roughness was found to be 0.07 ft for bendway weirs and 0.15 ft for spur-dikes. Table 4 summarizes the results for the calibration. MAPD for both the bendway weir and spur-dike calibrations was higher than that of the baseline calibration. Such a result should be expected, as the introduction of structures complicates the flow field, limiting the accuracy of both the numerical model and the velocity measurements in the physical model.

Table 4. Calibration summary for the numerical model of Scurlock et al. (2014a)

Configuration	Flow depth MAPD	Velocity at 60% Depth MAPD
Baseline 12 ft^3/s	3.78%	11.67%
Bendway Weir (BW05)	4.61%	14.30%
Spur-dike (SD05)	6.00%	30.29%

Shin et al. (2018) modified Scurlock's model to assess the influence of bendway weirs on the flow distribution in river bends. The channel was extended downstream of the S-curve bend to allow the instream structures to create their own tail water conditions (Figure 10). The model mesh was modified to a cell size of 0.15 ft x 0.414 ft x 0.034 ft with 55 million total cells. The model was then recalibrated, with the flow rate being reduced to 10.5 ft^3/s and the roughness of both the channel and the bendway weirs set to 0.07 ft, as in Scurlock et al. (2014a). The model from Shin et al. (2018) was the starting point for the numerical models in the present study of rock vanes.

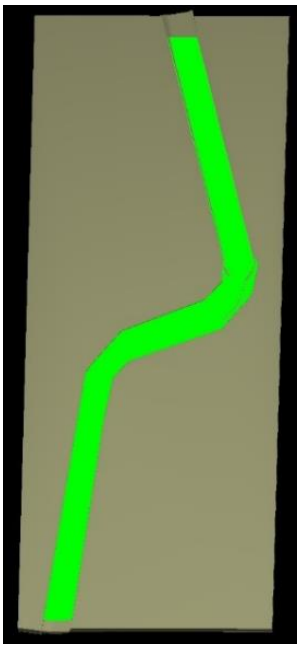

Figure 10. Channel with downstream extension from Shin et al. (2018)

CHAPTER 3. DOWNSTREAM MODEL IMPROVEMENTS

The numerical models in the present study are built upon CSU's previous numerical models used to evaluate bendway weirs (Scurlock et al. 2014a, Shin et al. 2018) with several modifications to meet the current research objectives. Two separate numerical models were used for this study. One, the downstream model, uses the same channel topography as Shin et al. (2018) to model structures in the downstream bend. A second model, denoted as the upstream model, uses a modified topography to create inlet conditions for the upstream bend that are more representative of a meandering river channel than the previous models. Development of the upstream model is discussed in Chapter 5.

As with their predecessors, the present models use the commercially available FLOW-3D modelling package. The FLOW-3D software uses the Fractional-Area-Volume-Obstacle-Representation (FAVOR) method to generate a mesh of the flow domain and assign a fractional fill volume to mesh cells containing solid objects. FLOW-3D is widely used for modelling open-channel flows and is well suited to modelling flows around instream structures (Abad 2008, Kolden 2013, Plymesser 2014). As in earlier models, the Re-Normalisation Group (RNG) k-ε turbulence model was used. Scurlock et al. (2014a) provides an overview of the application and limitations of the RNG k-ε model for modelling flows around transverse structures.

Mesh and Coordinate System

Investigating the three-dimensional flow field around rock vanes and bendway weirs requires a model with sufficiently fine spatial resolution to capture the main turbulence structures formed around the vanes and weirs. To accomplish this task, the mesh was designed to have as fine a resolution around the structures as possible, while maintaining a sufficiently short run time to allow many different structure configurations to be evaluated.

In order to provide maximum resolution around the structures while minimizing computational time, the flow domain of the downstream model consisted of six mesh blocks of varying cell size. Using multiple mesh blocks allows the total number of cells to be reduced by better fitting the mesh to the flow domain, thus minimizing the volume of mesh occupying regions without flow. The varying resolution of the mesh blocks allows for fine resolution around the structures where the flow field is most complex while using a coarser resolution away from the structures where the flow field is simpler and not of interest to the project.

With the new downstream model mesh, the total number of cells was reduced to 16,563,000 from the 55,000,000 used by Shin et al. (2018) while increasing the resolution around the structures from 0.15 ft x 0.414 ft x 0.034 ft to 0.125 ft x 0.125 ft x 0.034 ft. Table 5 lists the boundaries of the mesh blocks and their resolutions, with Figure 11 showing the plan view layout of the mesh blocks on the channel topography.

Table 5. Mesh block information for the downstream model

Mesh Block	Minimum (ft)			Maximum (ft)			Resolution (ft)			Number of Cells
	X	Y	Z	X	Y	Z	X	Y	Z	
1	81.000	135.000	97.175	145.000	299.000	98.875	0.400	0.400	0.068	1,640,000
2	85.000	66.000	97.175	148.000	135.000	98.875	0.200	0.200	0.034	5,433,750
3	58.000	47.000	97.175	85.000	83.000	98.875	0.125	0.125	0.034	3,110,400
4	34.000	9.000	97.175	58.000	66.000	98.875	0.125	0.125	0.034	4,377,600
5	26.000	-40.000	97.175	51.000	9.000	98.875	0.200	0.200	0.034	1,531,250
6	14.000	-134.000	97.175	46.000	-40.000	98.875	0.400	0.400	0.068	470,000
									Total:	16,563,000

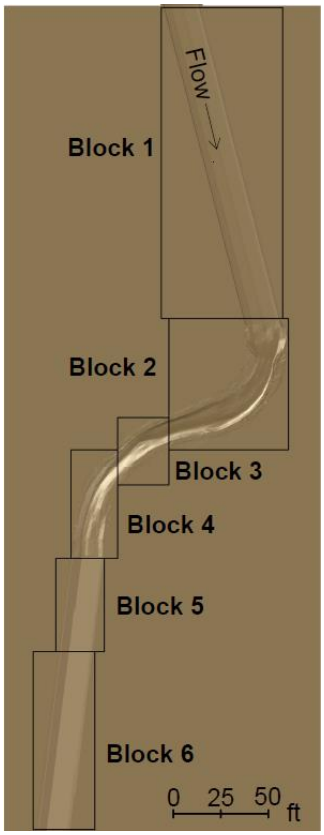

Figure 11. Downstream model flow domain and mesh block layout

The model coordinate system was modified from that of Shin et al. (2018) so that the coordinate system in FLOW-3D aligned with the coordinate system in AutoCAD from which the topography was generated. The equation to transform the coordinate system used in the S-curve physical model to the new numerical coordinate system is given in Equation 8. The coordinate system is the same in both the upstream and downstream models.

$$\begin{bmatrix} x_{num} \\ y_{num} \end{bmatrix} = \begin{bmatrix} cos\phi & -sin\phi \\ sin\phi & cos\phi \end{bmatrix} \begin{bmatrix} x_{phys} \\ y_{phys} \end{bmatrix} + \begin{bmatrix} \Delta x \\ \Delta y \end{bmatrix} \quad (8)$$

Where:

ϕ = -38.543°

Δx = 2.1916 ft

Δy = 25.4035 ft

Initial, Boundary, and Finish Conditions

The upstream boundary condition was modified to use the natural inlet boundary condition added in version 11.1 of FLOW-3D. The natural inlet boundary condition allows the inlet water surface elevation to be determined by the downstream conditions in the model, rather than set at a fixed elevation. Specifying a natural inlet boundary with subcritical flow improved the performance of the model by eliminating areas of unstable flow at the inlet and decreasing the model run time.

The initial conditions of the model were also improved to allow the model to reach steady state faster. Rather than initializing the model with a constant water surface elevation across the flow domain as in Shin et al. (2018), nine different fluid regions were used. Using multiple fluid regions allowed the initial water surface to be "stair-stepped" along the channel, providing a closer approximation of the steady state condition. Table 6 lists the fluid regions and their initial surface elevations.

Table 6. Initial fluid regions of the downstream model

	Minimum (ft)		Maximum (ft)		Fluid Elevation (ft)
Region	X	Y	X	Y	
1a	81	258	145	299	98.760
1b	81	217	145	258	98.730
1c	81	176	145	217	98.680
1d	81	135	145	176	98.630
2	85	66	148	135	98.570
3	58	47	85	83	98.551
4	34	9	58	66	98.520
5	26	-40	51	9	98.481
6	14	-134	46	-40	98.425

For all test cases, the model was run until a steady state finish condition was achieved. Steady state was defined as less than 1% global deviation in total mass, total fluid energy, mass-

averaged mean kinetic energy, mass-averaged mean turbulent energy, and mass-averaged turbulent dissipation over a 60-second interval.

Baseline Performance

The modified downstream model was run in a baseline condition with no transverse structures to compare its performance to the physical hydraulic model and the numerical models of Shin et al. (2018) and Scurlock et al. (2014a). The model was set up to simulate the physical model baseline test with a nominal flow rate of 12 ft^3/s. To account for leakage in the physical model, the inlet flow rate was set to 10.5 ft^3/s, as determined by Shin et al. (2018). Figure 12 shows the depth-averaged velocity distribution from the physical model and the new numerical model.

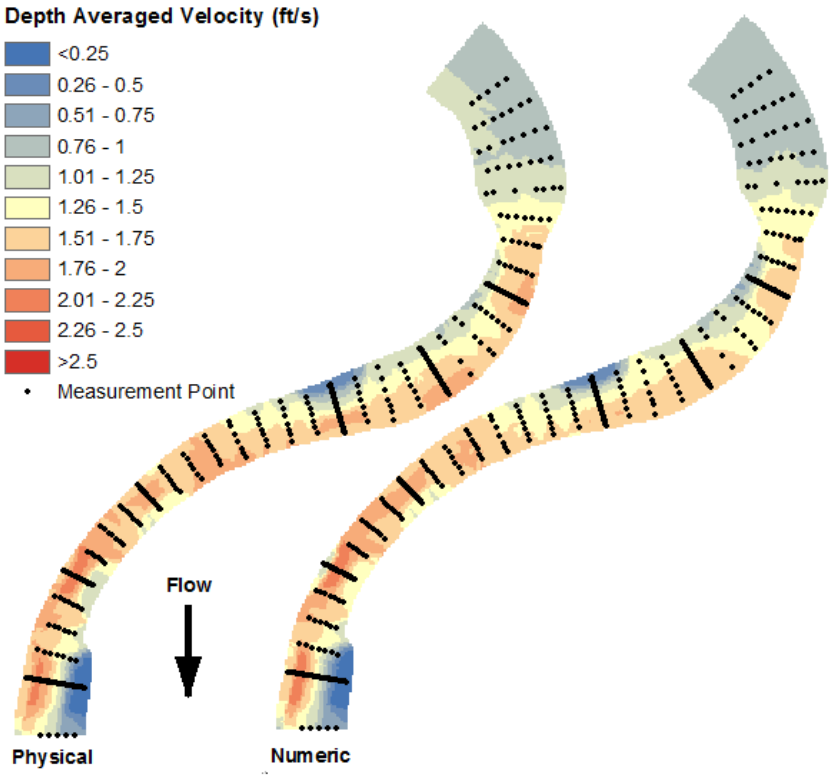

Figure 12. Depth averaged velocity from the physical and numerical models

Results of the physical and numerical models were compared at each location where velocity and depth measurements were taken in the physical model. Equations 9 and 10 give the formulas used to compute the error and absolute percent error at each data collection point. To summarize the performance of the model across the flow domain, the Mean Absolute Percent Error (MAPE) was computed for depth and depth-averaged velocity.

$$Error = Physical\ Value - Numerical\ Value \tag{9}$$

$$Absolute\ Perecent\ Error = \left|\frac{Physical\ Value - Numerical\ Value}{Physical\ Value}\right| * 100\% \tag{10}$$

For the baseline condition, the numerical model had a MAPE of 5.6% for depth and 13.8% for depth-averaged velocity compared to the physical model data. Figure 13 shows the spatial distribution of depth-averaged velocity errors. Depth-averaged velocity error is less than 10% across most the model domain. The only area with notably elevated error is a region along the bank at the transition between the upper and lower bends. Figure 14 shows the distribution of flow depth error. The largest depth error occurs at the upstream end of the S-curve and reflects the alteration of the channel geometry to create the upstream channel extension. This region is not of interest to the present study, so the large error is not a concern.

The depth MAPE of 5.6% is slightly larger than the 3.78% error of Scurlock et al. (2014a), but the depth-averaged velocity MAPE of 13.8% is a considerable improvement over that model's 20.4% error. The increase in the depth error is likely due to a combination of the model flow rate and the downstream boundary condition. The 2014 model used a flow rate of 11.5 ft^3/s, rather than 10.5 ft^3/s, which may have improved the depth error at the expense of the velocity error. Furthermore, the downstream boundary in the 2014 model was set immediately below the S-curve, without a length of straight channel to allow uniform flow to develop, which may have altered the depth in the lower portion of the model.

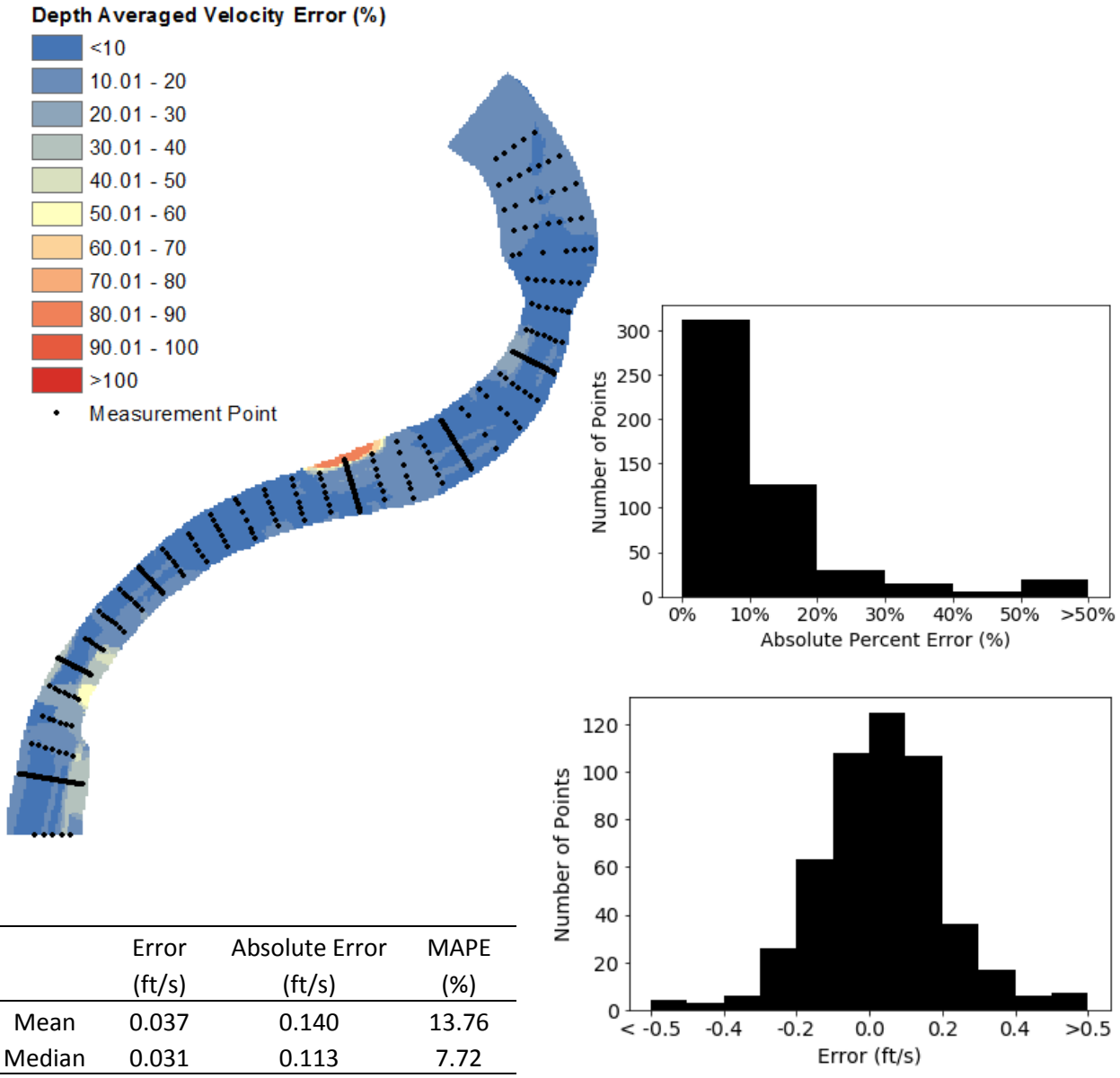

	Error (ft/s)	Absolute Error (ft/s)	MAPE (%)
Mean	0.037	0.140	13.76
Median	0.031	0.113	7.72

Figure 13. Error distribution for depth-averaged velocity for the baseline configuration

The improved model performed sufficiently well in the baseline scenario to build confidence in its representation of the basic flow processes in the S-curve. With this established, work proceeded to calibrating the model using physical model data for rock vanes.

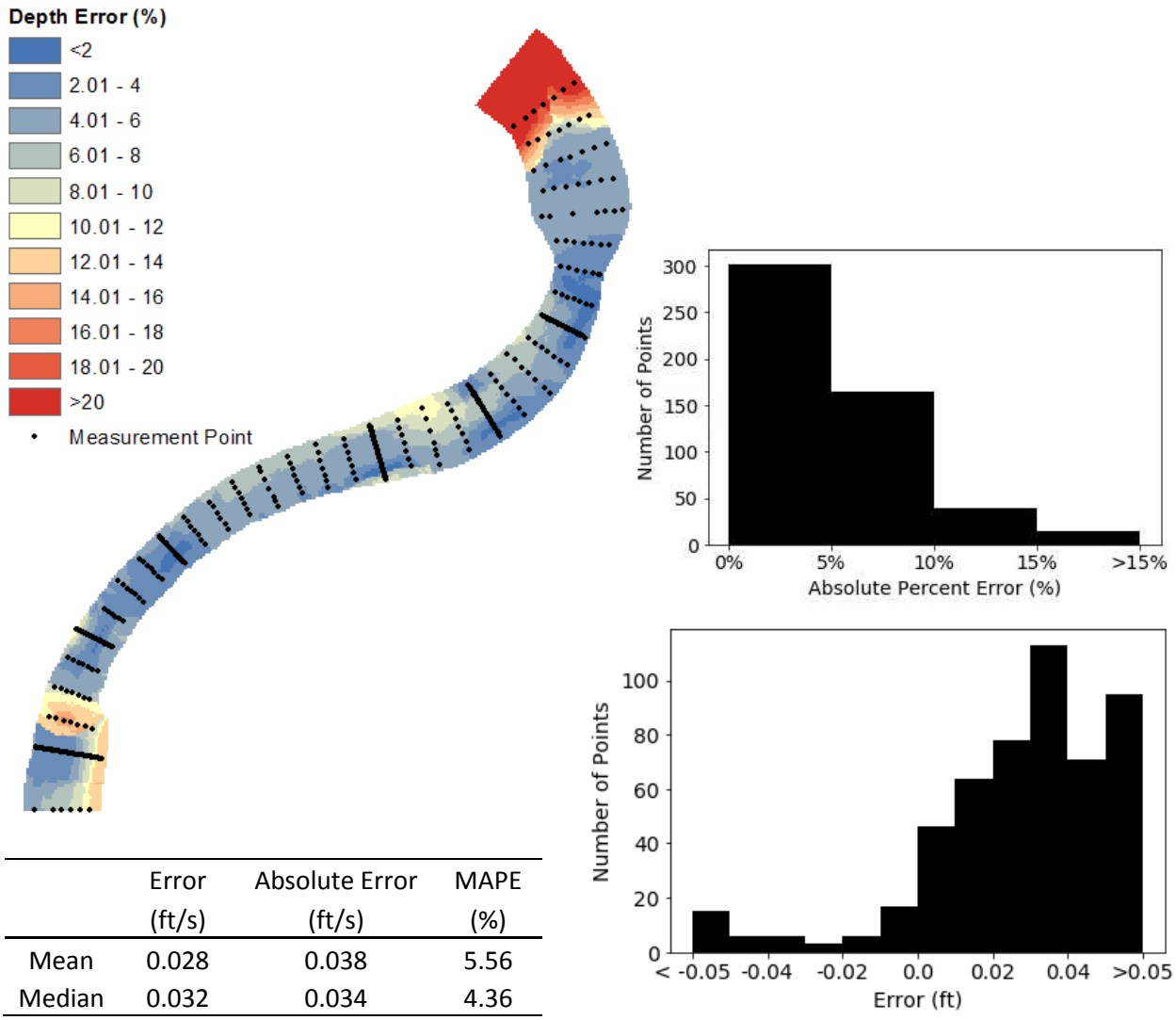

	Error (ft/s)	Absolute Error (ft/s)	MAPE (%)
Mean	0.028	0.038	5.56
Median	0.032	0.034	4.36

Figure 14. Error distribution for flow depth for the baseline configuration

CHAPTER 4. MODEL CALIBRATION AND VALIDATION

With the channel roughness already determined from the baseline condition, calibration focused only determining the roughness of the rock vane structures. The correct roughness of the rock vane structures could not be readily determined from direct measurements as it involves both the grain roughness created by the individual rock elements and the form roughness from the total height of the vane. The optimal roughness value was determined by calibration to the physical model, selecting the roughness value that minimized error in depth and depth-averaged velocity across the flow domain. Once roughness was determined by calibration, the numerical model was validated to ensure the calibrated roughness value produced acceptable performance on an independent data set.

Calibration

Data from the V01 configuration in the physical model were used for calibration. Because the rock vane physical model tests were performed several years after the baseline test, the flow rate in the model was computed from the V01 velocity measurements to account for changes in the leakage rate. Flow rate was computed at two cross-sections, designated A and B in the data files. Based on the computed flow rates of 11.31 ft^3/s at cross-section A and 11.08 ft^3/s at B, a flow rate of 11.25 ft^3/s was selected for the numerical model.

3D models of the rock vanes in V01 were drawn in AutoCAD Civil3D based on the dimensions in the design spreadsheets from the physical model structures. The surface of the structures was given a random riprap texture to represent the roughness of the riprap surface. The completed structures were then exported to FLOW-3D as a stereo lithography (STL) file. Appendix B details the procedure for drafting the rock vane structures. Figure 15 shows the layout of rock vanes in the V01 configuration.

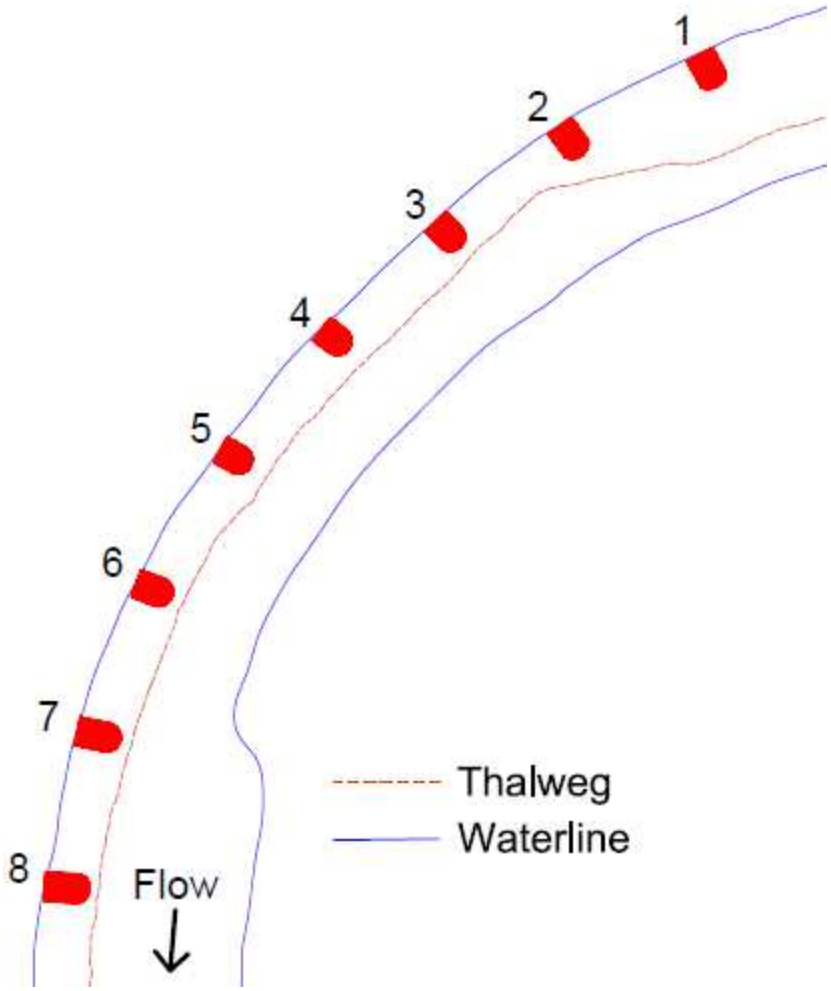

Figure 15. Layout of rock vanes (shown in red) in the V01 configuration

The numerical model was run with four different values of vane roughness, ranging from 0.04 ft to 0.15 ft. For each calibration run, the MAPE was computed for depth and depth-averaged velocity. Figure 16 shows the results of the calibration runs.

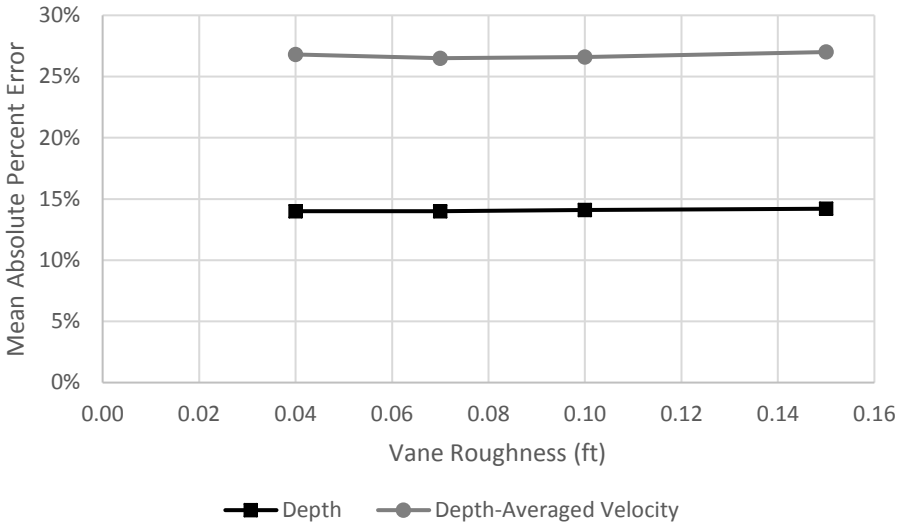

Figure 16. Calibration errors for depth and depth-averaged velocity

The results show very little sensitivity to the structure roughness, with the MAPE for both depth and depth-averaged velocity varying by less than 1% between the calibration runs. Such a result is not surprising, as the mesh resolution (0.034 ft in the z direction) is fine enough to capture the large roughness elements of the structures directly from the geometry, without relying on the specified surface roughness.

As the roughness of 0.07 ft gave marginally better performance, 0.07 ft was selected as the roughness value. This agrees with the calibration of previous numerical models, where both Shin et al. (2018) and Scurlock et al. (2014a) found 0.07 ft to be the optimal roughness value for bendway weirs, which have similar geometry to rock vanes.

Examining the spatial distribution of errors in depth-averaged velocity, Figure 17 shows that the numerical model provides a good representation of the physical data over most of the flow domain. Errors are concentrated at measurement points on and between the rock vanes and in the region of flow separation at the channel expansion. The flow in these areas is highly three-

dimensional and in some cases shallow, causing difficulty in collecting high-quality velocity measurements in the physical model.

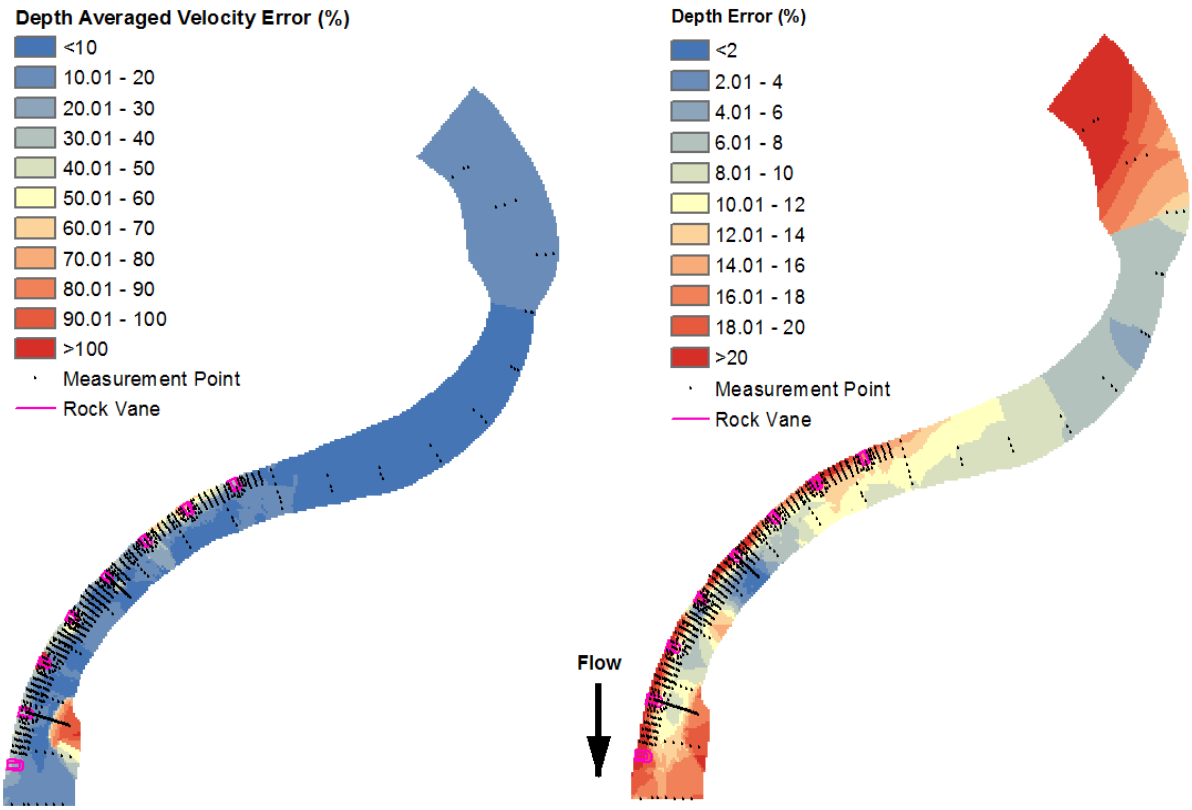

Figure 17. MAPE for depth-averaged velocity (left) and depth (right) for the V01 configuration

The complex nature of flow also limits the accuracy of the numerical model. The RNG *k*-ε turbulence model has weaknesses in areas of highly turbulent flow and flow separation (Scurlock et al. 2014a), such as the flows occurring in the regions of greatest difference. The combination of the channel curvature, rock vane structures, and channel expansion creates a complicated flow field that is both difficult to model numerically and difficult to measure in a physical model. That the numerical data and physical data have some regions of disagreement should not be surprising.

Overall, the calibrated model has good agreement with the physical data across most of the flow domain, with some regions of greater difference in areas with more complicated flow. The optimal roughness value of 0.07 ft determined for rock vanes is in agreement with the earlier studies determining the roughness of bendway weirs. With calibration complete, the model's performance was evaluated on a different rock vane configuration to validate the model.

Validation

To validate the downstream model's performance, it was run again to compare it to an independent set of data collected from the physical model. The V07 configuration was chosen for validation, since its structures are located in the downstream bend of the S-curve, which is the region of interest for the downstream model. The structures for the V07 configuration were drawn in AutoCAD Civil3D and exported to FLOW-3D in the same manner as the V01 structures. Figure 18 shows the layout of the V07 structures. The numerical model was run using the same rock vane roughness of 0.07 ft and flow rate of 11.5 ft^3/s determined from the calibration process.

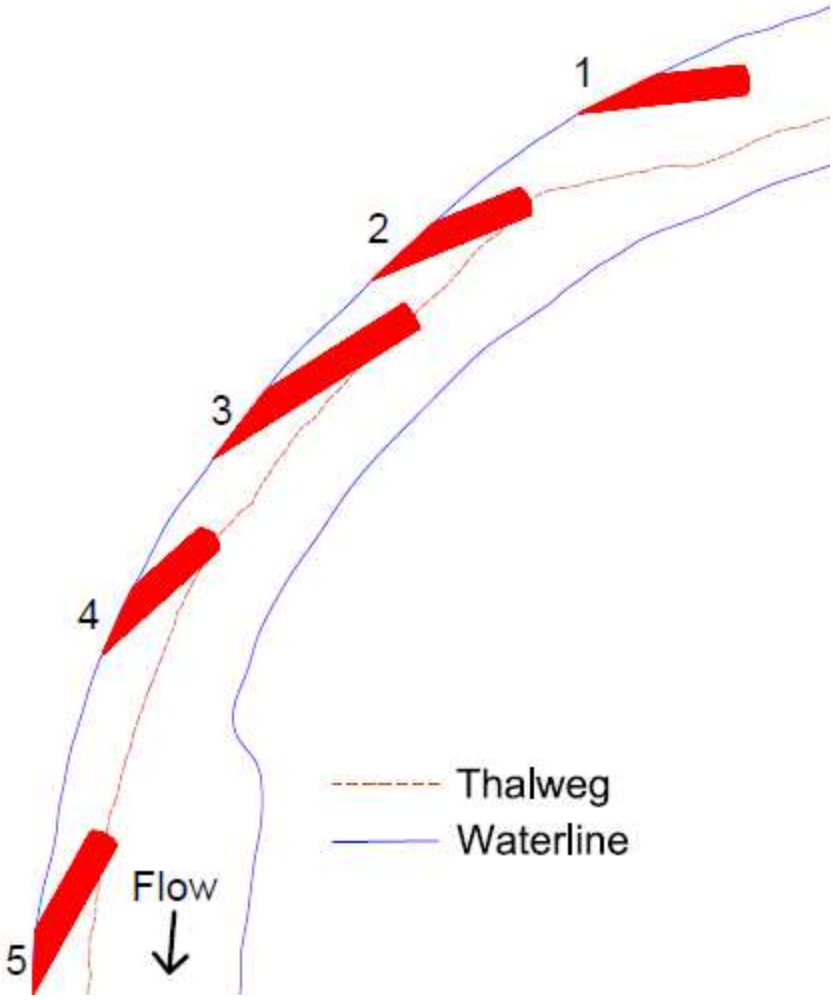

Figure 18. Layout of rock vanes in the V07 configuration used for model validation

The error of the numerical model compared to the physical model was computed in the same manner as in calibration, with MAPE computed for depth and depth-averaged velocity. The numerical model displayed improved performance for the V07 configuration, with MAPE of 9.7% for depth and 19.6% for depth-averaged velocity. The mean depth error was only 0.014 ft, indicating the mean flow depth in the numerical model is in good agreement with the physical model. Table 7 summarizes the model performance in the calibration and validation trials.

Table 7. Calibration and validation summary of the downstream model

Model Run	Flow Rate (ft^3/s)	Vane Roughness (ft)	Depth MAPE	Mean Depth Error (ft)	Depth Avg. Velocity MAPE
Baseline	10.5	-	5.6%	0.028	13.8%
V01	11.25	0.07	14.0%	0.104	26.5%
V07	11.25	0.07	9.7%	0.014	19.6%

The improved performance of the validation data over the calibration data suggests the model was correctly calibrated to the optimal parameter values. Examining the spatial error distribution (Figure 19), the largest velocity errors again occur between the vanes and at the expansion, in regions of more complex flow.

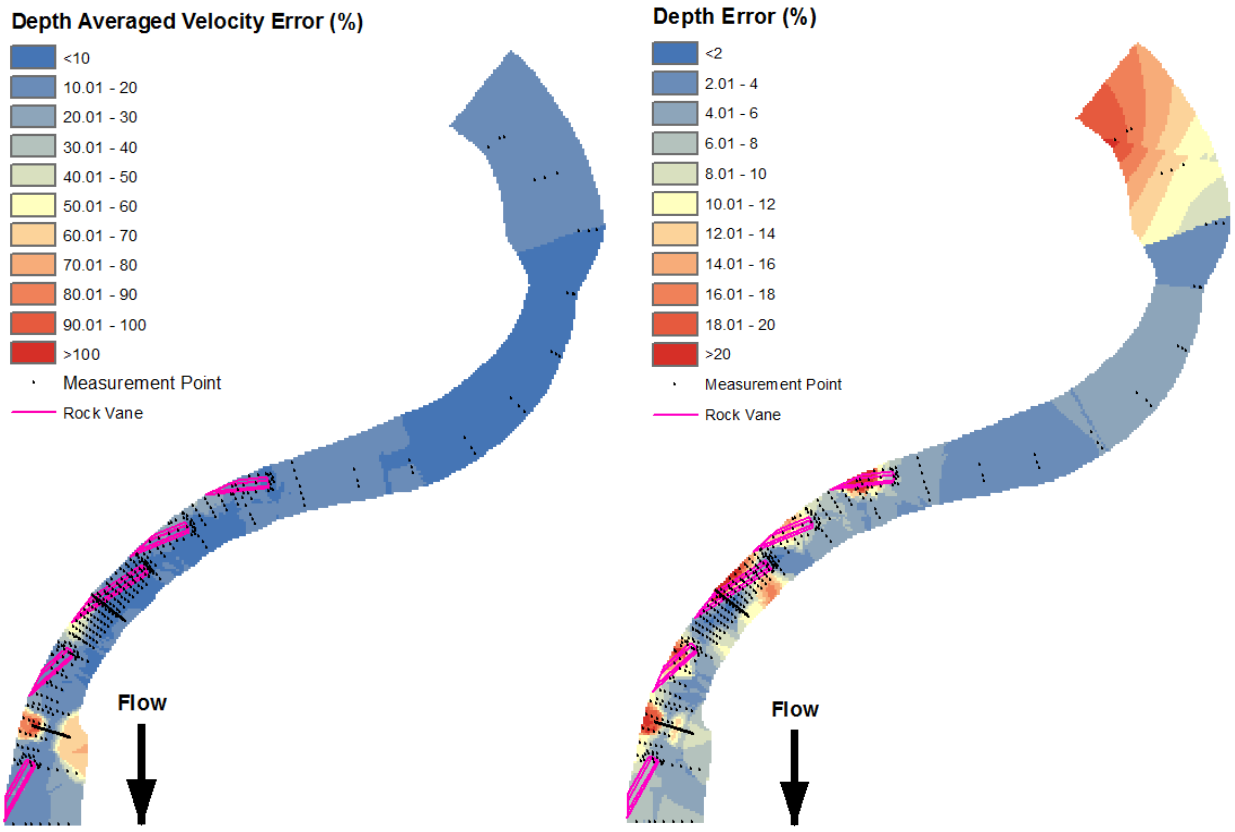

Figure 19. MAPE for depth-averaged velocity (left) and depth (right) for V07

One reason for the improved performance of the numerical model for the V07 configuration may be reduced turbulence around the rock vanes. Figure 20 and Figure 21, both showing the same portion of the model domain, illustrate the streamlines of modeled flow over rock vanes 5 and 6 in V01 and rock vane 4 in V07. The flow field in the V01 configuration is much more complex, with several eddies visible along the outer bank. In contrast, flow in the V07 configuration is relatively smooth. As previously discussed, areas of complex, highly three-dimensional flow hamper both the numerical model and the physical model measurements. The smoother flow around the vanes in V07 could be an important reason for better agreement between the physical and numerical data for V07 than V01.

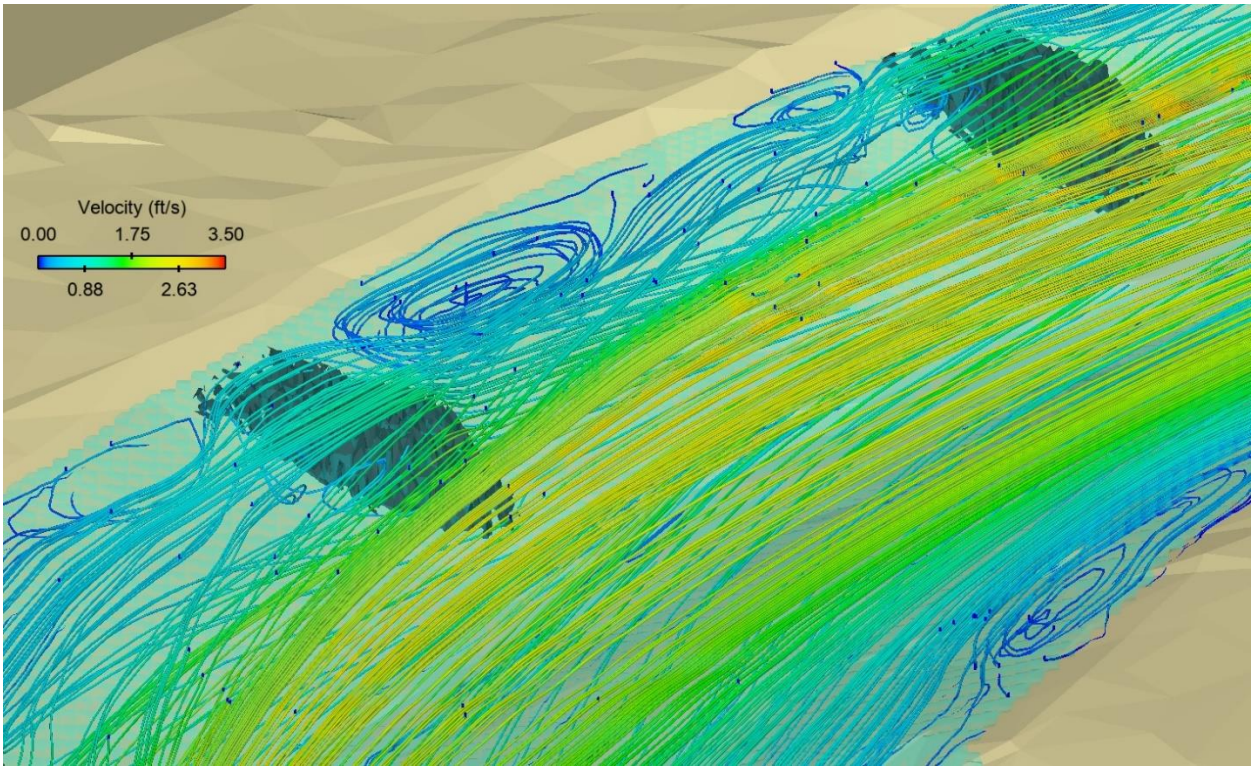

Figure 20. Flow around rock vanes 5 and 6 in V01

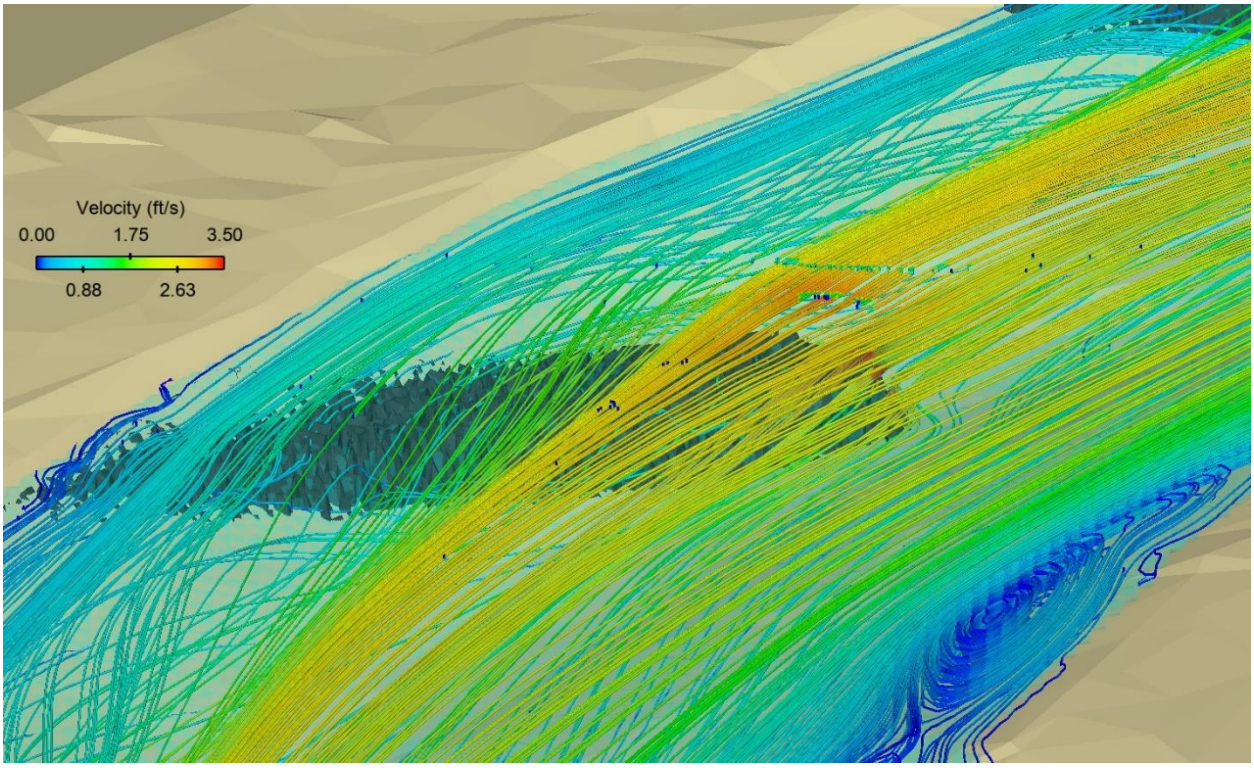

Figure 21. Flow around rock vane 4 in V07

The calibration and validation of the downstream numerical model indicate the basic model structure, including mesh size and boundary conditions, produces sufficiently accurate simulations of flow in the S-curve bend. Additionally, calibration determined the optimal value of roughness for rock vanes to be 0.07 ft, in agreement with the work of Shin et al. (2018) and Scurlock et al. (2014a) on bendway weirs. Based on these findings, a second, upstream, numerical model was created with a modified channel topography to produce better flow conditioning in the upstream bend.

CHAPTER 5. UPSTREAM BEND MODEL

The models developed by Shin et al. (2018) and Scurlock et al. (2014a) used a straight approach channel for the inlet to the upstream bend. The long, straight channel of constant slope caused uniform flow to develop in the channel with a nearly uniform lateral velocity distribution. The straight approach channel was representative of flow conditions in the CSU physical model, where the head box was designed to provide uniform flow into the model (Heintz 2002) but is not representative of the distribution of flow entering a typical meander bend in a river.

In meandering rivers, the lateral velocity distribution varies throughout a series of meander bends such that the highest velocity occurs near the outer bank of each bend, as shown in Figure 22. As a result, the velocity distribution for a bend with a long, straight approach is different from that in a bend with a series of meander bends upstream (Odgaard and Abad 2007). To make the inlet conditions of the upstream bend of the model more representative of a meandering river, a second numerical model was created.

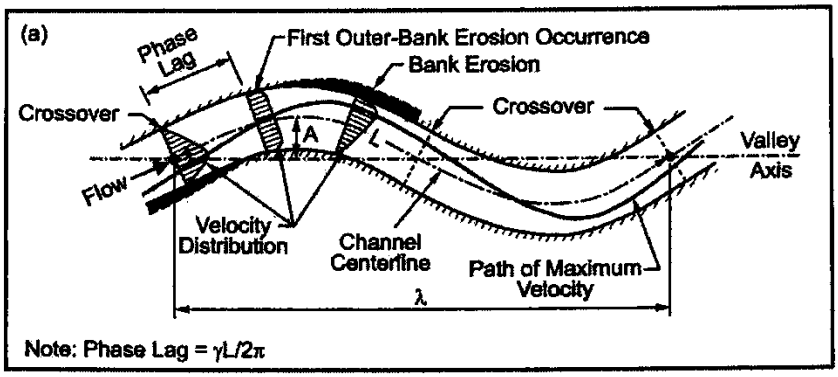

Figure 22. Variation in velocity distribution throughout a meander bend (Odgaard and Abad 2007)

The second model, referred to as the upstream model, replaced the straight inlet channel with two additional 90° bends. These bends condition the flow to be non-uniformly distributed

across the width of the channel. As a result, flow into the upstream bend is more representative of that in actual river channel, where meander bends typically occur in series of multiple bends. The new bends were created by extruding the upstream-most cross-section of the upstream bend to create two new bends, each with the same radius as the upstream bend. The additional bends have the same constant slope of 0.00086 ft/ft as the straight approach channel used in the model of the downstream bend.

To accommodate the additional bends in the upstream model, eight mesh blocks were used to model the flow domain compared to the six used in the downstream model. The mesh of the upstream model was designed similarly to that of the downstream model, with high-resolution mesh (0.125 ft x 0.125 ft x 0.034 ft) where structures would be located in the upstream bend and lower resolution mesh elsewhere to minimize model run time. Table 8 describes the mesh blocks used in the upstream model and Figure 23 shows the layout of the mesh blocks.

Table 8. Mesh block information for the upstream model

Mesh Block	Minimum (ft)			Maximum (ft)			Resolution (ft)			Number of Cells
	X	Y	Z	X	Y	Z	X	Y	Z	
1	117.000	190.000	97.175	167.000	250.000	98.875	0.400	0.400	0.068	468,750
2	113.000	148.000	97.175	143.000	190.000	98.875	0.200	0.200	0.034	1,575,000
3	117.000	98.000	97.175	147.000	148.000	98.875	0.125	0.125	0.034	4,800,000
4	85.000	66.000	97.175	139.000	98.000	98.875	0.125	0.125	0.034	5,529,600
5	58.000	47.000	97.175	85.000	83.000	98.875	0.200	0.200	0.034	1,215,000
6	34.000	10.000	97.175	58.000	66.000	98.875	0.200	0.200	0.034	1,680,000
7	26.000	-40.000	97.175	52.000	10.000	98.875	0.400	0.400	0.068	203,125
8	14.000	-134.000	97.175	46.000	-40.000	98.875	0.400	0.400	0.068	470,000
									Total:	15,941,475

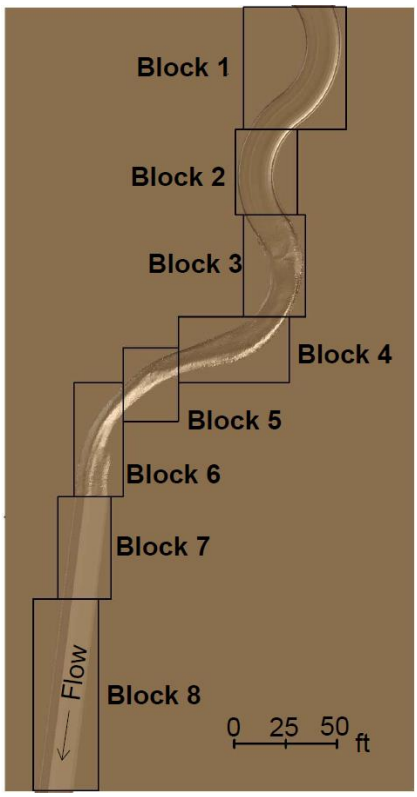

Figure 23. Upstream model flow domain and mesh block layout

Boundary conditions were identical to those used in the downstream model, except that the flow direction vector at the upstream boundary was changed to x = 0.1369 y = -0.9906 to align with the new channel geometry. The initial conditions were modified such that the initial fluid regions aligned with the new mesh block boundaries. Table 9 lists the boundaries and elevations of the initial fluid regions used in the upstream model.

Because of the additional bends added to the upstream model, it is not possible to calibrate the model to physical experiment data. In fact, the very purpose of the upstream model is to address shortcomings in the physical model experiment. However, because the upstream numerical model shares the same basic structure as the downstream numerical model, it should provide results of comparable quality. With numerical models prepared for both the upstream

and downstream bends in the S-curve, work proceeded on to testing configurations of rock vane and bendway weir structures.

Table 9. Initial fluid regions of the upstream model

Block	Minimum (ft)		Maximum (ft)		Fluid Elevation (ft)
	X	Y	X	Y	
1a	117	220	167	250	98.760
1b	117	190	167	220	98.730
2	113	148	143	190	98.680
3	117	98	147	148	98.630
4	85	66	139	98	98.570
5	58	47	85	83	98.551
6	34	10	58	66	98.520
7	26	-40	52	10	98.481
8	14	-134	46	-40	98.425

CHAPTER 6. TEST CONFIGURATIONS

Once preparation of the numerical models of the upstream and downstream bends was completed, work proceeded to the second objective of the study: to determine the effects on the bend flow field of varying the spacing and geometric parameters of rock vanes and bendway weirs. To accomplish this objective, 31 rock vane configurations were tested, along with 14 bendway weir configurations.

The test configurations were numbered following a scheme used in previous CSU studies of rock vanes and bendway weirs (Scurlock et al. 2014b, Thornton, et al. 2016). Configurations are designated with the indicator "V" for rock vane or "BW" for bendway weir followed by a test number. To distinguish from configurations in previous studies, rock vane tests were numbered starting with V11 and bendway weir tests were numbered starting at BW401.

Description of Test Configurations

Rock vane configurations V11-V16 were designed in the downstream bend based on the most successful configuration from Thornton et al. (2016), V01. The planform angle of the rock vanes was reduced to 60° and rock vanes with both 10% and 20% slopes were tested at crest lengths of $L_c = T_w/3$, $T_w/4$, and $T_w/6$. The spacing was the same as that used in V01, $L_{arc} = 1.15T_w$. To provide a comparison between the bends, configurations V17-V19 were tested in the upstream bend with the same 60° planform angle, spacing of $L_{arc} = 1.15T_w$, and a 10% crest slope. The projected lengths of V17-V19 were designed to correspond with the three projected lengths tested in V11-V16. Table 10 gives the geometric parameters of configurations V11-V19.

Table 10. Rock vane test configurations based on V01. DS indicates the configuration was tested in the downstream bend, US indicates the upstream bend.

Configuration	Crest Length L_c	Projected Length L_{proj}	Spacing L_{arc}	Angle θ	Crest Slope $tan\phi$	Bend
V11	$0.33T_w$	$0.29T_w$	$1.15T_w$	60°	10%	DS
V12	$0.33T_w$	$0.29T_w$	$1.15T_w$	60°	20%	DS
V13	$0.167T_w$	$0.14T_w$	$1.15T_w$	60°	10%	DS
V14	$0.167T_w$	$0.14T_w$	$1.15T_w$	60°	20%	DS
V15	$0.25T_w$	$0.22T_w$	$1.15T_w$	60°	10%	DS
V16	$0.25T_w$/	$0.22T_w$	$1.15T_w$	60°	20%	DS
V17	$0.34T_w$	$0.29T_w$	$1.15T_w$	60°	10%	US
V18	$0.16T_w$	$0.14T_w$	$1.15T_w$	60°	10%	US
V19	$0.26T_w$	$0.22T_w$	$1.15T_w$	60°	10%	US

Based on the existing design guidance summarized in Table 1, USBR selected the values in Table 11 as representative of geometric parameters in the current design guidance. Configurations V20-V41 were developed by systematically deviating individual vane parameters from the median values. Table 12 lists the parameters of configurations V20-V41. Note that spacing in Table 12 is given in terms of both T_w and L_{proj}, to enable direct comparison of spacing for configurations with varying lengths.

Table 11. Median values of rock vane parameters in existing design guides selected by USBR

Projected Length L_{proj}	Spacing L_{arc}	Angle θ	Crest Slope $tan\phi$
$0.25T_w$	$3L_{proj}$	45°	10%

Table 12. Rock vane configurations based on deviations from common design values.

Configuration	Projected Length L_{proj}	Spacing L_{arc}	Angle θ	Crest Slope $tan\phi$	Bend
V20	$0.25T_w$	$0.75T_w = 3L_{proj}$	45°	10%	DS
V21	$0.25T_w$	$0.75T_w = 3L_{proj}$	45°	20%	DS
V22	$0.25T_w$	$0.75T_w = 3L_{proj}$	45°	5%	DS
V23	$0.25T_w$	$0.75T_w = 3L_{proj}$	70°	10%	DS
V24	$0.25T_w$	$0.75T_w = 3L_{proj}$	25°	10%	DS
V25	$0.25T_w$	$1.5T_w = 6L_{proj}$	45°	10%	DS
V26	$0.25T_w$	$0.5T_w = 2L_{proj}$	45°	10%	DS
V27	$0.5T_w$	$1.5T_w = 3L_{proj}$	45°	10%	DS
V28	$0.167T_w$	$0.5T_w = 3L_{proj}$	45°	10%	DS
V29	$0.25T_w$	$0.75T_w = 3L_{proj}$	45°	10%	US
V30	$0.25T_w$	$0.75T_w = 3L_{proj}$	45°	20%	US
V31	$0.25T_w$	$0.75T_w = 3L_{proj}$	45°	5%	US
V32	$0.25T_w$	$0.75T_w = 3L_{proj}$	70°	10%	US
V33	$0.25T_w$	$0.75T_w = 3L_{proj}$	25°	10%	US
V34	$0.25T_w$	$1.5T_w = 6L_{proj}$	45°	10%	US
V35	$0.25T_w$	$0.5T_w = 2L_{proj}$	45°	10%	US
V36	$0.5T_w$	$1.5T_w = 3L_{proj}$	45°	10%	US
V37	$0.167T_w$	$0.5T_w = 3L_{proj}$	45°	10%	US
V38	$0.25T_w$	$2T_w = 8L_{proj}$	45°	10%	DS
V39	$0.25T_w$	$2T_w = 8L_{proj}$	45°	10%	US
V40	$0.25T_w$	$3T_w = 12L_{proj}$	45°	10%	DS
V41	$0.25T_w$	$3T_w = 12L_{proj}$	45°	10%	US

To compare the performance of rock vanes and bendway weirs, 14 different bendway weir configurations also were tested. The configurations, listed in Table 13, were designed with lengths and spacing that would provide direct comparison with the rock vane test configurations.

Table 13. Bendway weir test configurations

Configuration	Projected Length L_{proj}	Spacing L_{arc}	Angle θ	Height D - Δz	Bend
BW401	$0.25T_w$	$0.75T_w = 3L_{proj}$	70°	D/3	DS
BW402	$0.25T_w$	$0.75T_w = 3L_{proj}$	70°	D/2	DS
BW403	$0.25T_w$	$0.75T_w = 3L_{proj}$	70°	D/5	DS
BW404	$0.5T_w$	$1.5T_w = 3L_{proj}$	70°	D/3	DS
BW405	$0.125T_w$	$0.375T_w = 3L_{proj}$	70°	D/3	DS
BW406	$0.25T_w$	$0.375T_w = 1.5L_{proj}$	70°	D/3	DS
BW407	$0.25T_w$	$1.5T_w = 6L_{proj}$	70°	D/3	DS
BW408	$0.25T_w$	$0.75T_w = 3L_{proj}$	70°	D/3	US
BW409	$0.25T_w$	$0.75T_w = 3L_{proj}$	70°	D/2	US
BW410	$0.25T_w$	$0.75T_w = 3L_{proj}$	70°	D/5	US
BW411	$0.5T_w$	$1.5T_w = 3L_{proj}$	70°	D/3	US
BW412	$0.125T_w$	$0.375T_w = 3L_{proj}$	70°	D/3	US
BW413	$0.25T_w$	$0.375T_w = 1.5L_{proj}$	70°	D/3	US
BW414	$0.25T_w$	$1.5T_w = 6L_{proj}$	70°	D/3	US

Bend Geometry Parameters

Before computing numerical values for the parameters of each configuration, the geometric parameters of the upstream and downstream bends had to be determined. The geometry of the downstream bend was unaltered from that used in the physical model of Scurlock et al. (2014b), so the channel top-width (T_w), hydraulic depth (D), and average thalweg depth (D_b) were taken from the physical modelling report. The values for normal depth flow conditions were used, as the numerical model was calibrated to the normal depth condition.

All of the geometric characteristics of the upstream bend had to be recomputed because the geometry of the upstream bend was modified from that of the physical model. The channel top-width, flow area (A), and thalweg depth were evaluated at cross-sections 3-10 to match the range of cross-sections used to compute the upstream bend geometry in Scurlock et al. (2014b) (see Figure 6 for cross-section locations in the physical hydraulic model). The hydraulic depth

was computed at each cross-section as $D = A/T_w$ and the average values of the geometric parameters for the bend were computed, as shown in Table 14.

Table 14. Calculation of geometric parameters for the upstream bend

Cross Section	Top-Width T_w	Flow Area A	Hydraulic Depth D	Thalweg Depth D_b
	ft	ft^2	ft	ft
3	13.99	7.71	0.55	0.96
4	13.02	12.29	0.94	1.29
5	12.95	11.59	0.89	1.36
6	12.56	8.69	0.69	1.16
7	12.95	6.94	0.54	1.06
8	13.22	6.44	0.49	0.83
9	11.59	8.78	0.76	1.15
10	10.24	9.85	0.96	1.40
Average	12.6	9.0	0.73	1.2

The values of bend radius deserve some special attention, as they have been given inconsistently in previous reports. The regression equation in Scurlock et al. (2014b) states that the "radius of curvature of channel bend centerline" is to be considered in the design of bendway weirs. However, layout of the model geometry in AutoCAD revealed that the bend radii values in Scurlock et al. (2014b) are measured to the channel thalweg, not the channel centerline. It appears the radii values in Scurlock et al. (2014b) were measured using the methodology of Scurlock et al. (2012b) and erroneously reported to be centerline radii.

The true centerline radii were determined by locating the midpoint of the channel at cross-sections 3-8 for the upstream bend and 11-16 for the downstream bend. The radius from the midpoint of each cross-section to the center of curvature was measured in AutoCAD and the average radius was computed for each bend, as shown in Table 15. Table 16 summarizes the geometric parameters of each bend.

Table 15. Values used to calculate the average bend radius

Upstream Bend		Downstream Bend	
Cross-Section	Radius	Cross-Section	Radius
	ft		ft
3	39.63	11	68.23
4	40.24	12	68.42
5	40.77	13	68.10
6	40.76	14	68.90
7	40.64	15	69.05
8	40.42	16	67.26
Average	40	Average	68

Table 16. Average geometric parameters for the upstream and downstream bends

Bend	Top-Width	Hydraulic Depth	Thalweg Depth	Radius
	T_w	D	D_b	R_c
	ft	ft	ft	ft
Upstream	12.6	0.73	1.2	40
Downstream	9.3	0.74	1.2	68

Configuration Layout and Testing

With the geometry of each bend quantified, numerical values of the geometric parameters for each rock vane and bendway weir configuration were computed. Using the computed values, the structures were modelled in AutoCAD according to the procedure described in Appendix B. All structures were drawn with a crest width of W = 1.0 ft and a toe slope of 1H:1V.

The projected area is not constant for each structure in a given configuration, as the channel cross-section varies throughout the two bends. To account for the variation, the projected area of each configuration was computed as the average of the projected areas of all the structures in the configuration. Table 17 contains the parameter values for the rock vane configurations while the values for the bendway weir configurations are given in Table 18.

Table 17. Computed parameter values for rock vane test configurations

Configuration	Crest Length L_c (ft)	Projected Length L_{proj} (ft)	Spacing L_{arc} (ft)	Angle θ	Crest Slope $tan\phi$	Submergence Δz (ft)	Projected Area A^*	Bend
V11	3.1	2.7	10.7	60°	10%	0.31	20%	DS
V12	3.1	2.7	10.7	60°	20%	0.62	12%	DS
V13	1.5	1.3	10.7	60°	10%	0.15	7%	DS
V14	1.5	1.3	10.7	60°	20%	0.31	4%	DS
V15	2.3	2.0	10.7	60°	10%	0.23	13%	DS
V16	2.3	2.0	10.7	60°	20%	0.46	8%	DS
V17	4.3	3.6	14.4	60°	10%	0.43	26%	US
V18	2.0	1.8	14.4	60°	10%	0.20	14%	US
V19	3.2	2.8	14.4	60°	10%	0.32	21%	US
V20	3.3	2.3	7.0	45°	10%	0.33	15%	DS
V21	3.3	2.3	7.0	45°	20%	0.67	7%	DS
V22	3.3	2.3	7.0	45°	5%	0.17	20%	DS
V23	2.5	2.3	7.0	70°	10%	0.25	19%	DS
V24	6.0	2.3	7.0	25°	10%	0.60	8%	DS
V25	3.3	2.3	13.9	45°	10%	0.33	15%	DS
V26	3.3	2.3	4.6	45°	10%	0.33	15%	DS
V27	6.8	4.6	13.9	45°	10%	0.68	32%	DS
V28	2.2	1.5	4.6	45°	10%	0.22	8%	DS
V29	4.6	3.1	9.4	45°	10%	0.46	21%	US
V30	4.6	3.1	9.4	45°	20%	0.92	12%	US
V31	4.6	3.1	9.4	45°	5%	0.23	27%	US
V32	3.4	3.1	9.4	70°	10%	0.34	25%	US
V33	9.4	3.1	9.4	25°	10%	0.94	12%	US
V34	4.6	3.1	18.8	45°	10%	0.46	22%	US
V35	4.6	3.1	6.3	45°	10%	0.46	22%	US
V36	9.7	6.3	18.8	45°	10%	0.97	26%	US
V37	3.0	2.1	6.3	45°	10%	0.30	15%	US
V38	3.3	2.3	18.5	45°	10%	0.33	16%	DS
V39	4.6	3.1	25.1	45°	10%	0.46	20%	US
V40	3.3	2.3	27.8	45°	10%	0.33	15%	DS
V41	4.6	3.1	37.7	45°	10%	0.46	23%	US

Table 18. Computed parameter values for bendway weir test configurations

Configuration	Crest Length L_c	Projected Length L_{proj}	Spacing L_{arc}	Angle θ	Crest Slope $tan\phi$	Submergence Δz	Projected Area A^*	Bend
	(ft)	(ft)	(ft)			(ft)		
BW401	2.5	2.3	7.0	70°	0%	0.49	6%	DS
BW402	2.5	2.3	7.0	70°	0%	0.37	10%	DS
BW403	2.5	2.3	7.0	70°	0%	0.59	4%	DS
BW404	4.9	4.6	13.9	70°	0%	0.49	26%	DS
BW405	1.2	1.2	3.5	70°	0%	0.49	0%	DS
BW406	2.5	2.3	3.5	70°	0%	0.49	6%	DS
BW407	2.5	2.3	13.9	70°	0%	0.49	6%	DS
BW408	3.3	3.1	9.4	70°	0%	0.49	14%	US
BW409	3.3	3.1	9.4	70°	0%	0.37	18%	US
BW410	3.3	3.1	9.4	70°	0%	0.58	11%	US
BW411	6.7	6.3	18.8	70°	0%	0.49	24%	US
BW412	1.7	1.6	4.7	70°	0%	0.49	5%	US
BW413	3.3	3.1	4.7	70°	0%	0.49	14%	US
BW414	3.3	3.1	18.8	70°	0%	0.49	14%	US

To provide consistency in structure layout, a "base point" was selected in each bend at which a structure was placed in each configuration and from which the other structures were located. The selected "base points" were the location of rock vane 5 in the V01 configuration in the downstream bend and rock vane 4 in the V29 configuration in the upstream bend. Structures were placed upstream and downstream of the "base point" at intervals of L_{arc}, until structures were placed along the length of the bend. Figure 24 – Figure 35 show the location of structures in each configuration. The location of the thalweg of the fixed bed channel is indicated in the figures.

The models of each configuration were tested in FLOW-3D to evaluate their effect on the flow field in the model bends. A surface roughness of 0.07 ft was specified for each structure, in accordance with the results of model calibration. All models were run until steady-state conditions were achieved. As in the calibration runs, steady state was defined as less than 1%

global deviation in total mass, total fluid energy, mass-averaged mean kinetic energy, mass-averaged mean turbulent energy, and mass-averaged turbulent dissipation over a 60-second interval. Upon achieving steady-state, the simulation was stopped and the results stored for analysis.

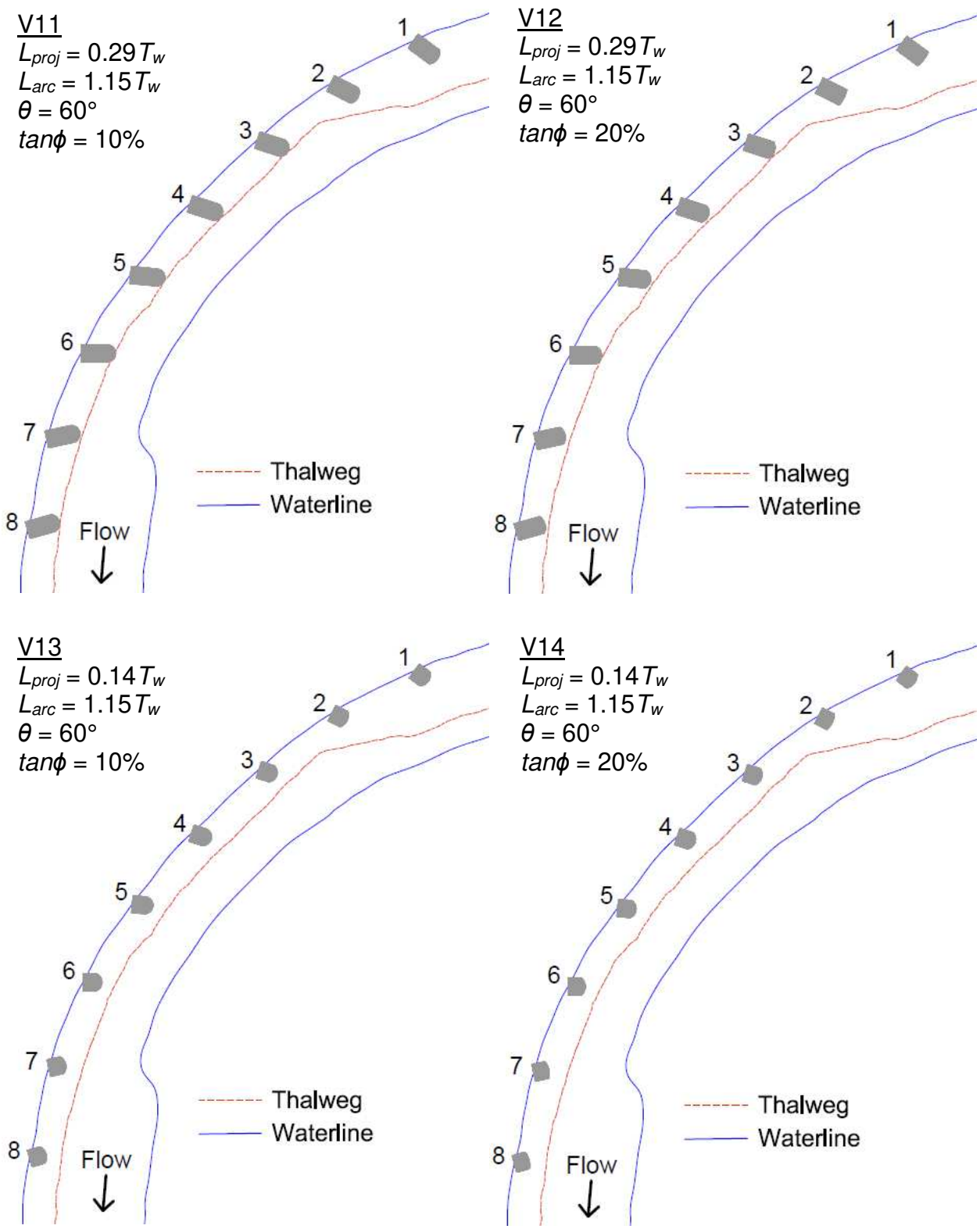

Figure 24. Locations of rock vanes in configurations V11-V14

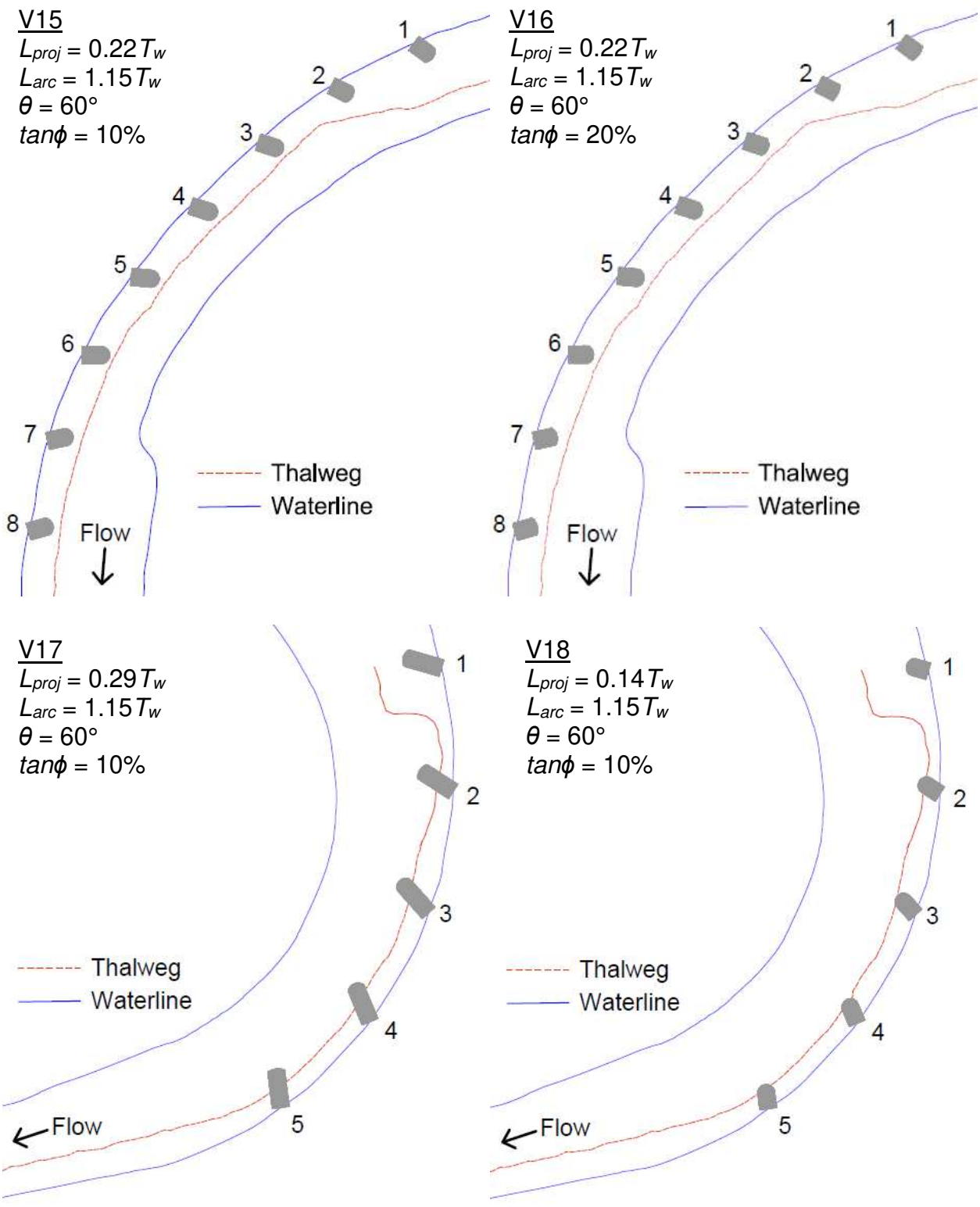

Figure 25 Locations of rock vanes in configurations V15-V18

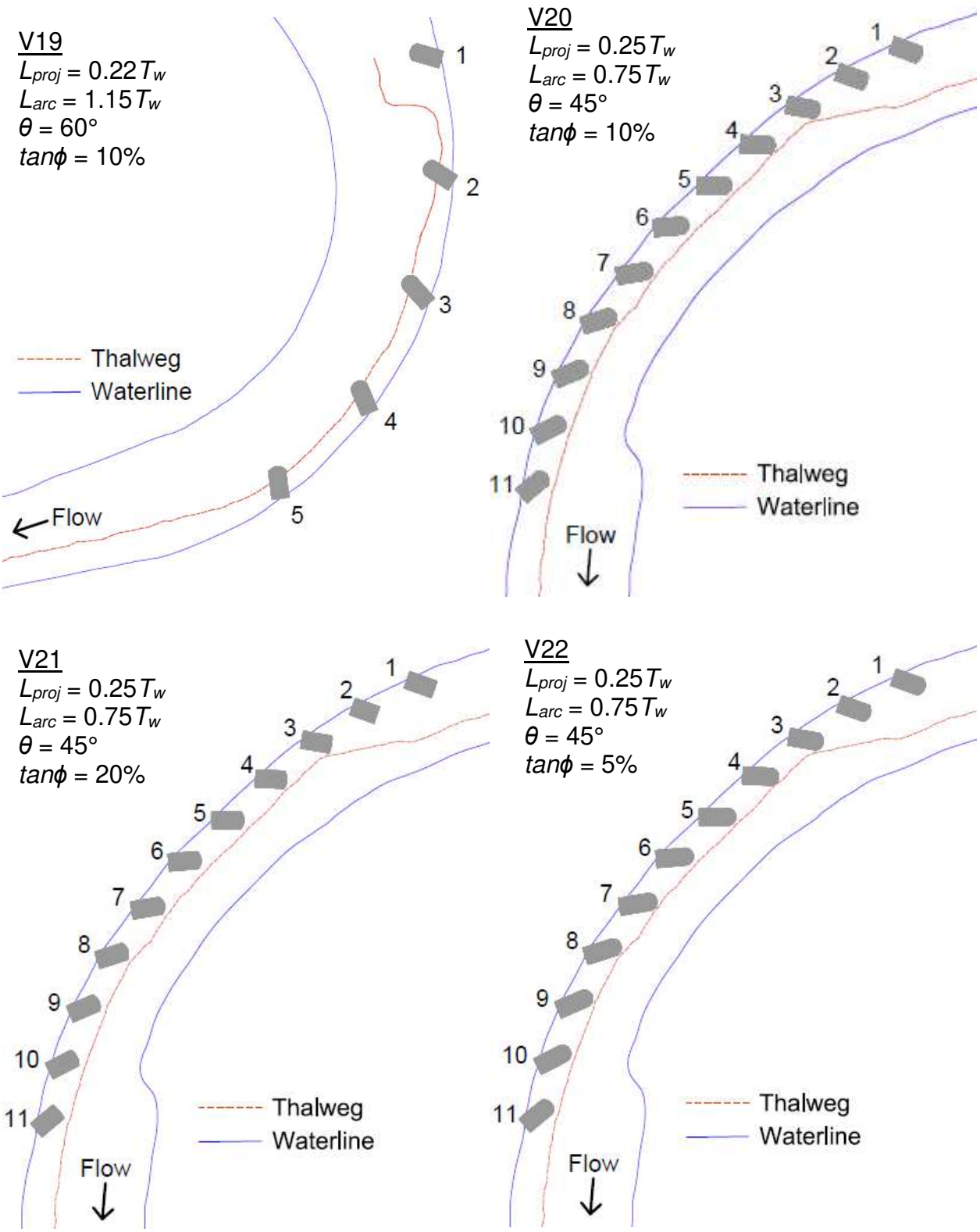

Figure 26. Locations of rock vanes in configurations V19-V22

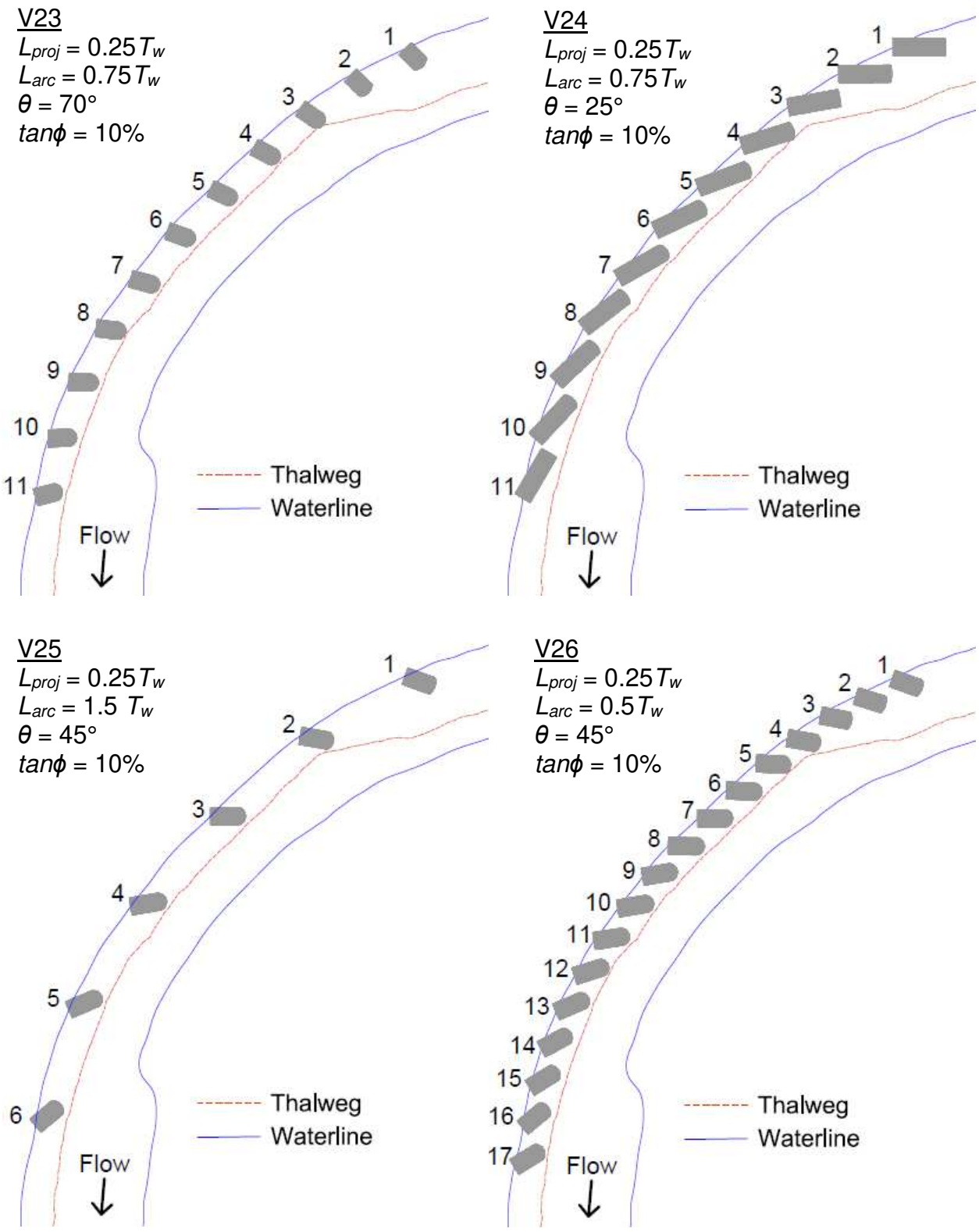

Figure 27. Locations of rock vanes in configurations V23-V26

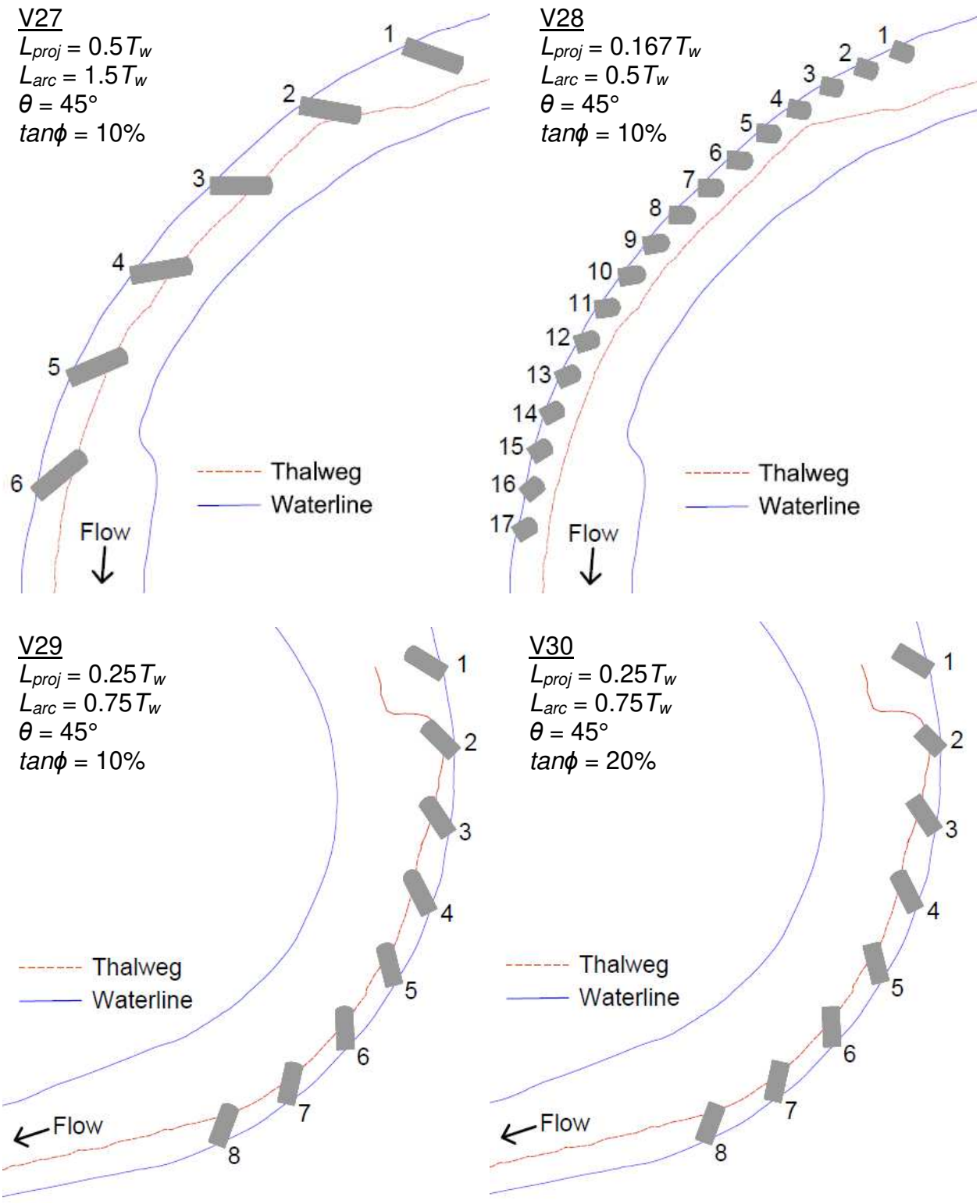

Figure 28. Locations of rock vanes in configurations V27-V30

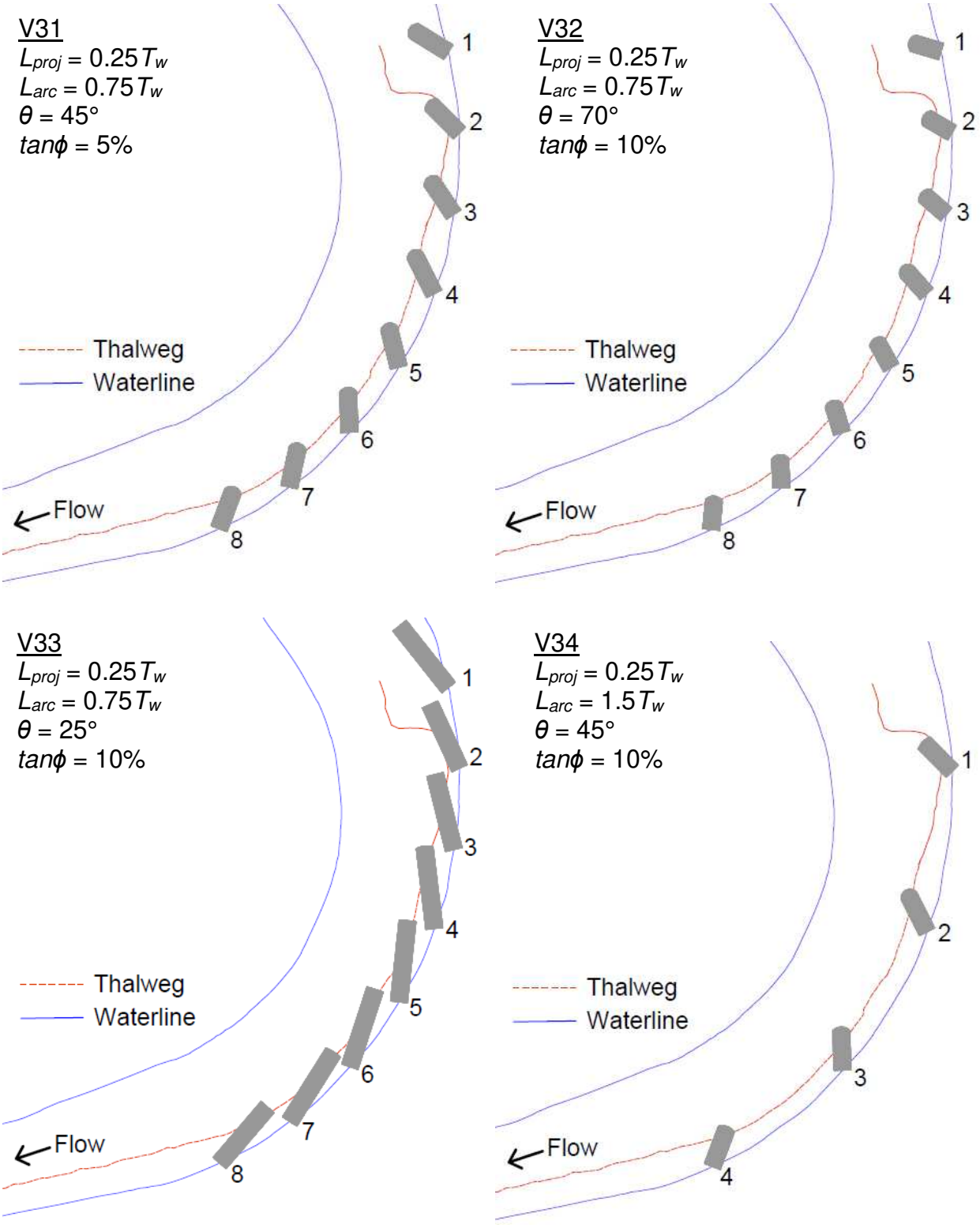

Figure 29. Locations of rock vanes in configurations V31-V34

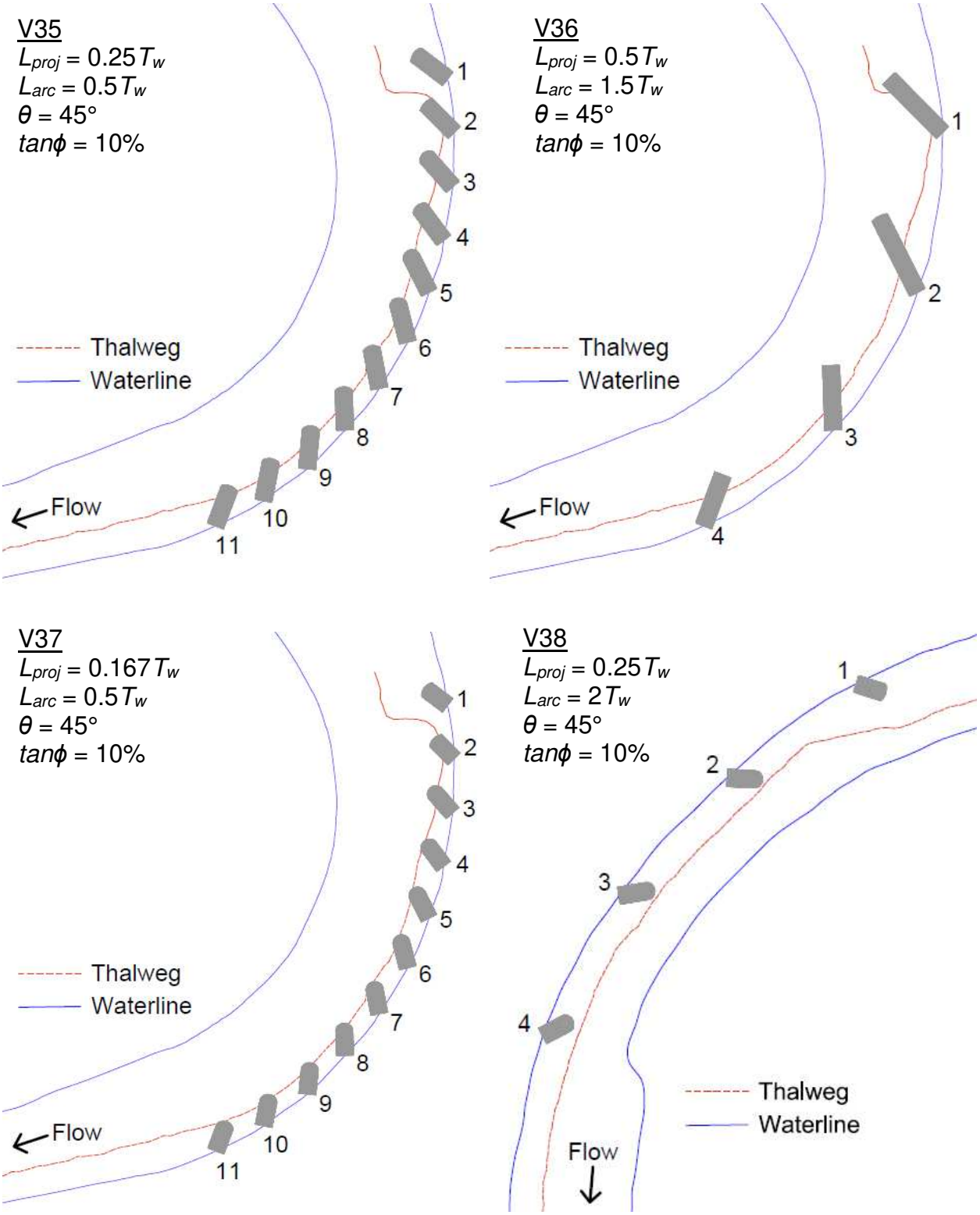

Figure 30. Locations of rock vanes in configurations V35-V38

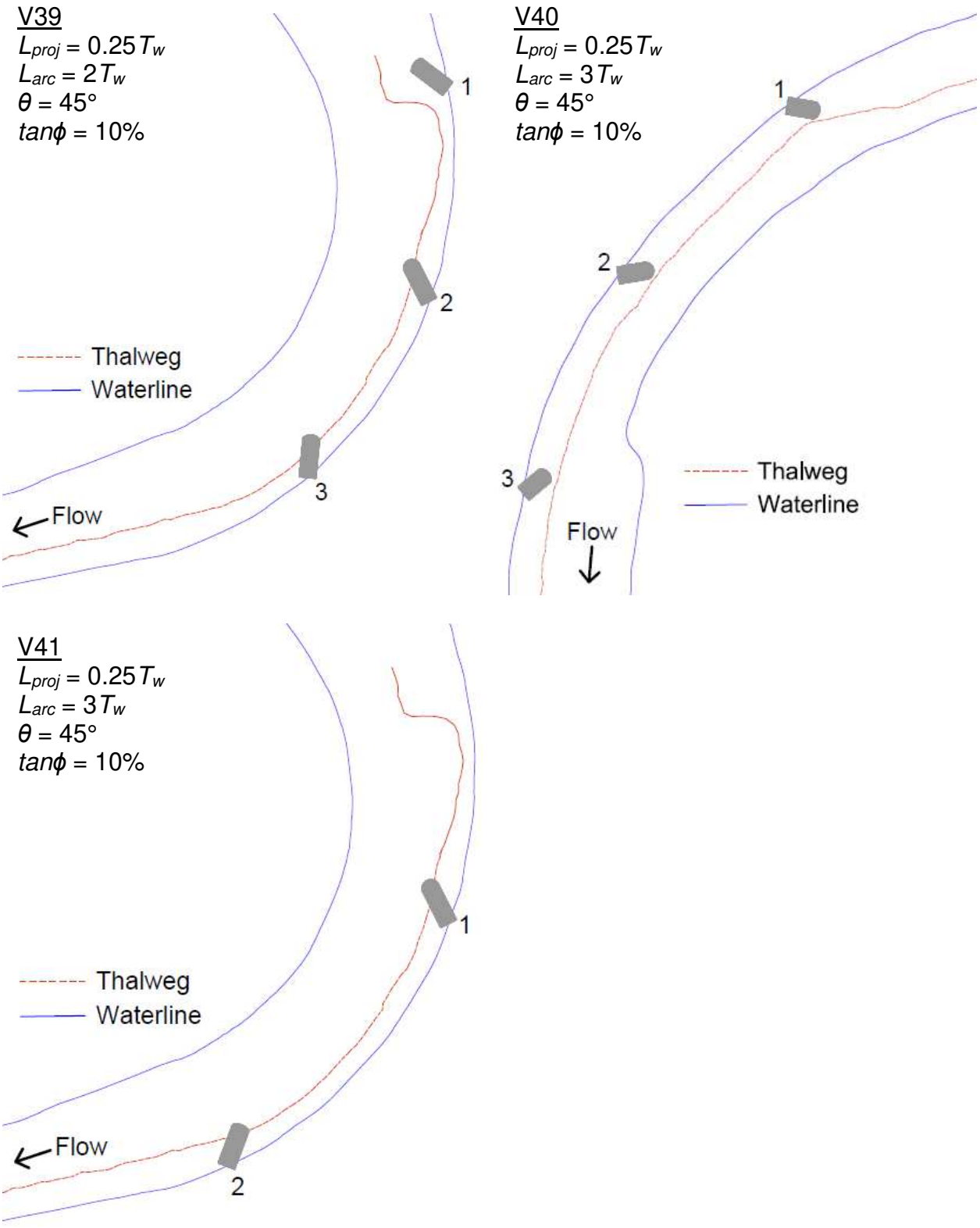

Figure 31. Locations of rock vanes in configurations V39-V41

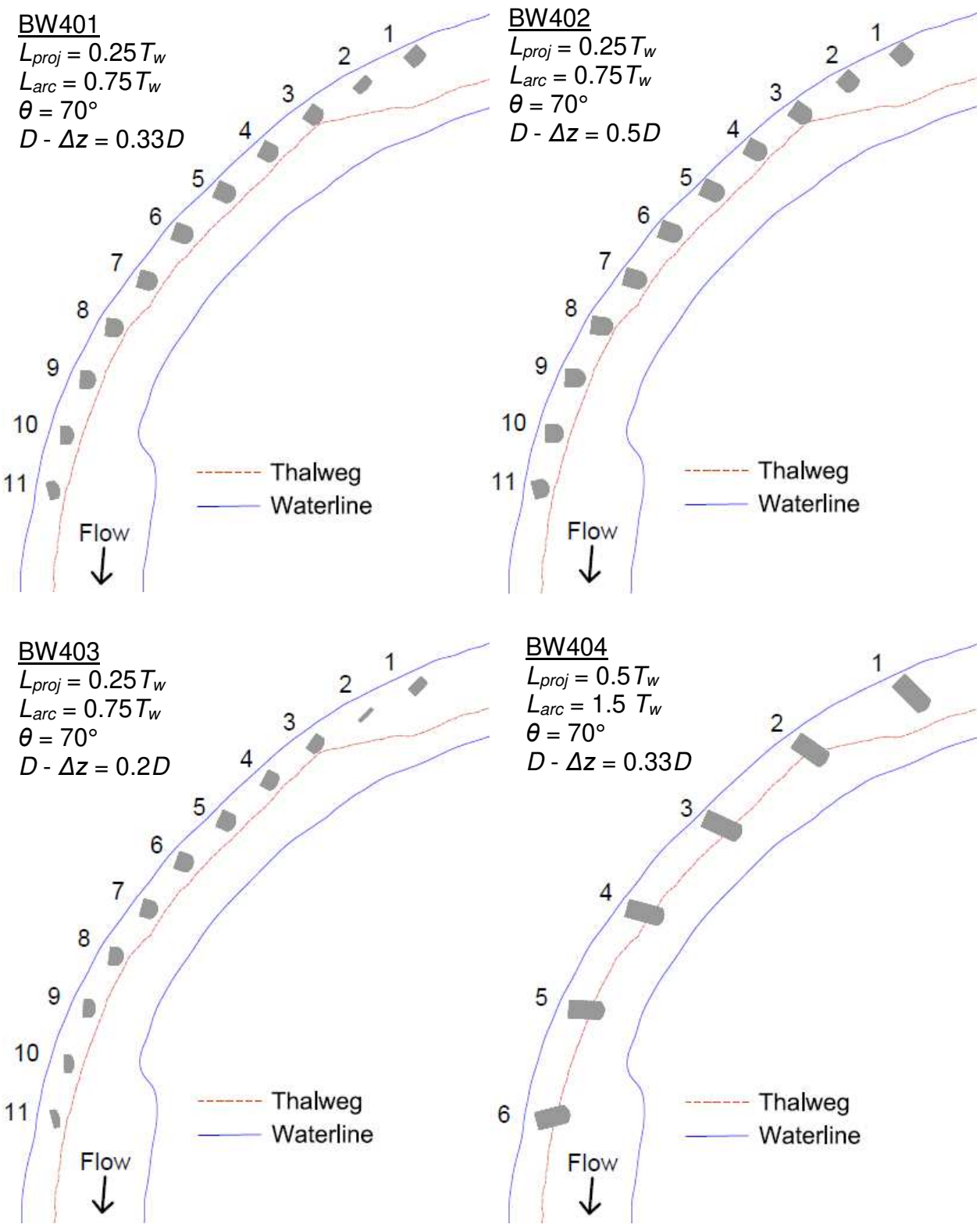

Figure 32. Locations of bendway weirs in configurations BW401-BW404

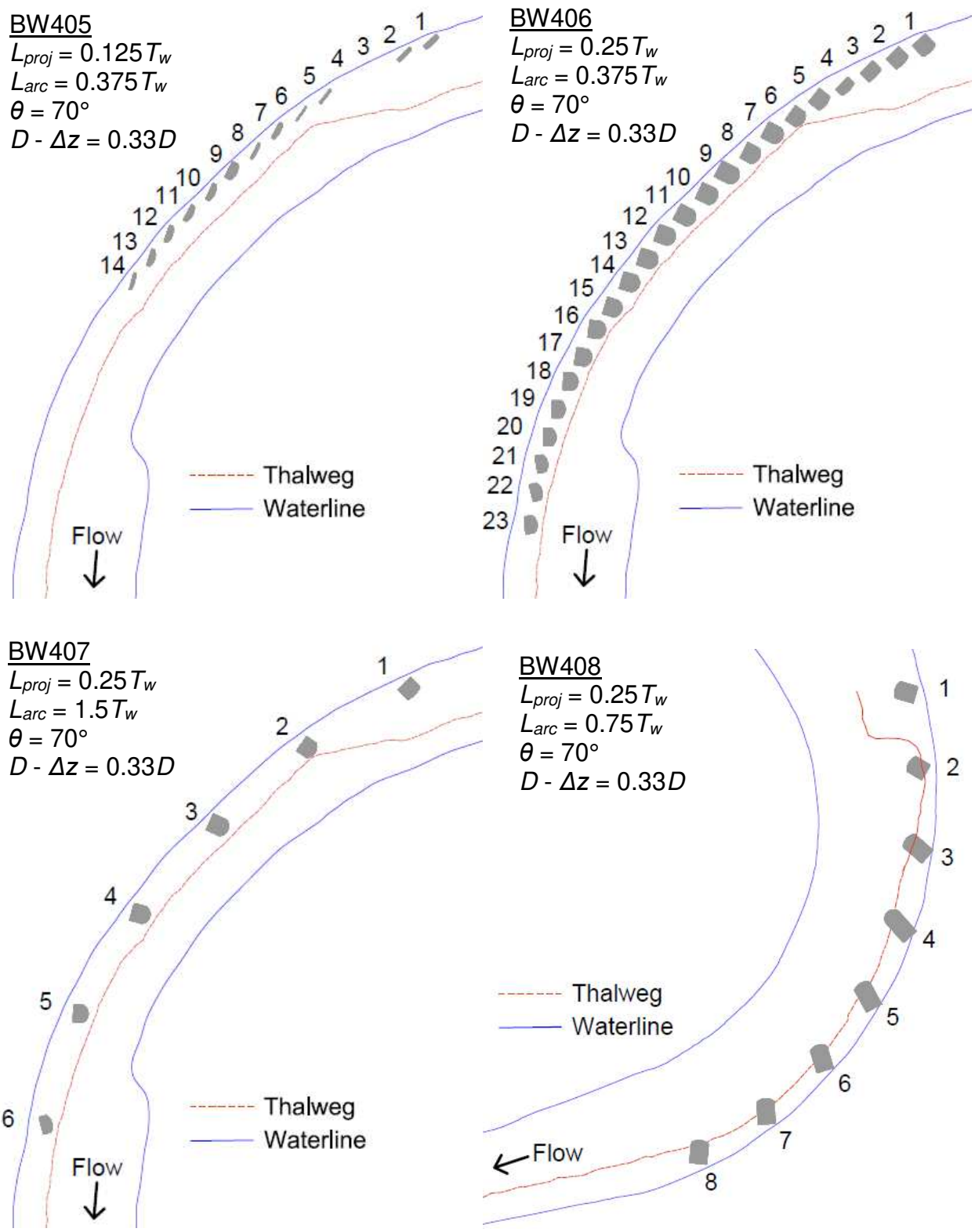

Figure 33. Locations of bendway weirs in configurations BW405-BW408

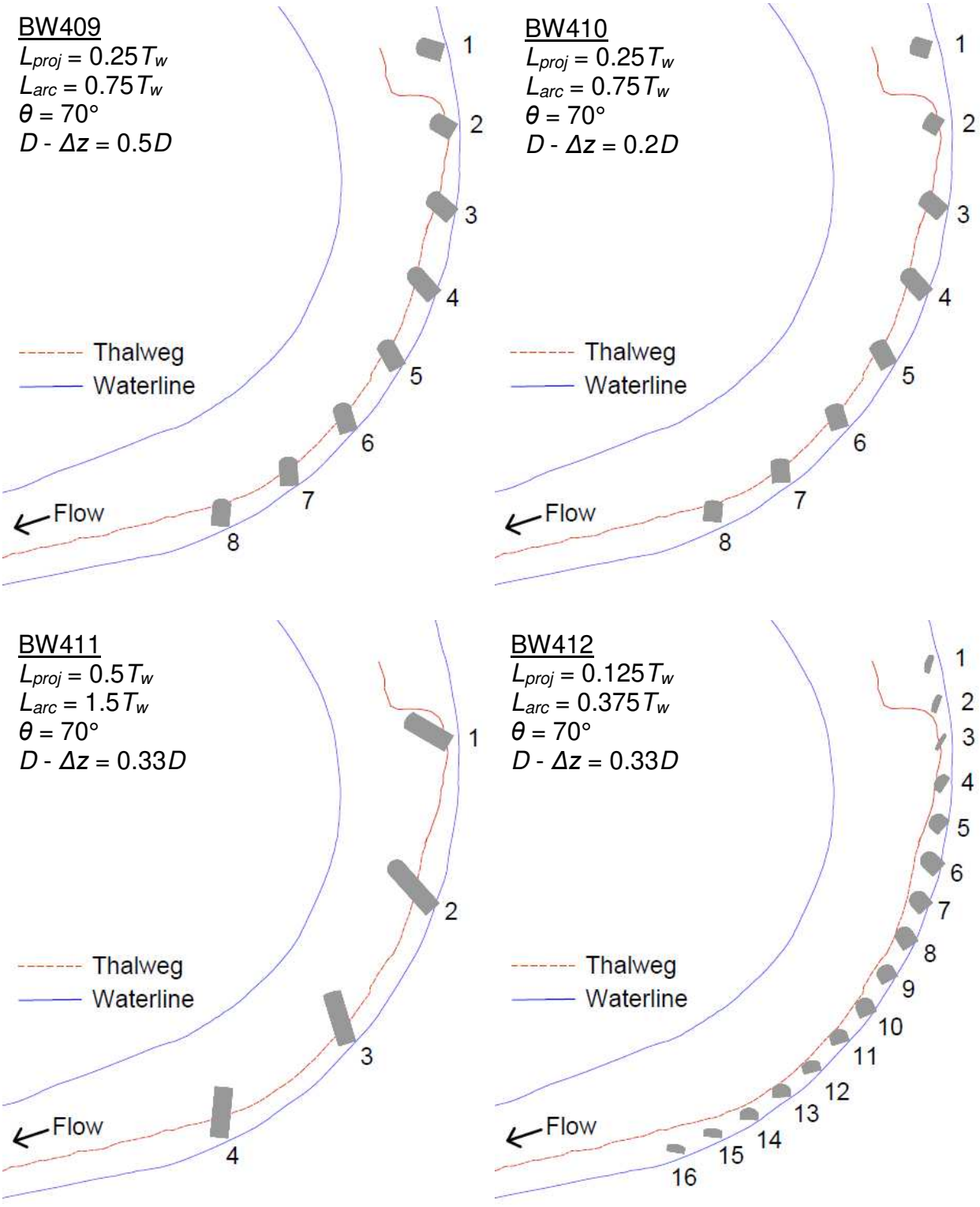

Figure 34. Locations of bendway weirs in configurations BW409-BW412

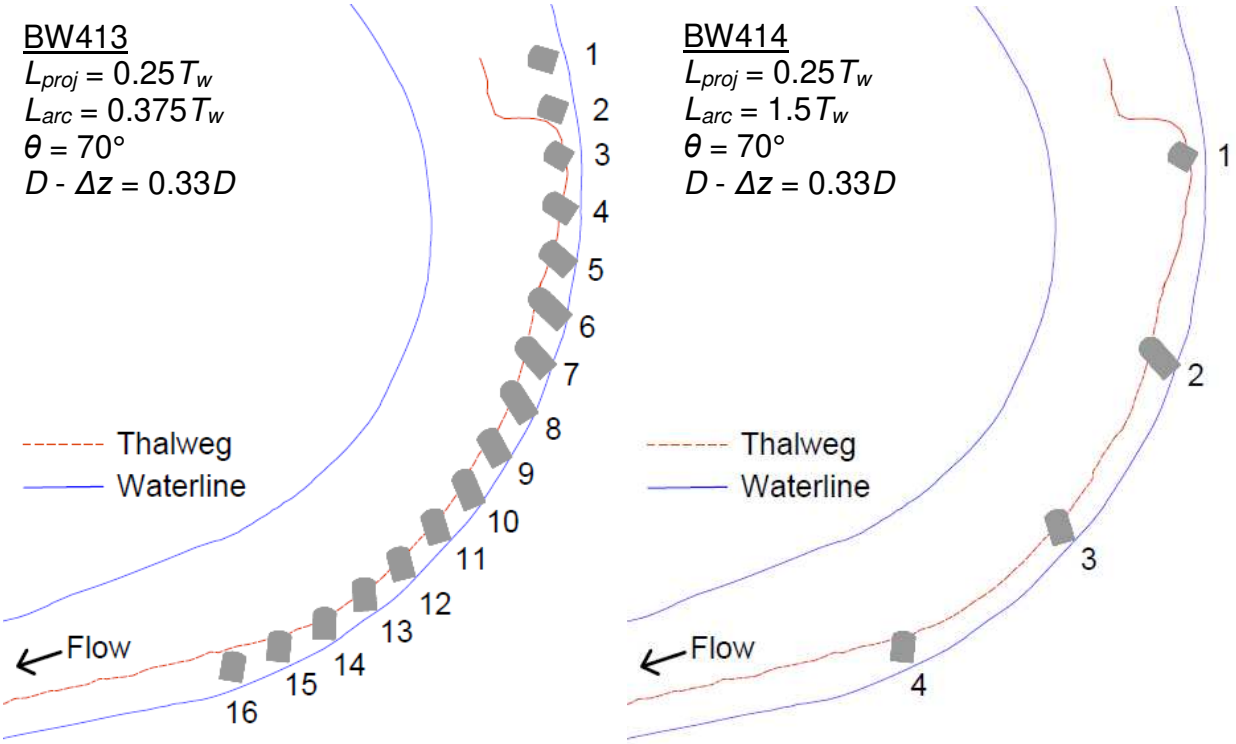

Figure 35. Locations of bendway weirs in configurations BW413 and BW414

CHAPTER 7. RESULTS AND ANALYSIS

Following completion of each numerical model run, the several gigabytes of data from the model were processed to extract the relevant information from each run. In addition to data from the 31 rock vane configurations and 14 bendway weir configurations described in Chapter 6, data from the calibration (V01) and validation (V07) configurations were used in analysis.

To evaluate the effectiveness of the various configurations in protecting the channel bank from erosion, the Average Velocity Ratio along the outer bank (AVR_o) was computed to quantify the reduction of velocity along the outer bank of a bend. Additionally, the Maximum Velocity Ratio at the tip of the structures (MVR_{tip}) was computed to quantify the increase in velocity at the structure tip and the resulting force on the structures. For bendway weirs only, the Maximum Velocity Ratio at the structure root (MVR_{root}) was evaluated to quantify the acceleration of flow around the root of the structure. Combined with images visualizing the flow field, the velocity ratios provide a straightforward method of evaluating the performance of the various configurations tested.

Figure 36 gives examples of depth-averaged velocity plots for the rock vane configuration V27 and bendway weir configuration BW404. Appendix C present plots of steady state depth-averaged velocity for all of the tested configurations.

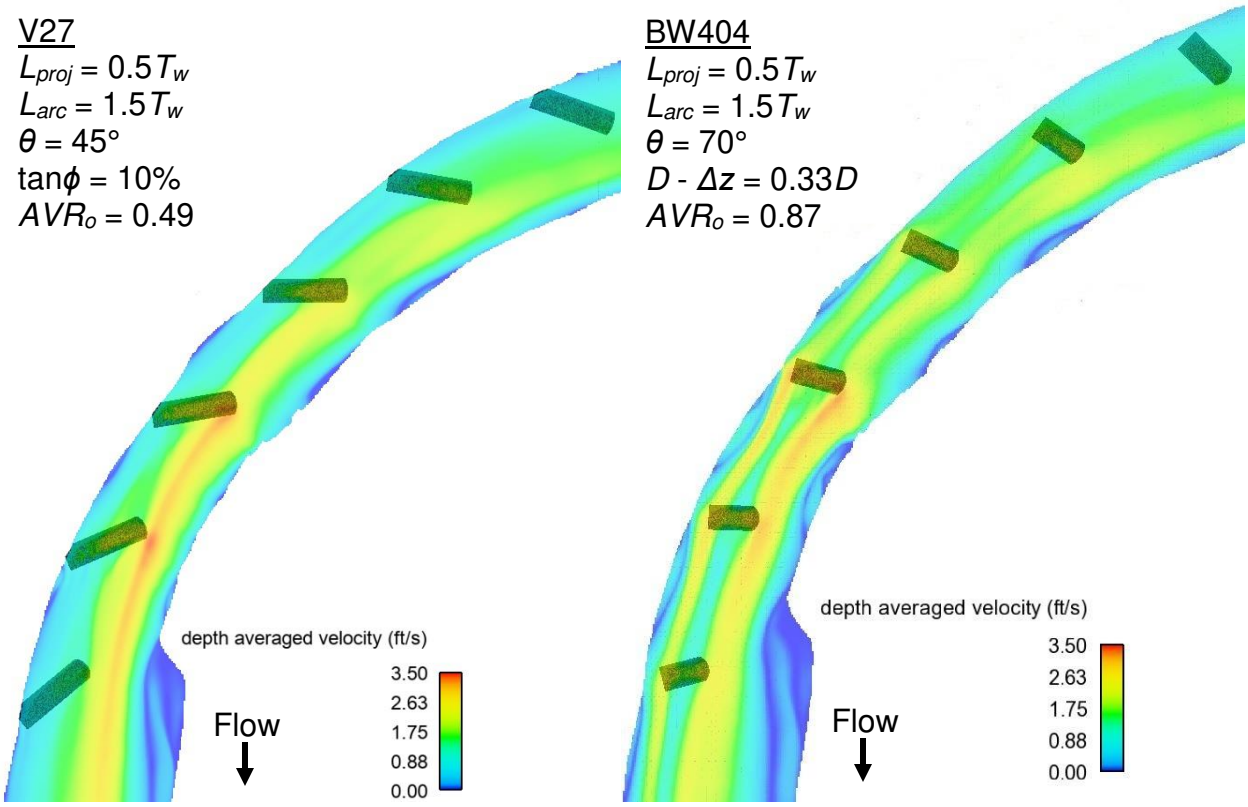

Figure 36. Steady state depth-averaged velocity for rock vane configuration V27 and bendway weir configuration BW404

Average Velocity Ratio

Velocity ratios have been used in previous studies of bendway weirs and rock vanes (e.g., Heintz 2002, Schmidt 2005, Scurlock et al. 2014b) to quantify the performance of different structure configurations. For the purpose of this study, the only average velocity ratio considered is the ratio given as Equation 11:

$$AVR_o = \frac{V_{o-structures}}{V_{baseline}} \quad (11)$$

Where:

AVR_o = Average Velocity Ratio along the outer bank

$V_{o\text{-}structures}$ = Average velocity along the outer bank of the bend after the installation of structures

$V_{baseline}$ = Average velocity at the entrance of the bend before the installation of structures

The region for the measurement of $V_{o\text{-}structures}$ is the region between bendway weir or rock vane structures bounded by the baseline waterline and a line parallel to the waterline at a distance of $T_w/5$ out from the bank; Figure 37 shows the region. The measurement region excludes areas on top of rock vanes or bendway weirs because flow accelerates over the structures, increasing the velocity. As the riprap material of the structures should provide high resistance to erosion, the isolated locations of higher velocity on top of the structures should not contribute to erosion of the outer bank.

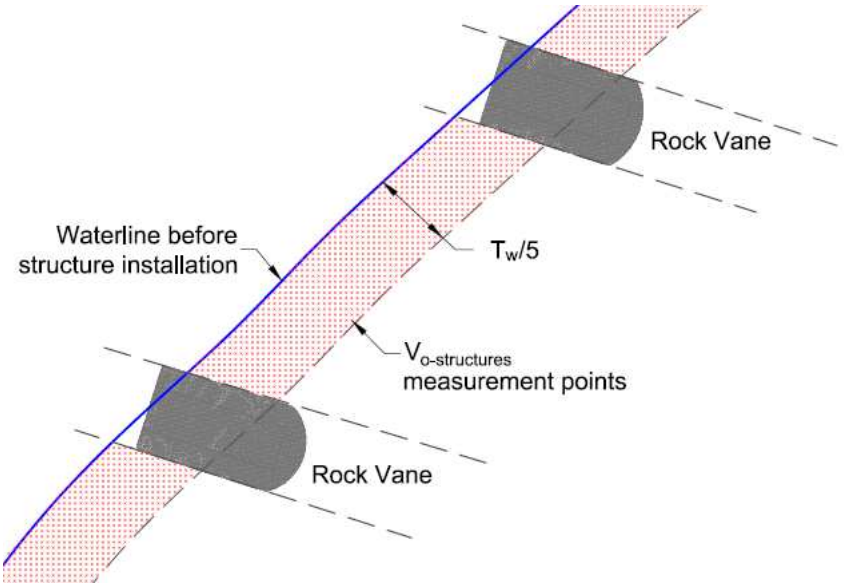

Figure 37. Measurement region for velocity along the outer bank after the installation of structures ($V_{o\text{-}structure}$)

The upstream and downstream extent of measurement for $V_{o\text{-}structures}$ should encompass the central portion of the bend. For this study, $V_{o\text{-}structures}$ was computed between physical model cross-sections 3 and 8 in the upstream bend and cross-sections 11 and 16 in the downstream bend, as illustrated in Figure 38 and Figure 39. For each configuration, $V_{o\text{-}structures}$ was computed as the average depth-averaged velocity of all of the grid cells in the measurement region, excluding the cells located on top of structures.

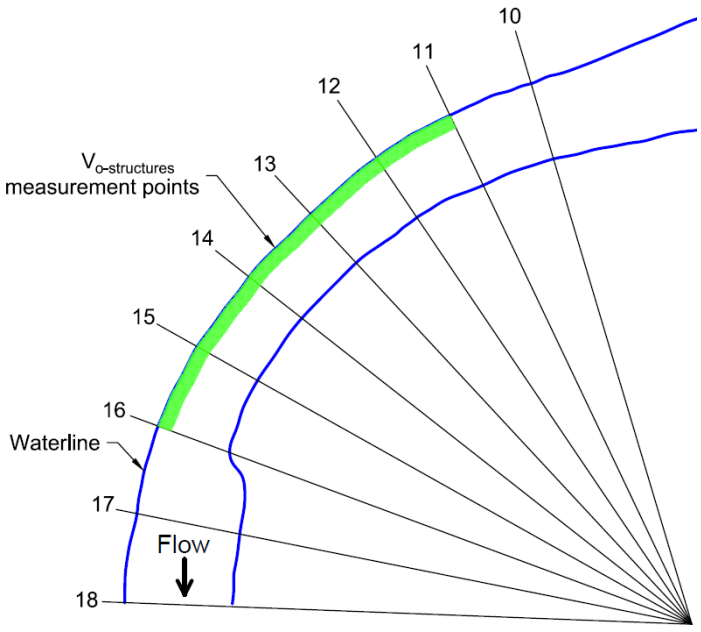

Figure 38. The region (green) containing points used to measure $V_{o\text{-}structures}$ in the downstream bend

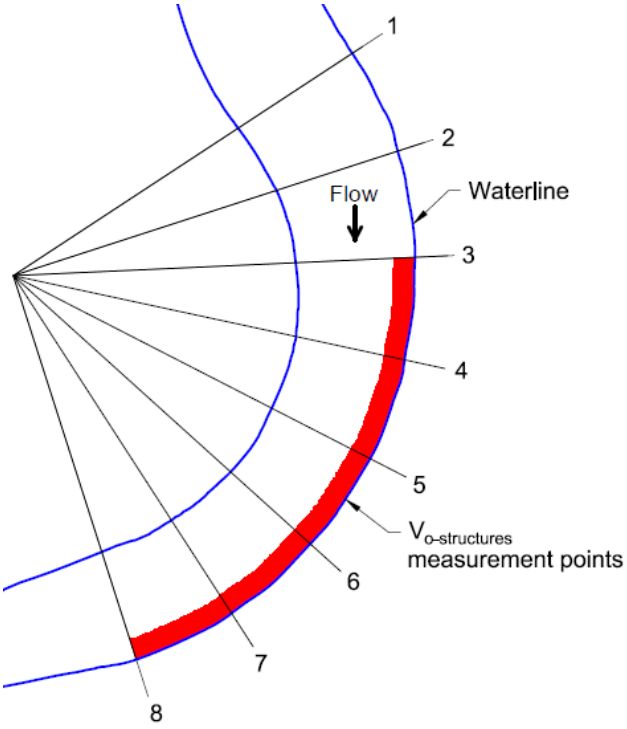

Figure 39. The region (red) containing points used to measure $V_{o\text{-}structures}$ in the upstream bend

The average velocity at the entrance to each bend before the installation of structures ($V_{baseline}$) is defined herein as the volumetric flow rate (Q) divided by the cross-sectional area of flow at the entrance of the bend ($A_{entrance}$):

$$V_{baseline} = \frac{Q}{A_{entrance}} \tag{12}$$

For the downstream bend, the flow area at the bend entrance was taken at cross-section 11 and determined to be 7.55 ft^2, based on the report of Scurlock et al. (2014b). In the upstream bend, entrance flow area was evaluated at cross-section 3, where the flow area was computed to be 7.71 ft^2 (Table 14). Using the model flow rate of 11.25 ft^3/s, the baseline velocity was computed to be 1.49 ft/s for the downstream bend and 1.46 ft/s for the upstream bend.

It is important to note that, because the points used to compute $V_{o\text{-}structures}$ are confined to a region near the outer bank, AVR_o may be less than one even if there are no structures present. Such is the case for both bends in this study. For the upstream bend, the average velocity along the outer bank without any structures installed ($V_{o\text{-}baseline}$) is 1.12 ft/s. The resulting velocity ratio is $AVR_o = V_{o\text{-}baseline} / V_{baseline} = 0.77$ with no structures installed in the upstream bend. Likewise, in the downstream bend, the average velocity along the outer bank without any structures installed is $V_{o\text{-}baseline} = 1.31$ ft/s, resulting in $AVR_o = 0.88$. Appendix D provides values for an alternative analysis method computing the outer bank velocity ratio as $V_{o\text{-}structures} / V_{o\text{-}baseline}$, resulting in velocity ratios of 1.0 without structures installed.

Because the computed AVR_o value is less than one in each bend without any structures present, care is needed when interpreting the results of the velocity ratio analysis. If the AVR_o value of a configuration is greater than 0.77 in the upstream bend or 0.88 in the downstream bend, the configuration has no effect in reducing velocity along the outer bank. Table 19 summarizes the average velocity ratio values determined for the rock vane configurations.

Table 19. Average Velocity Ratio analysis for the rock vane configurations

Configuration	Outer-bank Velocity (ft/s) $V_{o\text{-}structures}$	Bend Entrance Velocity $V_{baseline}$	Average Velocity Ratio AVR_o	Bend
V01	0.56	1.49	0.38	DS
V07	0.90	1.49	0.61	DS
V11	0.52	1.49	0.35	DS
V12	0.73	1.49	0.49	DS
V13	0.66	1.49	0.44	DS
V14	0.85	1.49	0.57	DS
V15	0.51	1.49	0.34	DS
V16	0.74	1.49	0.50	DS
V17	0.35	1.46	0.24	US
V18	0.51	1.46	0.35	US
V19	0.36	1.46	0.24	US
V20	0.46	1.49	0.31	DS
V21	0.70	1.49	0.47	DS
V22	0.41	1.49	0.27	DS
V23	0.52	1.49	0.35	DS
V24	0.65	1.49	0.43	DS
V25	0.58	1.49	0.39	DS
V26	0.47	1.49	0.32	DS
V27	0.73	1.49	0.49	DS
V28	0.42	1.49	0.28	DS
V29	0.47	1.46	0.32	US
V30	0.61	1.46	0.42	US
V31	0.35	1.46	0.24	US
V32	0.39	1.46	0.27	US
V33	0.68	1.46	0.47	US
V34	0.54	1.46	0.37	US
V35	0.32	1.46	0.22	US
V36	0.53	1.46	0.36	US
V37	0.37	1.46	0.25	US
V38	0.62	1.49	0.42	DS
V39	0.53	1.46	0.43	US
V40	0.85	1.49	0.57	DS
V41	0.65	1.46	0.45	US
Maximum	-	-	0.61	-
Minimum	-	-	0.22	-
Average	-	-	0.38	-

The AVR_o results for the bendway weir tests are summarized in Table 20. The values of AVR_o have very little variation between configurations in the downstream bend, ranging from 0.74 to 0.87. In fact, only one bendway weir configuration in the downstream bend has an AVR_o outside the range of 0.84–0.87. The variation in the upstream bend is somewhat larger, ranging from 0.44 to 0.65.

Table 20. Average Velocity Ratios for the bendway weir configurations

Configuration	Outer-bank Velocity (ft/s) $V_{o\text{-}structures}$	Bend Entrance Velocity $V_{baseline}$	Average Velocity Ratio AVR_o	Bend
BW401	1.28	1.49	0.86	DS
BW402	1.10	1.49	0.74	DS
BW403	1.29	1.49	0.87	DS
BW404	1.29	1.49	0.87	DS
BW405	1.28	1.49	0.86	DS
BW406	1.27	1.49	0.85	DS
BW407	1.25	1.49	0.84	DS
BW408	0.84	1.46	0.58	US
BW409	0.70	1.46	0.48	US
BW410	0.95	1.46	0.65	US
BW411	0.80	1.46	0.55	US
BW412	0.83	1.46	0.57	US
BW413	0.64	1.46	0.44	US
BW414	0.89	1.46	0.61	US
Maximum	-	-	0.87	-
Minimum	-	-	0.44	-
Average	-	-	0.70	-

Maximum Tip Velocity

Rock vanes and bendway weirs must be designed to withstand the hydraulic forces produced by the flow of water around the structures. To estimate these forces, it is desirable to estimate the maximum velocity a structure will experience. The maximum velocity ratio at the structure tip (MVR_{tip}) provides such an estimate. Defined in Equation 13, MVR_{tip} is the ratio of

the maximum velocity near the tip of any structure in a given configuration to the average velocity at the entrance of the bend before structures were installed:

$$MVR_{tip} = \frac{V_{tip-max}}{V_{baseline}} \quad (13)$$

Where:

MVR_{tip} = Maximum Velocity Ratio at the structure tip

$V_{tip\text{-}max}$ = Maximum depth-averaged velocity near the tip of a rock vane or bendway weir in a given configuration

$V_{baseline}$ = Average velocity at the entrance of the bend before the installation of structures

Because MVR_{tip} is computed using the maximum tip velocity of any structure in a configuration, it gives a mildly conservative measure of the velocity experienced by the other structures in a configuration. Such conservatism is desirable for purposes of designing for structural stability and is a more meaningful design value than the average velocity at the tip of all structures in a configuration.

MVR_{tip} was evaluated for each configuration of rock vanes and bendway weirs tested. The maximum velocity at the tip of each structure was determined by examining the depth-averaged velocity at all grid cells near the tip of a structure to locate the greatest value. “Near the tip” is defined as any mesh cell containing a portion of the sloped tip of a rock vane or bendway weir. Figure 40 illustrates the cells located in the tip region of a bendway weir.

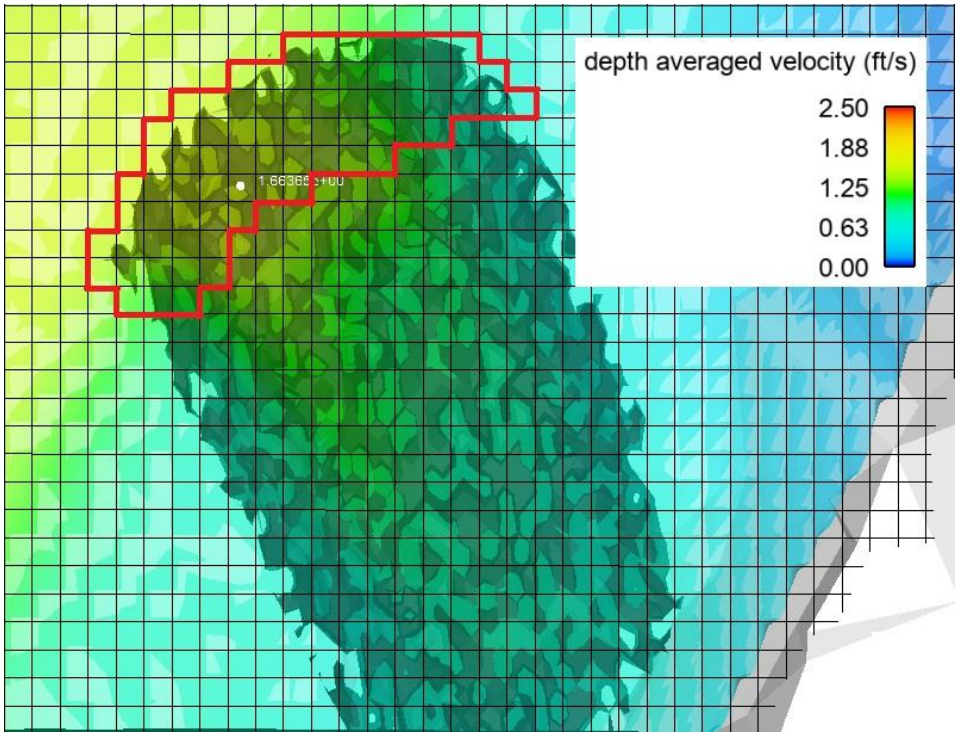

Figure 40. Bendway Weir 5 from configuration BW409 with mesh cells in the tip region outlined in red

Table 21 lists the measured MVR_{tip} values for the rock vane configurations while Table 22 lists the values for the bendway weir configurations. MVR_{tip} was not computed for bendway weir configuration BW405, as the structures in that configuration consisted of little more than a few rocks protruding from the streambed and were too short to have a clearly defined tip region.

Table 21. Maximum Tip Velocity Ratios for rock vane configurations

Configuration	Maximum Tip Velocity (ft/s) $V_{tip\text{-}max}$	Bend Entrance Velocity $V_{baseline}$	Maximum Tip Velocity Ratio MVR_{tip}	Bend
V01	2.55	1.49	1.71	DS
V07	3.02	1.49	2.03	DS
V11	2.82	1.49	1.89	DS
V12	3.01	1.49	2.02	DS
V13	2.52	1.49	1.69	DS
V14	2.38	1.49	1.60	DS
V15	2.77	1.49	1.86	DS
V16	2.79	1.49	1.87	DS
V17	2.53	1.46	1.73	US
V18	1.77	1.46	1.21	US
V19	2.21	1.46	1.51	US
V20	2.95	1.49	1.98	DS
V21	2.85	1.49	1.91	DS
V22	2.95	1.49	1.98	DS
V23	3.01	1.49	2.02	DS
V24	2.81	1.49	1.89	DS
V25	2.96	1.49	1.99	DS
V26	2.98	1.49	2.00	DS
V27	3.33	1.49	2.23	DS
V28	2.50	1.49	1.68	DS
V29	1.98	1.46	1.36	US
V30	1.81	1.46	1.24	US
V31	2.13	1.46	1.46	US
V32	2.29	1.46	1.57	US
V33	1.67	1.46	1.14	US
V34	1.97	1.46	1.35	US
V35	2.47	1.46	1.69	US
V36	2.19	1.46	1.50	US
V37	2.16	1.46	1.48	US
V38	2.94	1.49	1.97	DS
V39	1.80	1.46	1.23	US
V40	3.35	1.49	2.25	DS
V41	2.20	1.46	1.51	US
Maximum	-	-	2.25	-
Minimum	-	-	1.14	-
Average	-	-	1.71	-

Table 22. Maximum Tip Velocity Ratios for bendway weir configurations

Configuration	Maximum Tip Velocity (ft/s) $V_{tip\text{-}max}$	Bend Entrance Velocity $V_{baseline}$	Maximum Tip Velocity Ratio MVR_{tip}	Bend
BW401	2.64	1.48	1.77	DS
BW402	2.73	1.48	1.83	DS
BW403	2.59	1.49	1.74	DS
BW404	3.26	1.49	2.19	DS
BW405	-	1.49	-	DS
BW406	2.55	1.49	1.71	DS
BW407	2.69	1.49	1.81	DS
BW408	1.86	1.46	1.27	US
BW409	2.01	1.46	1.38	US
BW410	1.77	1.46	1.21	US
BW411	2.05	1.46	1.40	US
BW412	1.86	1.46	1.27	US
BW413	2.04	1.46	1.40	US
BW414	1.96	1.46	1.34	US
Maximum	-	-	2.19	-
Minimum	-	-	1.21	-
Average	-	-	1.56	-

The MVR_{tip} data are visualized in the box-and-whisker plot presented as Figure 41. The box-and-whisker plot allows the variation of the data to be visualized, with the ends of the box representing the upper and lower quartiles and the lines (whiskers) extending from the box representing the range of observations, excluding outliers. The line through the box indicates the median and the "x" symbol indicates the mean.

It is apparent that structures in the upstream bend tend to have lower values of MVR_{tip} than those in the downstream bend. Every bendway weir in the upstream bend has an MVR_{tip} value less than the lowest MVR_{tip} for a bendway weir in the upstream bend. For rock vanes, all but two configurations in the upstream bend have an MVR_{tip} value less than the lowest MVR_{tip} in the downstream bend.

The results indicate the maximum velocity at the tip of a structure depends on not only the structure geometry, but also on the properties of the bend in which it is installed. The upstream bend has an average flow area of 9.0 ft^2 in the baseline condition, compared with 6.9 ft^2 for the downstream bend. For a flow rate of 11.25 ft^3/s, the average velocity will be 1.25 ft/s along the length of the upstream bend and 1.63 ft/s along the downstream bend. Figure 42 illustrates the difference in baseline flow velocity between the two bends.

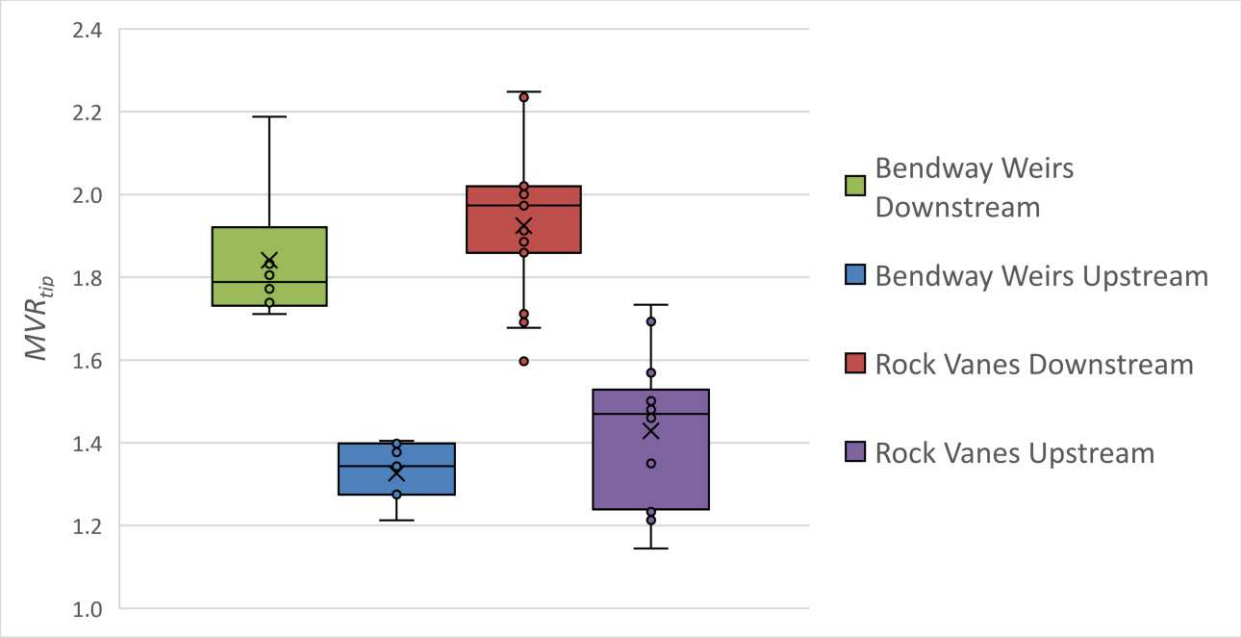

Figure 41. Box-and-whisker plot of MVR_{tip} values for bendway weirs and rock vanes

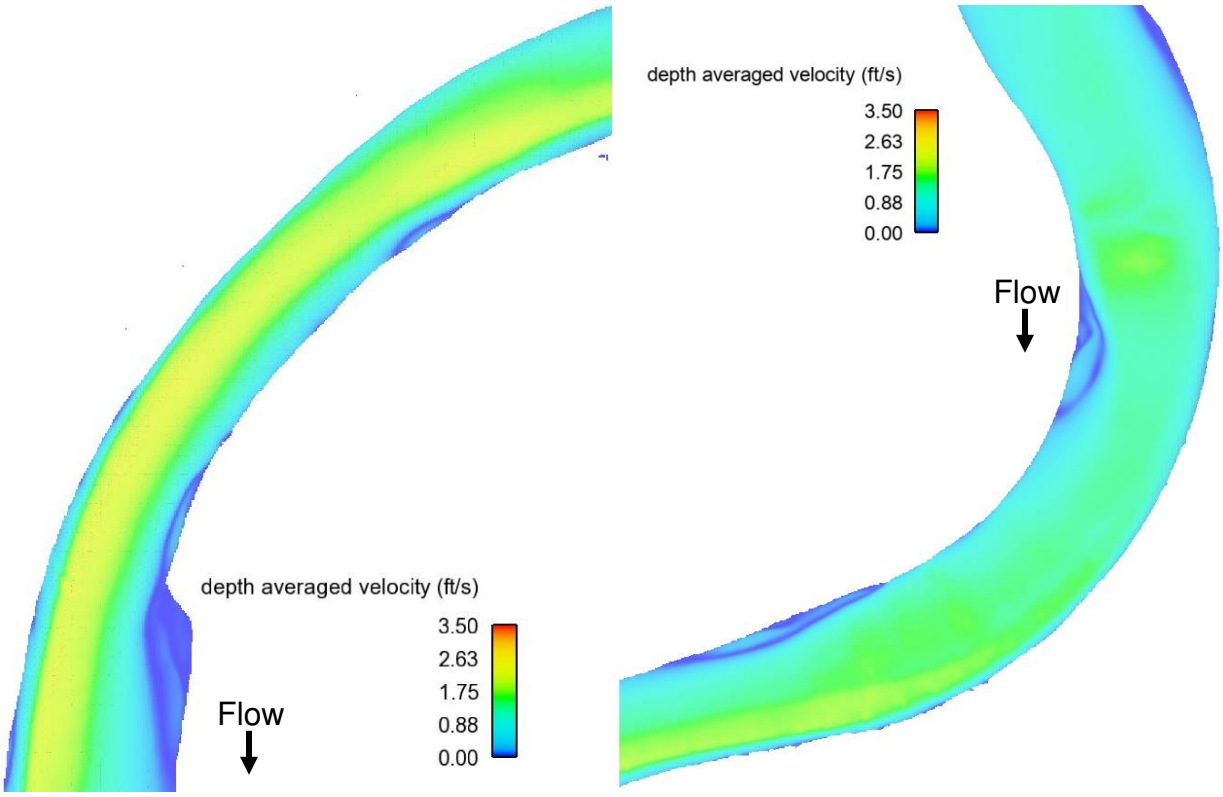

Figure 42. Depth-averaged velocity without structures installed for the downstream bend (left) and the upstream bend (right)

While the downstream bend has a greater average velocity along the length of the bend, the flow velocity at the entrance of each bend is nearly the same (1.49 ft/s in the downstream bend versus 1.46 ft/s in the upstream bend). As a result, the values of MVR_{tip}, which normalize maximum tip velocity to entrance velocity, are almost always greater in the downstream bend. This result underscores the importance of considering the geometry and entrance velocity of a bend in addition to the geometry of the structures when designing a rock vane or bendway weir installation.

Maximum Root Velocity

For bendway weirs, an additional design consideration is the velocity of flow at the root of the structure. Flow tends to accelerate around the root, resulting in higher velocities directly

adjacent to the bank. It is important to quantify the increase in velocity so that appropriate counter-measures can be taken to protect the bank. The maximum velocity ratio at the structure root (MVR_{root}) is the ratio of the maximum velocity near the root of any structure in a given configuration to the velocity at the entrance of the bend before structures were installed, given as Equation 14:

$$MVR_{tip} = \frac{V_{root-max}}{V_{baseline}} \quad (14)$$

Where:

MVR_{root} = Maximum Velocity Ratio at the structure root

$V_{root\text{-}max}$ = Maximum depth-averaged velocity near the root of a bendway weir in a given configuration

$V_{baseline}$ = Average velocity at the entrance of the bend before the installation of structures

Flow acceleration around the root of a structure is only a concern for bendway weirs. Rock vanes intersect the bank at the design water-surface elevation, preventing flow from passing around the root of the structure at the design flow. Therefore, MVR_{root} was only computed for bendway weirs, not rock vanes.

The maximum velocity at the root of each bendway weir was determined by examining the depth-averaged velocity at all grid cells near the root of a structure to locate the greatest value. “Near the root” is defined as any mesh cell containing a portion of a bendway weir at its intersection with the bank. Table 23 presents computed MVR_{root} values for the bendway weir configurations tested. MVR_{root} was not computed for configuration BW405, as the structures in that configuration were too short to have a well-defined root.

Table 23. Maximum Root Velocity Ratios for bendway weir configurations

Configuration	Maximum Root Velocity (ft/s) $V_{root\text{-}max}$	Bend Entrance Velocity $V_{baseline}$	Maximum Root Velocity Ratio MVR_{root}	Bend
BW401	2.40	1.48	1.61	DS
BW402	2.26	1.48	1.52	DS
BW403	2.37	1.48	1.59	DS
BW404	3.20	1.48	2.15	DS
BW405	-	1.48	-	DS
BW406	2.35	1.48	1.58	DS
BW407	2.39	1.48	1.60	DS
BW408	1.80	1.17	1.23	US
BW409	1.67	1.17	1.14	US
BW410	1.89	1.17	1.30	US
BW411	1.61	1.17	1.10	US
BW412	1.66	1.17	1.14	US
BW413	1.59	1.17	1.09	US
BW414	1.90	1.17	1.30	US
Maximum	-	-	2.15	-
Minimum	-	-	1.09	-
Average	-	-	1.41	-

Visualizing the MVR_{root} results on a box-and-whisker plot (Figure 43), MVR_{root} values are tightly grouped for each bend, except for the outlier in the downstream bend, BW404. The BW404 configuration has a projected length of $T_w/2$ and blocks 26% of the flow area, redirecting an unusually large portion of the flow between the bendway weir roots and the outer bank.

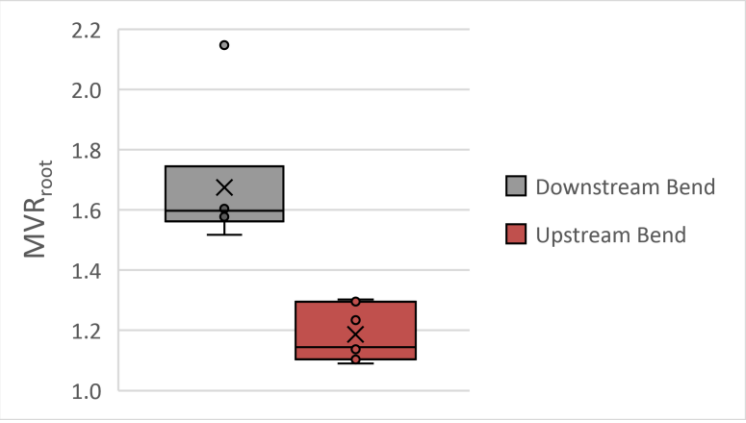

Figure 43. Box-and-whisker plot of MVR_{root} values for bendway weirs

Comparison of Rock Vane and Bendway Weir Performance

Examining the computed values of AVR_o, it is apparent that most bendway weir configurations did little to reduce velocity along the outer bank of each bend. In the downstream bend, the average velocity along the outer bank was 1.31 ft/s without structures installed. That the best bendway weir configuration in the downstream bend (BW402) only reduced the outer bank velocity to 1.10 ft/s ($AVR_o = 0.74$) indicates bendway weirs were largely ineffective at protecting the outer bank in the downstream bend.

The bendway weirs were more effective in the upstream bend, with all configurations having an AVR_o value less than 0.74, the lowest value in the downstream stream bend. While the bendway weirs did produce some appreciable velocity reductions in the upstream bend, they still had disappointing results compared to the rock vanes. The best performing bendway weir configuration (BW413) had an AVR_o of 0.44. However, all but two rock vane configurations in the upstream bend provided even greater velocity reductions.

The best explanation for the difference in velocity reduction of bendway weirs between the two bends is the difference in the bends' cross-sections. In the upstream bend, the thalweg is very close to the outer bank, while in the downstream bend it is closer to the center of the channel. As a result, bendway weirs in the upstream bend block a greater portion of the flow area than those in the downstream bend.

The best-performing bendway weir configuration in the downstream bend, BW402, blocked only 10% of the flow area. BW409, designed with the same geometric criteria in the upstream bend, blocked 18% of the flow area; nearly twice as much. Figure 44 shows bendway weir 3 in the BW402 configuration in the downstream bend. The channel thalweg is located away from the outer bank so that only the toe of the structure extends to the thalweg. In contrast,

Figure 45 shows bendway weir 3 in the BW409 configuration in the upstream bend. Because the thalweg of the upstream bend is very close to the outer bank, the crest of the bendway weir crosses the thalweg and blocks a much greater portion of the flow area.

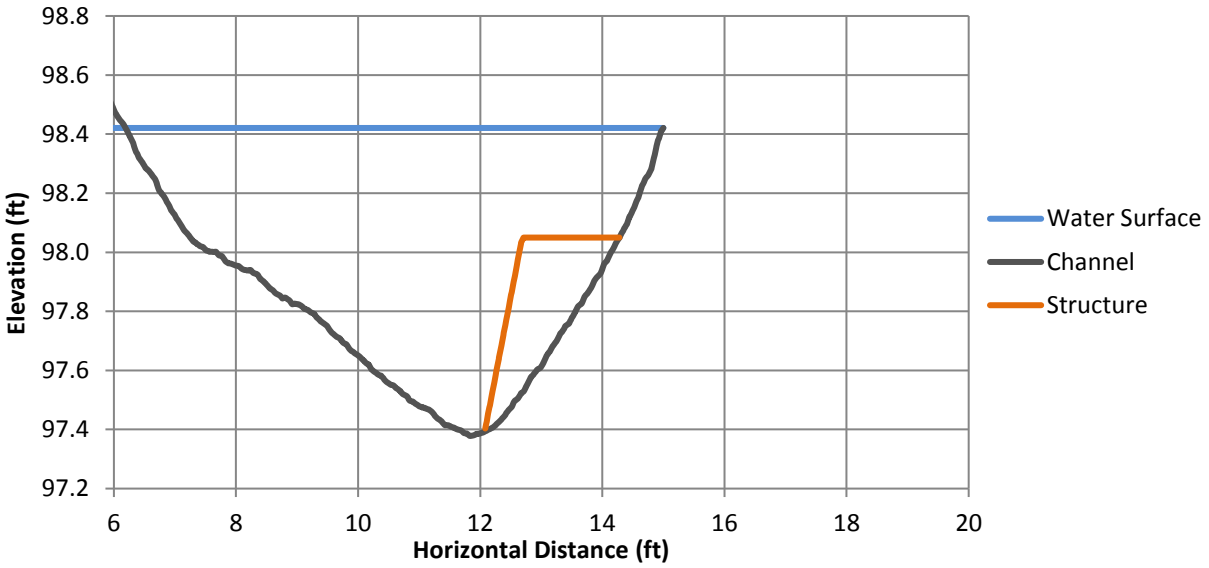

Figure 44. Weir 3 in the BW402 configuration in the downstream bend. Only the toe of the structure extends to the channel thalweg.

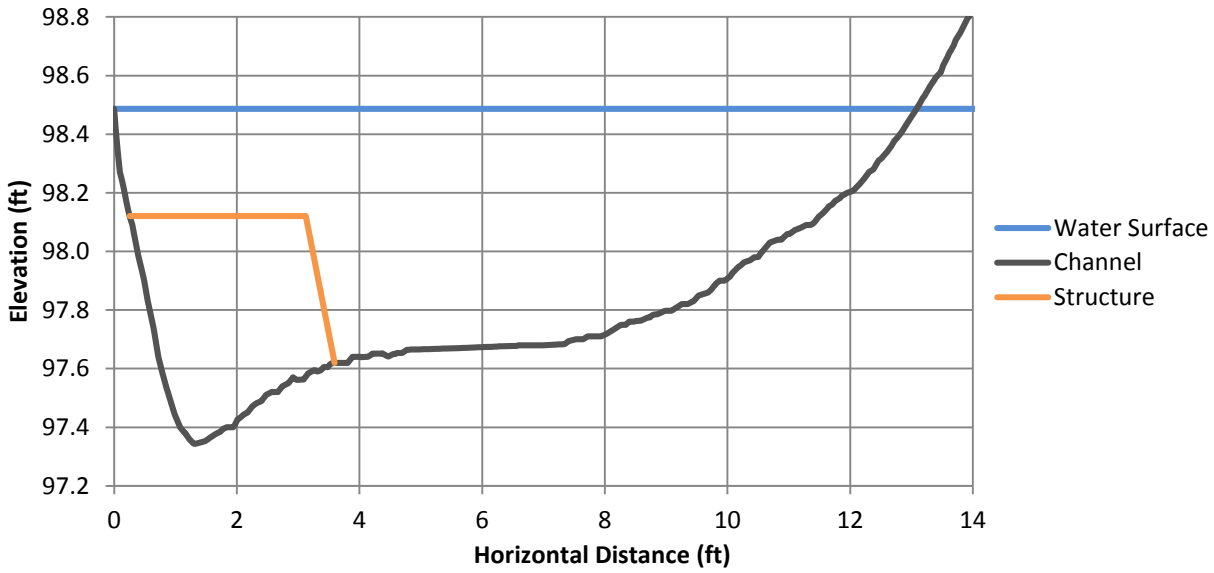

Figure 45. Weir 3 in the BW409 configuration in the upstream bend. The crest of the structure extends across the thalweg.

Differences in flow blockage also help explain the differences in outer bank velocities associated with the rock vane and bendway weir installations. Because bendway weirs do not extend to the waterline, they tend to produce a band of high-velocity flow between the root of the structure and the waterline. Configuration BW404 (Figure 36) vividly illustrates this phenomenon. The bendway weirs in BW404 redirect flow around both the structure tip and the structure root, resulting in a high-velocity region of flow along the outer bank with $AVR_o = 0.87$. In contrast, the V27 rock vane configuration, built with the same spacing and projected length, produced much lower velocity along the outer bank (Figure 36) with $AVR_o = 0.49$.

The streamlines around structures in each configuration show an important difference in the flow fields. Figure 46 illustrates streamlines around the fourth bendway weir in the BW404 configuration. Many streamlines pass between the root of the bendway weir and the bank or over the weir crest while relatively few streamlines are directed around the tip of the bendway weir. Flow velocity at the root of the structure exceeds 3 ft/s. Figure 47 illustrates a much different flow field around the fourth rock vane in the V27 configuration. Fewer streamlines pass over the crest of the rock vane whereas many streamlines are directed around the vane tip and the streamlines near the bank have velocities of only about 2 ft/s.

The difference in flow field between rock vanes and bendway weirs can be explained by their geometries. Bendway weirs are built with a horizontal crest, which is completely submerged at the design flow. The submerged crest allows a relatively large portion of the flow to pass over the crest of the bendway weir. In contrast, rock vanes have a sloped crest that extends up to the waterline elevation. As a result, rock vanes block more flow area near the waterline, helping to direct flow around the tip of the structure rather than over the crest. The

result is a lower unit discharge and lower velocity along the bank compared to a similarly designed bendway weir.

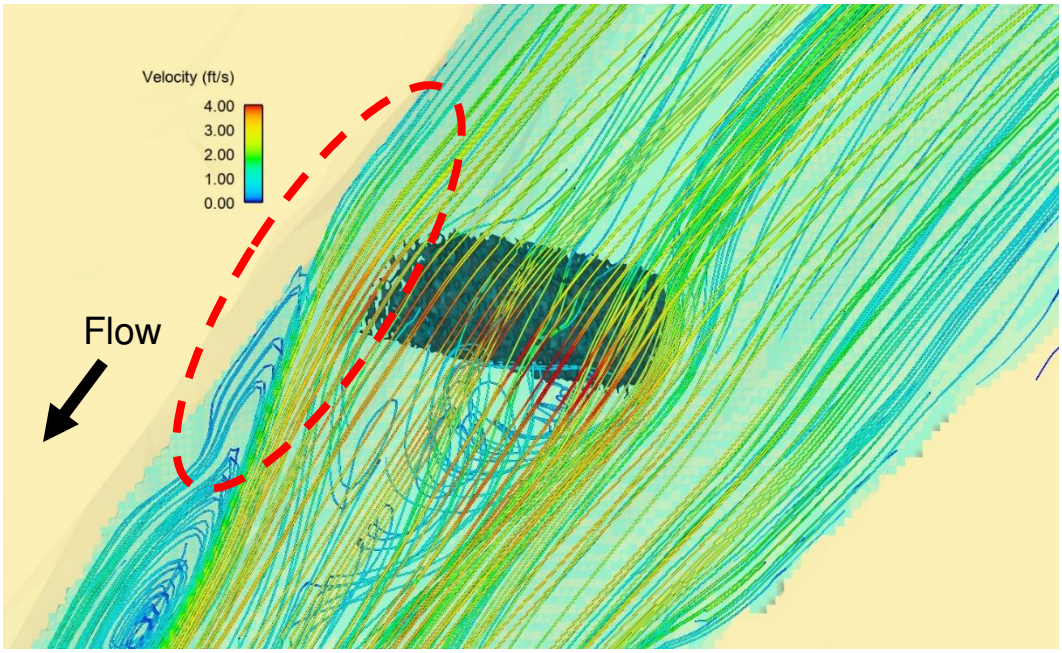

Figure 46. Streamlines around bendway weir 4 in the BW404 configuration. Note the closely spaced streamlines and >3ft/s velocity near the root of the structure.

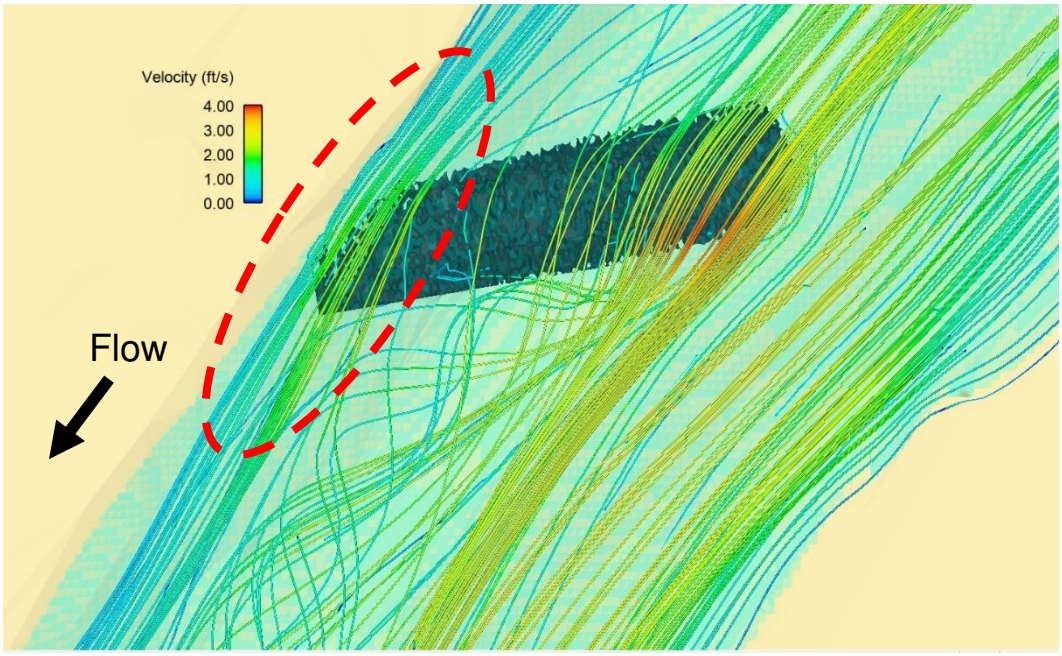

Figure 47. Rock Vane 4 in the V27 configuration. Note the very few streamlines near the bank compared to the many streamlines at the tip of the structure.

In summary, the geometric differences between bendway weirs and rock vanes result in different flow fields around the two types of structures and explain why rock vanes tend to produce lower velocities along the outer bank than bendway weirs. The next sections discuss the effects on the flow field of altering individual parameters of rock vane geometry. Because the results indicate bendway weirs are less effective than rock vanes at reducing flow velocity along the outer bank, a detailed analysis of their geometry will not be provided.

Effect of Rock Vane Planform Angle (θ)

The planform angle of rock vanes appears to play a relatively modest role in the velocity reduction along the outer bank. Configurations V20, V23, and V24 consist of rock vanes with the same projected length, spacing, and crest slope constructed at angles of 45°, 70°, and 25° in the downstream bend. Configurations V29, V32, and V33 do likewise in the upstream bend. Figure 48 shows the values of AVR_o for the configurations.

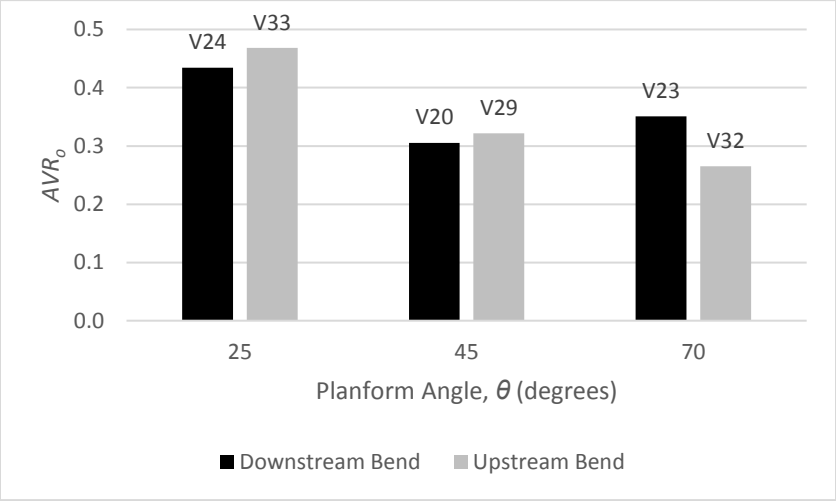

Figure 48. Variation of Average Velocity Ratio along the outer bank with rock vane planform angle. All configurations plotted have the same projected length (T_w/4), crest slope (10%), and spacing (L_{arc}=0.75T_w).

In the downstream bend, configuration V20 (θ = 45°, AVR_o = 0.31) performed slightly better than did V23 (θ = 70°, AVR_o = 0.35). However, in the upstream bend, V29 (θ = 45°, AVR_o

= 0.32) did not perform as well as did V32 ($\theta = 70°$, $AVR_o = 0.27$). The differences in AVR_o are relatively modest in both cases, less than 0.05, and all four configurations reduced velocity along the outer bank by more than 50%.

Rock vane configurations V24 and V33 (installed at $\theta = 25°$) both performed worse than their 45° counterparts. The velocity ratio for V24 is $AVR_o = 0.43$ and that for V33 is 0.47. The likely reason for the relatively poor performance of the 25° angle vanes is the fact that they block relatively little of the flow area. V24 blocks 8.4% of the flow, compared with 15.2% for V20. Likewise, V33 blocks 11.5% of the flow area compared with 21.3% for V29. In both cases, reducing the planform angle from 45° to 25° reduces the area of flow blocked by almost half.

One configuration of rock vanes (V01) was tested with an angle of $\theta = 85°$. The results are not directly comparable to the six configurations described above, but the resulting velocity ratio of $AVR_o = 0.38$ demonstrates that even angles close to 90° can provide large reductions in velocity along the outer bank.

These results indicate that rock vanes installed at any angle from 45° to 85° can provide good performance for channel control. This finding agrees with other studies in the literature. Brown (1985) found that for spur-dikes, a structure similar in geometry to rock vanes, the length of streambank protected downstream of the structure tip does not vary with the planform angle. Toniolo and Duvoy (2010) concluded that rock vanes installed at angles even greater than 90° could still provide good bank protection. The planform angle of rock vanes therefore appears to be a variable of secondary importance.

However, due caution should be taken when constructing rock vanes at angles less than $\theta = 45°$. The area of the flow blockage decreases with rock vane angle and this blockage effect becomes more pronounced at very small angles. Therefore, it may be difficult to design a

structure that provides sufficient velocity reduction along the outer bank. Appendix E describes geometric constraints for rock vanes installed at small angles.

Effect of Rock Vane Crest Slope ($tan\phi$)

The numerical modelling indicates that reducing the crest slope and, hence, tip submergence of a given rock vane configuration reduces the value of AVR_o. Configurations V20, V21, and V22 in the downstream bend, and V29, V30, and V31 in the upstream bend, tested rock vanes at crest slopes of 10%, 20%, and 5% respectively. As Figure 49 illustrates, decreasing the crest slope consistently decreased the value of AVR_o in both the upstream and downstream bends.

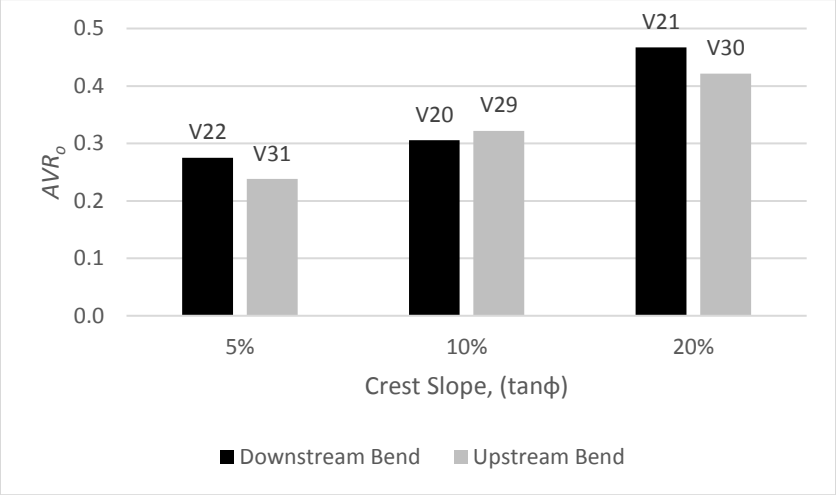

Figure 49. Variation of Average Velocity Ratio along the outer bank with rock vane crest slope. All configurations plotted have the same projected length ($T_w/4$), planform angle (45°), and spacing ($L_{arc} = 0.75T_w$)

Other tests confirm this result. Configurations V11-V16 were constructed with the same spacing and planform angle. Figure 50 shows that, for three different projected lengths (expressed as L_{proj}/T_w), rock vanes with a 10% crest slope have a lower value of AVR_o than do rock vanes with a 20% crest slope.

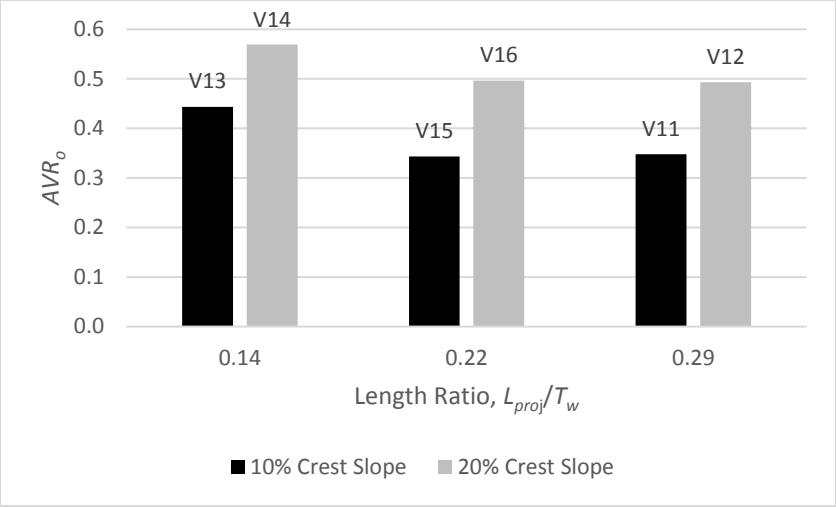

Figure 50. Average Velocity Ratio along the outer bank for crest slopes of 10% and 20% at different projected lengths. All configurations plotted have the same planform angle (60°) and spacing ($L_{arc} = 1.15T_w$) and are located in the downstream bend.

The clear conclusion is that for a given projected length, planform angle, and spacing, rock vanes with smaller crest slopes and smaller tip submergence will produce lower velocities along the outer bank. However, a smaller crest slope will not always be desirable in practice, as structures with steeper slopes require less material to construct and hence are somewhat more economical.

Effect of Rock Vane Projected Length (L_{proj})

The effect of projected length on rock vane performance is rather complex. While rock vanes with a projected length of zero provide no velocity reduction along the bank, ever-longer rock vanes do not provide ever-greater velocity reduction.

Configurations V11-V16 test rock vanes with three different projected lengths at both 10% and 20% crest slopes. As Figure 50 shows, increasing the projected length from $0.14T_w$ to $0.22T_w$ decreased AVR_o for both a 10% and 20% crest slope. However, further increasing the projected length to $0.29T_w$ resulted in almost no change in AVR_o compared to structures with a

length of $0.22T_w$. This suggests the velocity along the outer banks approaches a lower limit when $L_{proj} = 0.22T_w - 0.29T_w$.

Further evidence for the limiting effect of projected length is provided by configurations V25 & V27 in the downstream bend and V34 & V36 in the upstream bend. Doubling the rock vane projected length from $0.25T_w$ (V25) to $0.5T_w$ (V27) resulted in a greater average velocity along the outer bank in the downstream bend; AVR_o increased from 0.39 (V25) to 0.50 (V27). In the upstream bend, doubling the projected length decreased AVR_o very slightly from 0.37 (V34) to 0.36 (V36), as Figure 51 shows. That increasing projected length sometimes increases velocity along the outer bank indicates there exists an optimal project length that minimizes velocity along the outer bank.

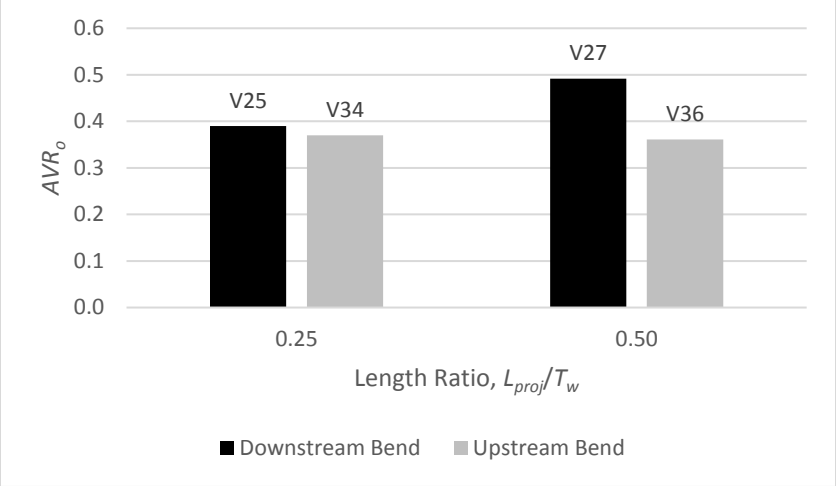

Figure 51. Average Velocity Ratio along the outer bank for projected lengths of $0.25T_w$ and $0.5T_w$. All configurations plotted have the same planform angle (45°), crest slope (10%), and spacing ($L_{arc} = 1.5T_w$)

The reason longer projected lengths do not always decrease velocity along the outer bank can be explained in terms of how rock vanes redirect flow. Once rock vanes become too long, more flow is directed over the top of the structure rather than around the tip of the structure. Figure 52 shows streamlines at Vane 4 in configuration V25. Note that very few streamlines pass over the rock vane crest compared to the large number directed around the rock vane's tip.

Figure 53 shows Vane 4 in configuration V27; far more streamlines pass over the crest and fewer are directed around the tip.

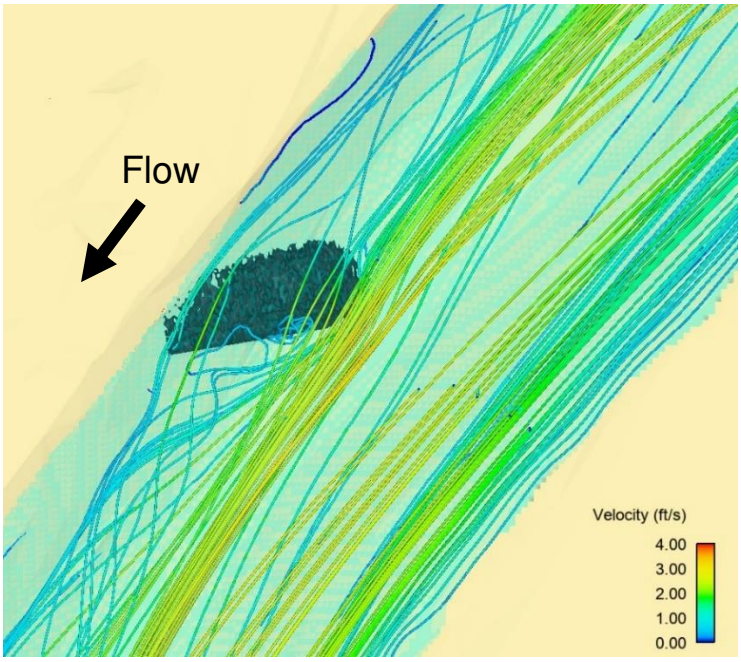

Figure 52. Streamlines at Vane 4 in configuration V25. Very few streamlines pass over the crest of the vane, while many streamlines are directed around the tip.

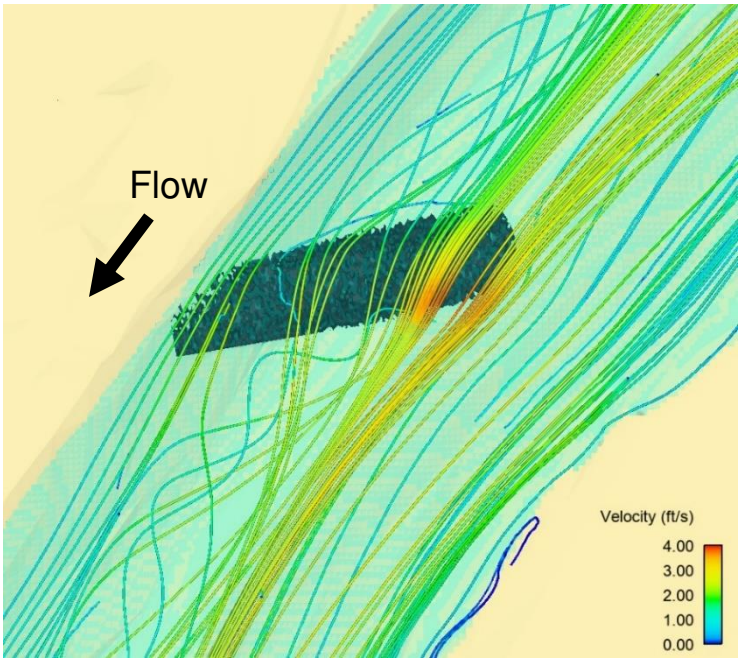

Figure 53. Streamlines at Vane 4 in configuration V27. More streamlines pass over the crest of the structure while fewer are directed around the tip.

In summary, the data suggest that there exists an optimal projected length for rock vanes. Rock vanes shorter than the optimal length will not deflect enough flow to provide optimal bank protection whereas rock vanes longer than the optimal length will cause more flow to pass over the crest of the structure, reducing bank protection. Based on the tests in this study, the optimal projected length is in the neighborhood of $0.2T_w - 0.3T_w$.

Effect of Bend Tightness (R_c/T_w)

No definitive determinations on the effect of bend tightness (R_c/T_w) can be made from this study. While the study examined two bends of different radii, the bends also differed in cross-section. As a result, it is impossible to discern what differences in rock vane performance are attributable to bend tightness versus cross-section geometry. A forthcoming study examining bends of four different radii may shed addition light on the effect bend radius.

The ratio R_c/T_w does affect the relationship between other geometric parameters of rock vanes. The relationship between projected length, crest slope, planform angle, and tip submergence is a function of R_c/T_w. Thus, for rock vanes of a given projected length, crest slope, and planform angle, the tip submergence will vary with varying values of R_c/T_w.

Effect of Rock Vane Spacing (L_{arc})

The spacing of rock vanes required for effective bank protection is related to the extent of the wake region formed downstream of a rock vane. The spacing must be short enough that the region between adjacent rock vanes will be sufficiently sheltered by the wake to provide the desired reduction in flow velocity along the outer bank. Figure 54 shows the wake region downstream of a rock vane in configuration V41.

As the graph in Figure 55 shows, increasing rock vane spacing generally increases the velocity along the outer bank. One exception was observed – decreasing spacing in the

downstream bend from $L_{arc} = 0.75T_w$ (V20) to $L_{arc} = 0.5T_w$ (V26) resulted in a slight increase in AVR_o values from 0.31 to 0.32. The slight increase appears to indicate that once spacing is sufficiently small, further reductions in spacing will not result in reductions in velocity along the outer bank.

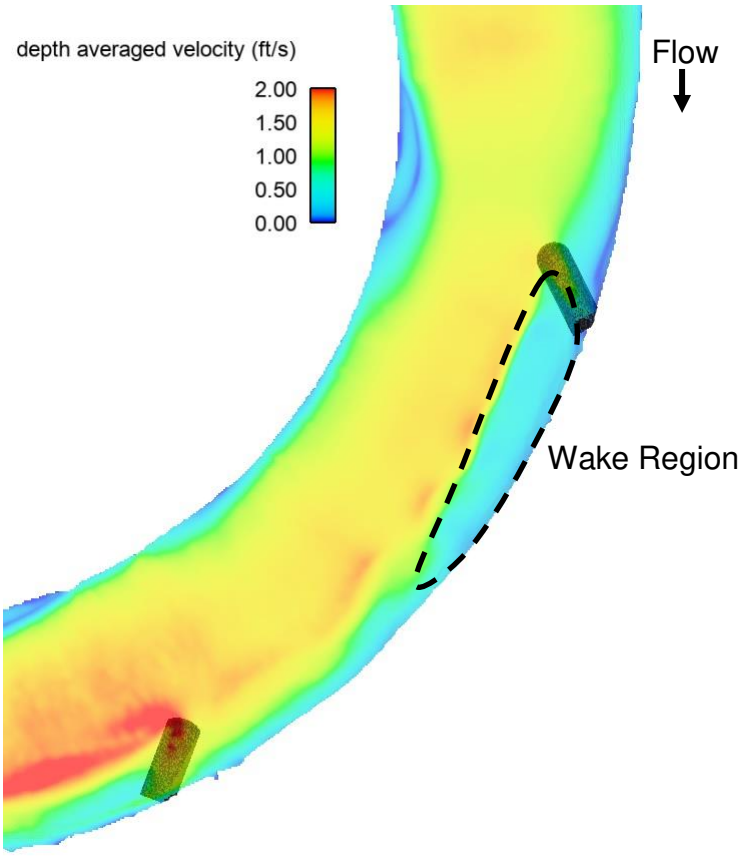

Figure 54. Plot of depth-averaged velocity showing the low-velocity wake region downstream of a rock vane in configuration V41

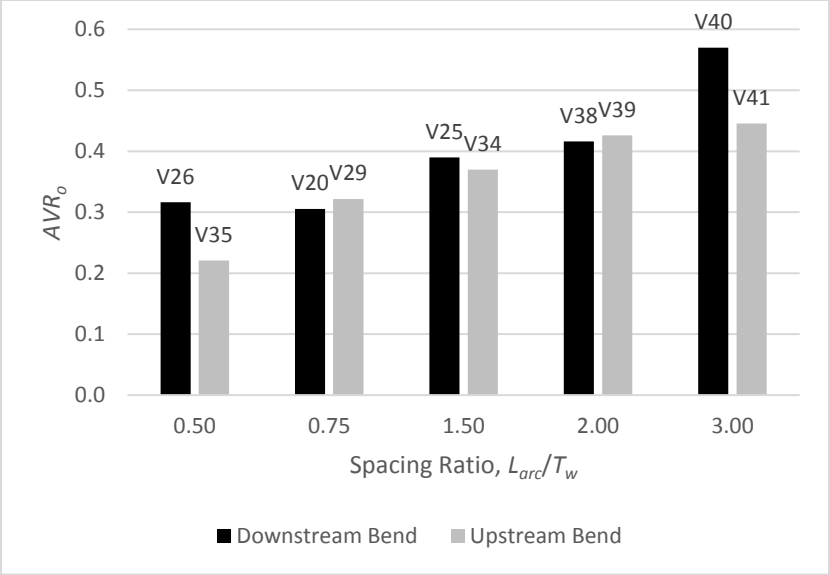

Figure 55. Average Velocity Ratio along the outer bank for spacing of $0.5T_w = 2L_{proj}$ to $3T_w = 12L_{proj}$. All configurations plotted have the same planform angle (45°), crest slope (10%), and projected length ($L_{proj} = 0.25T_w$)

For a spacing greater than $0.75T_w$, increasing the spacing consistently increased the velocity along the outer bank in both the upstream and downstream bends. Doubling the spacing from $0.75T_w$ to $1.5T_w$ results in rather modest increases in outer bank velocity. AVR_o increased from 0.31 (V20) to 0.39 (V25) in the downstream bend and from 0.32 (V29) to 0.37 (V34) in the upstream bend. Doubling the spacing again from $1.5T_w$ to $3.0T_w$ increased AVR_o from 0.39 (V25) to 0.57 (V40) in the downstream bend and from 0.37 (V34) to 0.45 (V41) in the upstream bend.

Rock vane spacing is a parameter designers can adjust to balance the cost of a rock vane installation with the degree of bank protection provided. Increasing the spacing of rock vanes decreases the number of structures (and hence volume of riprap) required to protect a given length of stream bank. Analysis and hydraulic modelling should allow the designer to select a rock vane spacing that provides the necessary velocity reduction to stabilize the bank while minimizing the number of structures required.

Effect of Area of Flow Blockage (*A)**

Projected area is by far the most complicated parameter considered in rock vane design because it depends upon the values of many variables: projected length, planform angle, crest slope, top-width, radius of curvature, and channel cross-section. For a channel of varying cross-section, it is even slightly dependent upon rock vane spacing.

Examining Figure 56, which plots the values of A^* and AVR_o for all of the tested bendway weir and rock vane configurations, it is apparent that configurations blocking greatly different portions of the flow area can produce similar velocity reductions along the outer bank. AVR_o values less than 0.50 were observed in the downstream bend from configurations blocking as little as 7% of the flow area and as much as 32%. In the upstream bend configurations with flow blockages ranging from 12% to 27% produced AVR_o values less than 0.50.

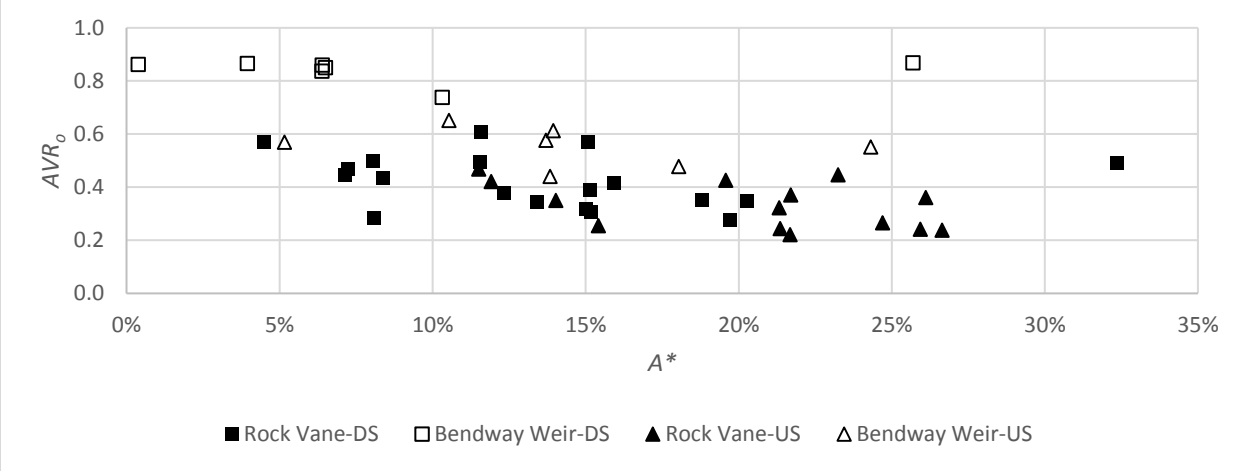

Figure 56. Plot of flow blockage area (A^*) and AVR_o for all bendway weir and rock vane configurations tested in the upstream (US) and downstream (DS) bends

These results indicate that while projected area may be useful for quantifying the combined effects of rock vane geometry, the basic geometric parameters of projected length, crest slope, planform angle, and spacing must still be considered individually. In other words, the

effectiveness of a given rock vane or bendway weir configuration is determined not just by how much of the flow area is blocked, but also by the geometry of the blocked area in the channel.

The importance of the geometry of the blockage area is apparent from examining the difference between bendway weir and rock vane performance. Bendway weirs tend to have greater AVR_o values than rock vanes, even when they block similar portions of the flow area. The geometric difference between bendway weirs and rock vanes – that rock vanes intersect the bank at the design water surface elevation while bendway weirs have a flat, fully submerged crest clearly effects their performance at reducing velocity along the outer bank.

Because projected area is interconnected with almost every other variable of rock vane design, little can be said of its effect on rock vane performance beyond what can be concluded regarding crest length and tip submergence:

1. Longer projected lengths cause more flow blockage and reduce outer bank velocities, up to a certain point; and,

2. Smaller crest slopes decrease tip submergence and increase flow blockage, resulting in decreased velocity along the outer bank.

However, projected area remains a valuable parameter which incorporates information about the channel cross-section not included in other parameters.

Volume of Riprap

While not one of the geometric parameters used in the design of rock vanes or bendway weirs, the volume of riprap used to construct bank protection is an important factor in the cost of a project. In terms of cost, an optimal bank protection design will use the smallest volume of riprap necessary to protect the streambank at the design flow. Examining a plot of AVR_o versus volume of riprap (as computed with AutoCAD Civil3D) in Figure 57 reveals that many of the

tested configurations offer similar degrees of velocity reduction while using greatly different volumes of riprap.

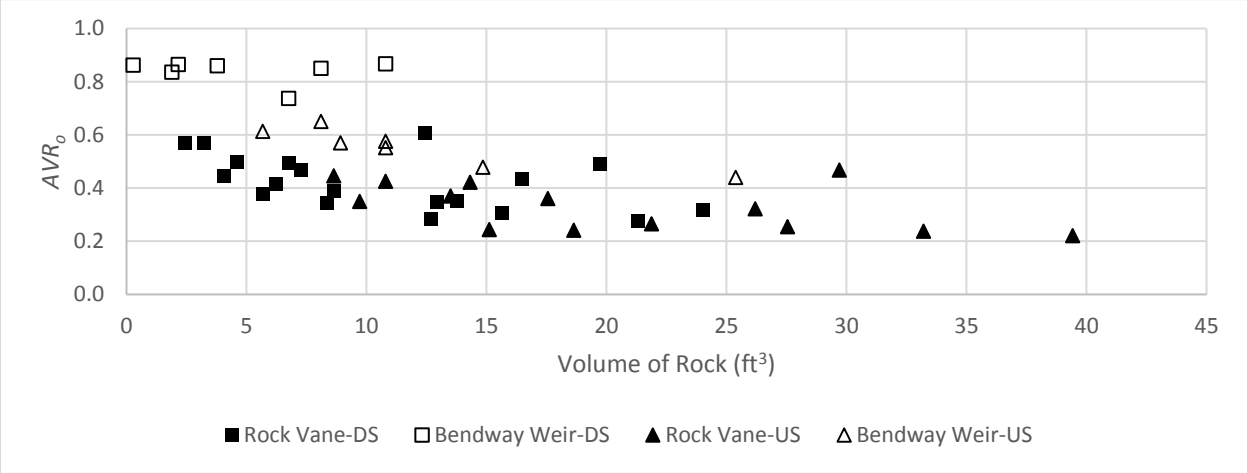

Figure 57. Plot of the volume of riprap required for all of the tested bendway weir and rock vane configurations in the upstream (US) and downstream (DS) bends

The arrangement of the riprap in the geometry of the structures is the crucial factor in determining the effectiveness of a configuration. A good rock vane design can achieve large reductions in outer bank velocity with modest quantities of riprap. Likewise, a careless design can use a great deal of riprap and produce little reduction in velocity along the outer bank. It is therefore crucial that analysis and modelling of any proposed rock vane installation consider both the effectiveness and economics of the proposed design.

Equation Development

The velocity ratio AVR_o provides a convenient measure of the bank protection provided by an array of rock vanes or bendway weirs. It would therefore be helpful for design engineers if a simple method of predicting the AVR_o value of a given configuration of structures could be found.

Beginning with Heintz (2002), numerous investigators have tried to find a simple equation to predict velocity ratios from the geometric parameters of the structures and the river

channel. Schmidt (2005) undertook an extensive dimensionless analysis, starting with 39 dimensionless terms. These were whittled down to equations using four to seven terms to predict various velocity ratios. Scurlock et al. (2012a) produced an equation with six dimensionless terms, a variation of which was included in Baird et al. (2015) and presented in this document as Equation 7.

The diversity of velocity ratio equations indicates one of the drawbacks of relationships derived from dimensional analysis – the results are not unique. While dimensional analysis can show that a parameter is a function of certain dimensionless terms, it cannot provide the form of that function. As a result, the creators of previous velocity ratio equations have generally chosen the simple power function form such as Equation 7.

However, it is possible to derive a physically based relationship between average velocity along the outer bank and rock vane geometry using the principle of continuity and a simplified model of flow through an installation of rock vanes. Figure 58a sketches two rock vanes installed in a straight channel. Considering a control volume bounded by the rock vanes, the flow along the outer bank can be broken down into components of flow entering or leaving the control volume over the crest of the rock vanes and flow entering or leaving in the wake region of the upstream vane.

If the flow over the crest of the vanes (Q_{crest}) is the same for both of the vanes bounding the control volume, the net flow entering the control volume through the wake region must be zero. To simplify analysis, flow is assumed to enter the control volume at a constant velocity (V_{wake}) and constant angle (α) for a distance of $0.5L_{arc}$ downstream of rock vane 1. Further, it is assumed to exit symmetrically, at the same velocity and angle for a distance of $0.5L_{arc}$ upstream

of rock vane 2. The flow depth at the tips of the rock vanes will be taken as the thalweg depth (D_b).

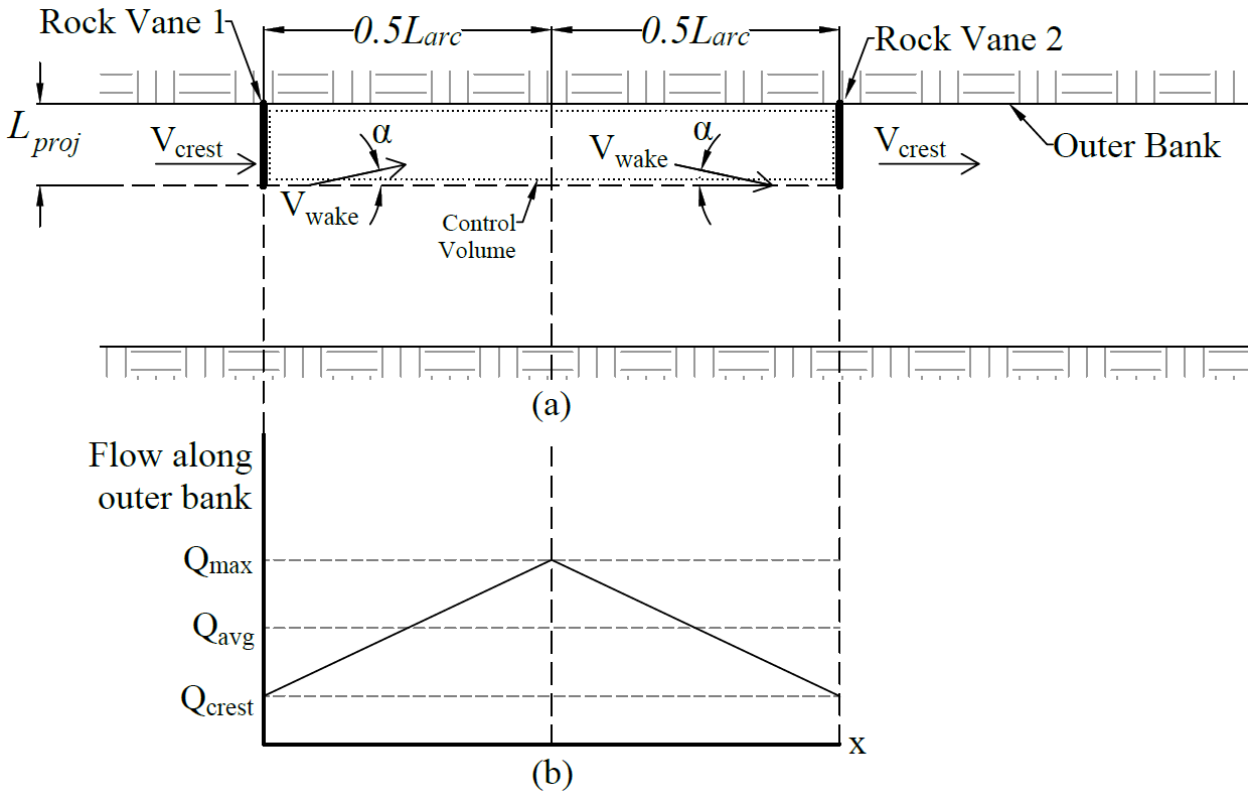

Figure 58. Simplified flow between rock vanes in a straight channel; (a) illustrates the layout of rock vanes and the velocity components; and, (b) illustrates the variation in flow rate along the outer bank between the rock vanes.

Figure 58b illustrates the variation of discharge within a distance L_{proj} of the outer bank along the length of the control volume. The maximum flow rate in the control volume (Q_{max}) can be computed as:

$$Q_{max} = Q_{crest} + V_{wake} sin\alpha D_b \left(\frac{L_{arc}}{2}\right) \quad (15)$$

The average flow rate in the control volume is then:

$$Q_{avg} = Q_{crest} + \frac{1}{2}(Q_{max} - Q_{crest}) = Q_{crest} + \frac{1}{4} V_{wake} sin\alpha L_{arc} D_b \quad (16)$$

In terms of the area of flow over the crest ($0.5L_{proj}\Delta z$) and the velocity over the crest (V_{crest}), the average flow rate is:

$$Q_{avg} = Q_{crest} + 0.25V_{wake}sin\alpha L_{arc}D_b = 0.5V_{crest}L_{proj}\Delta z + 0.25V_{wake}sin\alpha L_{arc}D_b \quad (17)$$

The average velocity in the control volume (V_{avg}) is determined by dividing the average flow rate by the flow area of the control volume ($0.5L_{proj}\Delta z + A^*A_{avg}$), where A^* is the percentage of flow area blocked by the rock vanes and A_{avg} is the average flow area in the channel:

$$V_{avg} = \frac{Q_{avg}}{A_{avg}} = \frac{0.5V_{crest}L_{proj}\Delta z + 0.25V_{wake}sin\alpha L_{arc}D_b}{0.5L_{proj}\Delta z + A^*A_{avg}} \quad (18)$$

The average velocity in the control volume can now be substituted for the $V_{o\text{-}structures}$ term in the definition of AVR_o:

$$AVR_o = \frac{V_{o-structures}}{V_{baseline}} \approx \frac{V_{avg}}{V_{baseline}} = \frac{0.5V_{crest}L_{proj}\Delta z + 0.25V_{wake}sin\alpha L_{arc}D_b}{V_{baseline}\left(0.5L_{proj}\Delta z + A^*A_{avg}\right)} \quad (19)$$

Separating the rock vane geometry from the other terms,

$$AVR_o = \left(\frac{0.5V_{crest}}{V_{baseline}}\right)\frac{L_{proj}\Delta z}{\left(0.5L_{proj}\Delta z + A^*A_{avg}\right)} + \left(\frac{0.25V_{wake}sin\alpha}{V_{baseline}}\right)\frac{L_{arc}D_b}{\left(0.5L_{proj}\Delta z + A^*A_{avg}\right)} \quad (20)$$

To provide a simple design equation, it is assumed that the non-geometric terms are nearly constant between configurations and can be replaced by regression coefficients,

$$AVR_o = a_1\frac{L_{proj}\Delta z}{\left(0.5L_{proj}\Delta z + A^*A_{avg}\right)} + a_2\frac{L_{arc}D_b}{\left(0.5L_{proj}\Delta z + A^*A_{avg}\right)} \quad (21)$$

Best-fit regression coefficients were determined by performing non-linear regression using the R statistical package. The fitted regression coefficient values are $a_1 = 0.348$ and $a_2 = 0.019$, as shown in Equation 22. Both coefficients are statistically significant at $p < 0.001$.

$$AVR_o = \frac{0.348L_{proj}\Delta z + 0.019L_{arc}D_b}{0.5L_{proj}\Delta z + A^*A_{avg}} \quad (22)$$

Figure 59 plots values of AVR_o predicted by Equation 22 against the values measured from the numerical model for each of the rock vane configurations tested. Overall, the equation provides good predictions of AVR_o, predicting 29 of 33 values within ±0.1 of the observed value and having a coefficient of determination of $r^2 = 0.83$.

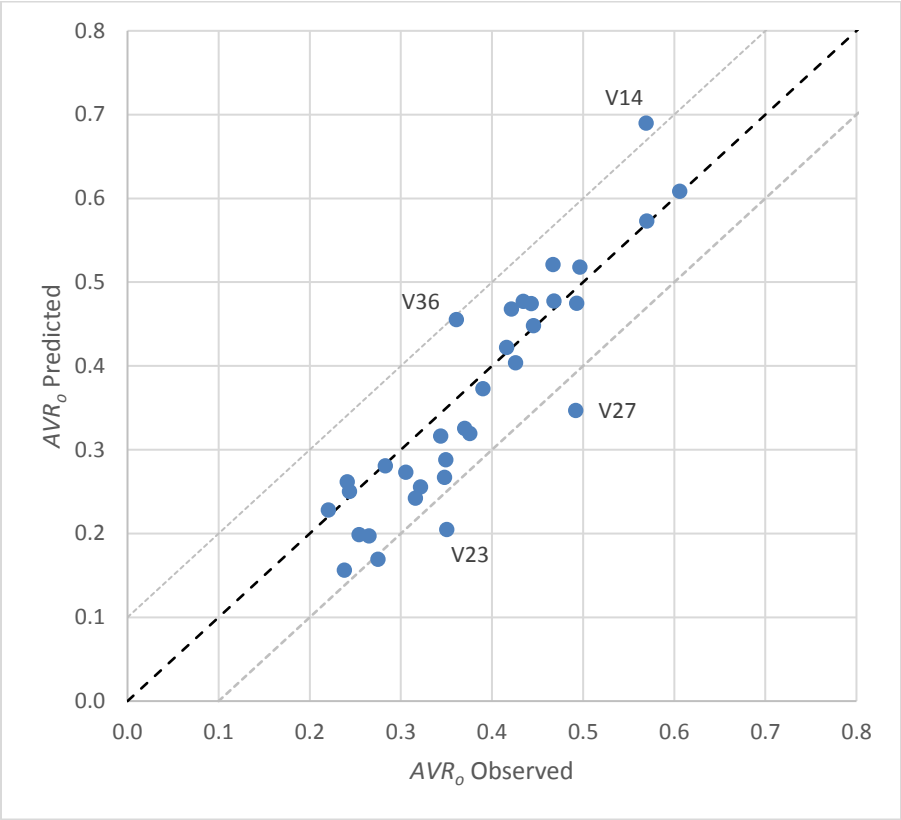

Figure 59. Predictions of AVR_o values from Equation 22 versus observed values from the modelled rock vane configurations.

Equation 22 has several interesting properties. First, the denominator is actually independent of Δz, as any decrease in area above the crest of the structure ($0.5L_{proj}\Delta z$) will be offset by a corresponding increase in area blocked by the structure (A^*A_{avg}). Therefore, decreasing Δz will always result in a decrease in the predicted value of AVR_o. This behavior agrees with the numerical simulations, where decreasing tip submergence always decreased the observed value of AVR_o.

Likewise, decreasing the structure spacing (L_{arc}) will always decrease the predicted AVR_o value of a given configuration. This behavior also agrees with the data from the simulations, as decreasing spacing resulted in decreased values of AVR_o, except for one case where AVR_o increased by 0.01.

The outlying data points in Figure 59 reveal some of the limitations of the design equation. The equation gives rather poor predictions for V27 and V36, the configurations with the greatest projected lengths ($L_{proj} = 0.5T_w$). As noted earlier, very long rock vanes redirect flow differently than shorter rock vanes, a difference the design equation may not adequately capture. V14 has the smallest projected area of any configuration ($A^* = 4\%$), which may account for the over-prediction of its AVR_o value. For the V23 configuration, the large difference between the predicted and observed value of AVR_o likely results from the equation lacking a term directly accounting for planform angle. V23, installed at $\theta = 70°$, performed worse than an otherwise identical configuration installed at $\theta = 45°$ (V20), contrary to the prediction of the equation. Future work to improve the equation should focus on very long rock vanes, very small projected areas, and accounting for planform angle.

In summary, Equation 22 agrees well with the numerical modelling results both statistically (in terms of goodness of fit) and conceptually (in terms of the flow field). The equation enables a designer to estimate the reduction in outer bank velocity a particular rock vane configuration will produce in a particular bend from the geometry of the bend (A_{avg} and D_b) and the rock vanes (L_{proj}, Δz, L_{arc}, and A^*). The designer can then iteratively determine the configuration geometry that will provide the desired bank protect with the least volume of rock. However, the equation cannot capture all of the peculiarities of a particular river bend so it

should only be used as a preliminary design tool. The final design of a rock vane configuration should be verified using a 2D or 3D numerical model.

CHAPTER 8. CONCLUSIONS AND RECOMMNEDATIONS

This study used 3D numerical models (implemented in FLOW-3D) to examine the effect of various configurations of bendway weirs and rock vanes on the flow field along two channel bends typical of the Middle Rio Grande. Of interest was the capacity of such configurations to manage channel bends along the Middle Rio Grande and prevent the channel from shifting. This chapter summarizes the main conclusions gathered from the numerical models.

Conclusions

1. The numerical models were useful methods for ascertaining the effectiveness of rock-vane and bendway-weir configurations for managing alluvial bends along the Middle Rio Grande.
2. Rock vanes are shown to be the more effect rock structure for managing alluvial bends, in terms of limiting erosion of the outer bank and controlling thalweg position.
3. The geometry of bendway weirs limits their effectiveness in reducing velocity along the outer bank of a river bend. Some flow is redirected around the root of the structure, increasing velocity along the bank near the bendway weir, because bendway weirs are completely submerged at the design flow rate.
4. In contrast, rock vanes extend to the edge of water at the design flow rate. Flow is redirected only over the structure crest or around the structure tip, resulting in a greater reduction in velocity along the outer bank.
5. Rock vanes installed at a range of planform angles can reduce velocity along the bank by almost 80% compared to the baseline velocity. The best performance of a rock vane configuration occurred for rock vanes installed at angles ranging from 45° to 85°. Vanes installed at very small angles (25°) did not perform as well, because very small planform

angles greatly reduce the area of flow blocked by the vanes and limit the disruption of flow along the bank.

6. Decreasing rock vane crest slope reduced the velocity along the outer bank for every configuration tested. However, decreasing the crest slope increases the amount of riprap required to construct a rock vane. Selection of crest slope is therefore a balance between performance and economics. Crest slopes of 10% performed well in many different configurations, reducing velocity along the outer bank by as much as 78% compared to the baseline velocity. However, rock vanes with a 20% crest slope could reduce velocity along the outer bank by up to 68%.
7. The projected length of rock vanes must be sufficiently long to disrupt flow along the outer bank. However, ever-longer rock vanes will not provide ever-lower velocities along the bank, as longer rock vanes direct more flow over the crest of the structure, rather than around the tip. Numerical modelling results indicate the optimal length of rock vanes is in the range of $0.2T_w - 0.3T_w$, where T_w = top-width of channel under design conditions.
8. The ratio of bend radius, R_c, to channel top-width (R_c/T_w) affects the relationship between crest length (L_c), planform angle (θ), and projected length (L_{proj}). The curvature effect becomes more important for rock vanes installed at small planform angles in tightly curved bends. For such structures, it is necessary to use Equation 1 (reproduced below) to compute the projected length of rock vanes:

$$L_{proj} = R_c + \frac{T_w}{2} - \sqrt{L_c^2 + \left(R_c + \frac{T_w}{2}\right)^2 - 2L_c\left(R_c + \frac{T_w}{2}\right)\sin\theta} \qquad (1)$$

9. Decreasing rock vane spacing decreased the velocity along the outer bank for all but one test configuration. From the one exception (decreasing spacing from $0.75T_w$ to $0.5T_w$ in

the downstream bend), it appears that once spacing is sufficiently small, further decreases in spacing will not produce further reductions in outer bank velocity. This trend occurs in part because spacing should be related to the length of wake formed by a rock vane. As increasing spacing decreases the number of structures required to protect a given length of streambank, spacing is a good parameter for the designer to adjust when balancing the degree of bank protection with the cost of an installation.

10. The portion of the channel flow area blocked by a rock vane installation is a function of the channel cross-section and all of the other geometric parameters. It is useful in considering the combined effects of rock vane geometry, but is not a parameter the designer should attempt to adjust discretely.
11. Similar degrees of bank protection can be provided by configurations utilizing greatly different volumes of rock. An economical design will find the least volume of rock necessary to provide the necessary bank protection.
12. The maximum velocity at the tip of a rock vane is heavily dependent upon the geometry and entrance velocity of the bend in which the rock vane is constructed.
13. Equation 22, reproduced below, gives useful preliminary estimates of velocity reduction along the outer bank based on the geometry of the bend (A_{avg} and D_b) and the rock vanes installed in the bend (L_{proj}, Δz, L_{arc}, and A^*).

$$AVR_o = \frac{0.348L_{proj}\Delta z + 0.019L_{arc}D_b}{0.5L_{proj}\Delta z + A^*A_{avg}} \tag{22}$$

Design Recommendations

The results of this study indicate that large reductions (up to about 80%) in velocity along the outer bank of a bend can be achieved with many different rock vane configurations. The optimal rock vane configuration for any given site will depend upon the site-specific channel

geometry and the velocity reduction required to stabilize the bank. Based on the numerical modeling results, the values in Table 24 provide a good starting point for rock vane design.

Table 24. Recommend initial values for rock vane design

Projected Length L_{proj}	Spacing L_{arc}	Angle θ	Crest Slope $tan\phi$
$0.25T_w$	$1.5T_w = 6L_{proj}$	60°	10%

From these initial values, Equation 22 can be used to further refine the crest slope and spacing to provide the desired velocity reduction. Adjusting planform angle is likely to have minimal effect on the velocity reduction and projected length should not be adjusted outside the optimal range of $0.2T_w - 0.3T_w$. The effectiveness of the design should be confirmed with a 2D or 3D numerical model in order to account for all the peculiarities of a particular bend, which may not be adequately captured with the regression equation.

The numerical model should also be used to evaluate the maximum velocity that the tips of the structures are likely to experience. This study has shown that velocity at the tip of a rock vane is heavily dependent upon the characteristics of the bend in which the rock vane is placed. As a result, it is important that maximum tip velocity be evaluated using a model that accounts for the unique characteristics of each river bend.

All of the modeling and design recommendations in this study are based on rock vanes that have a crest intersecting the bank at the design water surface elevation. If the design water surface elevation is exceeded, the rock vanes are likely to begin behaving like bendway weirs, with flow being redirected around the root of the structure, diminishing the velocity reduction along the outer bank. Therefore, it is crucial that the designer exercise an appropriate degree of conservatism in selecting the design flow rate and computing the design water surface elevation.

REFERENCES

Abad, J. D., Rhoads, B. L., Güneralp, İ., & García, M. H. (2008). Flow Structure at Different Stages in a Meander-Bend with Bendway Weirs. *Journal of Hydraulic Engineering*, 1052-1063.

Baird, D., Fotherby, L., Klumpp, C., & Sculock, S. M. (2015). *Bank Stabilization Design Guidelines.* Denver, CO: Bureau of Reclamation.

Biedenharn, D. S., Elliott, C. M., & Watson, C. C. (1997). *The WES Stream Investigation and Streambank Stabilization Handbook.* Vicksburg, MS: U.S. Army Engineer Waterways Experiment Station.

Brown, S. A. (1985). *Design of Spur-type Streambank Stabilization Structures.* McLean, VA: Federal Highway Administration.

Cox, A. L. (2014). *Numerical Modeling of Transverse River Training Structures: Creating STL Files.* St. Louis, MO: Saint Louis University.

Darrow, J. D. (2004). *Effects of Bendway Weir Characteristics on Resulting Flow Conditions.* Fort Collins, CO: Colorado State University.

Heintz, M. L. (2002). *Investigation of Bendway Weir Spacing.* Fort Collins, CO: Colorado State University.

Jamieson, E. C., Rennie, C. D., & Townsend, R. D. (2009). Design of stream barbs for field scale application at Sawmill Creek, Ottawa. *WIT Transactions on Ecology and the Environment,*, 281-292.

Jamieson, E. C., Rennie, C. D., & Townsend, R. D. (2011). Stream barb performance in a semi-alluvial meandering channel. *WIT Transactions on Ecology and the Environment*, 227-238.

Jamieson, E. C., Ruta, M. A., Rennie, C. D., & Townsend, R. D. (2013). Monitoring stream barb performance in a semi-alluvial meandering channel: flow field dynamics and morphology. *Ecohydrology*, 611–626.

Johnson, P. A., Hey, R. D., Tessier, M., & Rosgen, D. L. (2001). Use of vanes for control of scour at vertical wall abutments. *Journal of Hydraulic Engineering*, 772-778.

Julien, P. Y., & Duncan, J. R. (2003). *Optimal Design Criteria of Bendway Weirs from Numeircal Simulations and Physical Model Studies.* Fort Collins, CO: Colorado State University.

Kasper, K. E. (2005). *Accuracy of HEC-RAS to Calculate Flow Depths and Total Energy Loss With and Without Bendway Weirs in a Meander Bend.* Fort Collins, CO: Colorado State University.

Kolden, E. (2013). *Modeling in a Three-Dimensional World: Whitewater Park Hydraulics and Their Impact on Aquatic Habitat in Colorado.* Fort Collins, CO: Colorado State University.

Lagasse, P. F., Clopper, P. E., Pagán-Ortiz, J. E., Zevenbergen, L. W., Arneson, L. A., Schall, J. D., & Girard, L. G. (2009). *Bridge Scour and Stream Instability Countermeasures.* Washington, D.C.: Federal Highway Administration.

Maryland Department of the Environment. (2000). *Maryland's Waterway Construction Guidelines.* Water Management Administration.

McCullah, J. A., & Gray, D. (2005). *Environmentally Sensitive Channel- and Bank- Protection Measures.* Washington, D.C.: Transportation Research Board, National Academies of Science.

Natural Resources Conservation Service. (2005). *Technical Note 23, Version 2.0 Design of Stream Barbs.* Portland, OR: United States Department of Agriculture.

Natural Resources Conservation Service. (2007). *Technical Supplement 14H Flow Changing Techniques Part 654 National Engineering Handbook.* United States Department of Agriculture.

Natural Resources Conservation Service. (2009). *Wisconsin Supplement Engineering Field Handbook Chapter 16 Streambank and Shoreline Protection.* United States Department of Agriculture.

Natural Resources Conservation Service. (2010). *Minnesota Technical Note No. 8 Design of Stream Barbs for Low Gradient Streams.* St. Paul, MN: United States Department of Agriculture.

Natural Resources Conservation Service. (2013). *Kansas Engineering Technical Note No. KS-1 (Revision 1).* Salina, KS: United States Department of Agriculture.

Odgaard, A. J., & Abad, J. D. (2007). River Meandering and Channel Stability. In *Sedimentation Engineering* (p. 449). Reston, VA: American Society of Civil Engineers.

Papanicolaou, A. N., Bressan, F., Fox, J., Kramer, C., & Kjos, L. (2018). Role of Structure Submergence on Scour Evolution in Gravel Bed Rivers: Application to Slope-Crested Structures. *Journal of Hydraulic Engineering*, 03117008-1 - 03117008-14.

Papanicolaou, A. N., Kjos, L. J., & Fox, J. F. (2004). *Investigation of Flow and Local Scour Characteristics around a Partially Submerged Permeable WSDOT Barb.* Pullman, WA: Washington State Transportation Center.

Plymesser, K. E. (2014). *Modeling Fish Passage and Energy Expenditure for American Shad in a Steeppass Fishway Using a Computational Fluid Dynamics Model.* Bozeman. MT: Montana State University.

Richard, G. (2001). *Quantification and Prediction of Lateral Channel Adjustments Downstream from Cochiti Dam, Rio Grande, NM.* Fort Collins, CO: Colorado State University.

Schmidt, P. G. (2005). *Effects of Bendway Weir Field Geometric Characteristics on Channel Flow Conditions.* Fort Collins, CO: Colorado State University.

Sclafani, P. (2010). *Methodology for Predicting Maximum Velocity and Shear Stress in a Sinuous Channel with Bendway Weirs Using 1-D Hec-Ras Modeling Results.* Fort Collins, CO: Colorado State University.

Scott, S. H., Jai, Y., Wang, S. S., & Xu, Y. (2001). *Analysis of Near-Field Hydrodynamics of Submerged Weirs.* Vicksburg, MS: U.S. Army Engineer Research and Development Center,Coastal and Hydraulics Laboratory.

Sculock, S. M., Cox, A. L., Thornton, C. I., & Abt, S. R. (2012). *Transverse Instream Structure Analysis: Maximum and Average Veloicty Ratios within the Prismatic Channel.* Fort Collins, CO: Colorado State University.

Scurlock, S. M., Cox, A. L., Baird, D. C., Thornton, C. I., & Abt, S. R. (2012). *Instream structure analysis: Procedures for the application of MVR and AVR in field design.* Fort Collins, CO: Colorado State University.

Scurlock, S. M., Cox, A. L., Thornton, C. I., & Abt, S. R. (2014). *Calibration and validation of a numerical model forevaluation of transverse in-stream structure research.* Denver, CO: Bureau of Reclamation.

Scurlock, S. M., Thornton, C. I., & Abt, S. R. (2014). *Evaluation of bendway-weir structures within the native topography channel.* Denver, CO: Bureau of Reclamation.

Shin, K., Ettema, R., & Thornton, C. I. (2018). *Native Channel Topography and Rock-Weir Structure Channel-Maintenance Techniques.* Fort Collins, CO: Colorado State University.

Sotiropoulos, F., & Diplas, P. (2014). *NCHRP Report 795 Design Methods for In-Stream Flow Control Structures.* Washington, D.C.: National Cooperative Highway Research Program.

Thornton, C. I., James, M., & Shin, K. (2016). *Testing of instream vane structures within the native-topography channel.* Fort Collins, CO: Colorado State University.

Toniolo, H., & Duvoy, P. (2010). *Study to Compare the Performance of Two Designs to Prevent River Bend Erosion in Arctic Environments.* Fairbanks, AK: University of Alaska Department of Civil and Environmental Engineering.

Walker, K. G., Thornton, C. I., Abt, S. R., & Cox, A. L. (2009). *Comparison of a Generalized Trapezoidal Hydraulic Model to a Native Topography Patterned Bed Surface Model of the Rio Grande.* Fort Collins, CO: Colorado State University.

Washington State Department of Transportation. (2017). *Hydraulics Manual.* Olympia, WA.

APPENDIX A. ROCK VANE GEOMETRIC RELATIONSHIPS

The basic geometric parameters of rock vanes were introduced in Chapter 1 and illustrated in Figure 1. From the geometry, several relationships can be derived which are of great use in the layout of rock vanes. This appendix will derive the equations relating crest length to projected length, the equation for the projected slope of a rock vane, and equations illustrating the limitations of structures with small planform angle in curved channels. All derivations assume a configuration of identical rock vanes equally spaced in a channel of constant cross-section and radius of curvature.

Projected Length as a Function of Crest Length

Figure 60 shows a rock vane of crest length, L_c, built at an angle, θ, to the outer bank of a bend with constant top-width, T_w, and a constant radius of curvature, R_c, measured along the centerline of the channel. The projected length of the rock vane, L_{proj}, defined as the perpendicular distance from the crest tip to the outer bank, can be determined as follows.

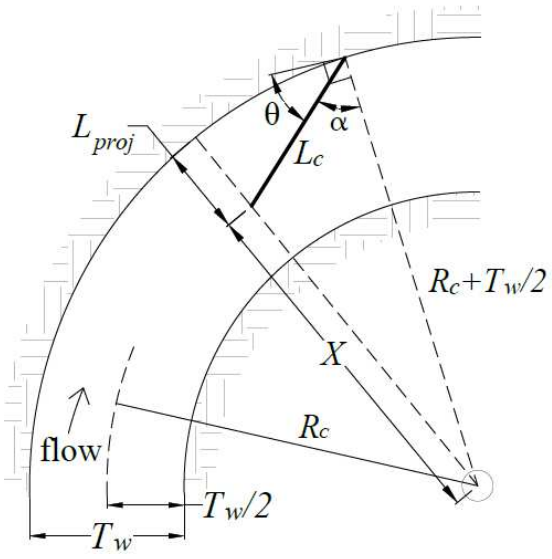

Figure 60. Geometric relationship of variables used to relate projected length to crest length

Define *X* as the distance between the tip of the rock vane and the center of curvature of the channel. By inspection of Figure 60, it is apparent that $X = R_c + \frac{T_w}{2} - L_{proj}$. Also, define α as the angle between the rock vane and a line radial to the outer bank at the vane root. Angle α is the complement of angle θ; i.e., $\alpha = 90° - \theta$.

Consider the triangle formed by the sides of length *X*, L_c, and $R_c+T_w/2$. Using the Law of Cosines, *X* is related to the other variables by the equation:

$$X^2 = L_c^2 + \left(R_c + \frac{T_w}{2}\right)^2 - 2L_c\left(R_c + \frac{T_w}{2}\right)cos\alpha \tag{23}$$

Because α is the complement of θ,

$$cos\alpha = \cos(90° - \theta) = sin\theta \tag{24}$$

So,

$$X^2 = L_c^2 + \left(R_c + \frac{T_w}{2}\right)^2 - 2L_c\left(R_c + \frac{T_w}{2}\right)sin\theta \tag{25}$$

Taking the square root of each side and recalling that $X = R_c + \frac{T_w}{2} - L_{proj}$ we obtain

$$X = \sqrt{L_c^2 + \left(R_c + \frac{T_w}{2}\right)^2 - 2L_c\left(R_c + \frac{T_w}{2}\right)sin\theta} = R_c + \frac{T_w}{2} - L_{proj} \tag{26}$$

Solving for L_{proj}, gives

$$L_{proj} = R_c + \frac{T_w}{2} - \sqrt{L_c^2 + \left(R_c + \frac{T_w}{2}\right)^2 - 2L_c\left(R_c + \frac{T_w}{2}\right)sin\theta} \quad \blacksquare \tag{27}$$

This equation gives an exact geometric relationship for the projected length of a rock vane as the shortest distance from the tip of the crest to the outer bank for a bend of constant top-width and radius of curvature.

Crest Length as a Function of Projected Length

When laying out rock vane configurations, it is useful to be able to determine crest length as a function of L_{proj}, θ, R_c, and T_w. Such a function is obtained by the following adventure in algebra:

Starting by squaring each side of Equation 26,

$$L_c^2 + \left(R_c + \frac{T_w}{2}\right)^2 - 2L_c\left(R_c + \frac{T_w}{2}\right) sin\theta = \left(R_c + \frac{T_w}{2} - L_{proj}\right)^2 \qquad (28)$$

Subtracting $\left(R_c + \frac{Tw}{2}\right)^2$ from each side and adding $\frac{\left(2\left(R_c + \frac{T_w}{2}\right) sin\theta\right)^2}{4} = \left(R_c + \frac{T_w}{2}\right)^2 \sin^2\theta$ to each side, then factoring the left-hand side yields,

$$\left(L_c - \left(R_c + \frac{T_w}{2}\right) sin\theta\right)^2 = \left(R_c + \frac{T_w}{2} - L_{proj}\right)^2 - \left(R_c + \frac{T_w}{2}\right)^2 + \left(R_c + \frac{T_w}{2}\right)^2 \sin^2\theta \qquad (29)$$

Expanding the first term on the right-hand side and simplifying,

$$\left(L_c - \left(R_c + \frac{T_w}{2}\right) sin\theta\right)^2 = L_{proj}^2 - 2L_{proj}\left(R_c + \frac{T_w}{2}\right) + \left(R_c + \frac{T_w}{2}\right)^2 \sin^2\theta \qquad (30)$$

Taking the square root of each side,

$$L_c - \left(R_c + \frac{T_w}{2}\right) sin\theta = -\sqrt{L_{proj}^2 - 2L_{proj}\left(R_c + \frac{T_w}{2}\right) + \left(R_c + \frac{T_w}{2}\right)^2 \sin^2\theta} \qquad (31)$$

Note that the negative square root is chosen on the right-hand side to give the shorter L_c necessary to produce a given L_{proj}. Solving for L_c,

$$L_c = \left(R_c + \frac{T_w}{2}\right) sin\theta - \sqrt{L_{proj}^2 - 2L_{proj}\left(R_c + \frac{T_w}{2}\right) + \left(R_c + \frac{T_w}{2}\right)^2 \sin^2\theta} \quad \blacksquare \qquad (32)$$

Maximum Possible Projected Length

Rock vanes installed at small planform angles are subject to very significant effects from channel curvature. As a result, the planform angle of a rock vane can limit its projected length i.e. extending the crest length may not continuously extend the projected length. While not likely

to be useful for practical design purposes, the equation derived in this section provides a geometric limit on the planform angle of rock vanes and helps explain why rock vanes lose effectiveness at very small angles.

The maximum projected length, $L_{proj\text{-}max}$, possible for a rock vane constructed at a given angle, θ, in a bend with constant top-width, T_w, and a constant radius of curvature, R_c, can be derived from the construction shown in Figure 61.

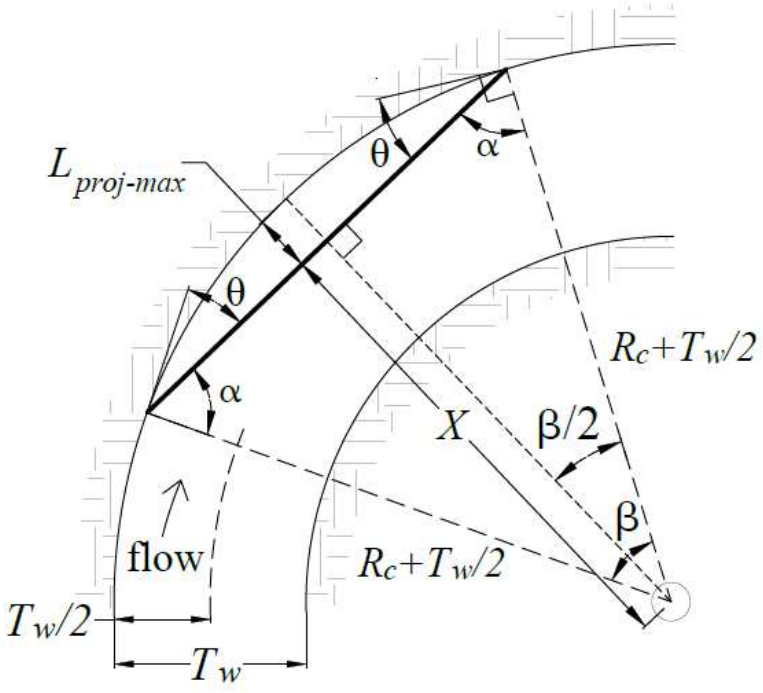

Figure 61. Geometric relationship of variables used to determine the maximum possible projected length for a given planform angle

The angle β is computed as

$$\beta = 180° - 2\alpha = 180° - 2(90° - \theta) = 180° - 180° + 2\theta = 2\theta \quad (33)$$

Therefore, $\frac{\beta}{2} = \theta$

From Figure 61,

$$L_{proj-max} = R_c + \frac{T_w}{2} - X \quad (34)$$

Rearranging,

$$X = R_c + \frac{T_w}{2} - L_{proj-max} \tag{35}$$

Examining Figure 61, by the definition of cosine,

$$\cos\left(\frac{\beta}{2}\right) = cos\theta = \frac{X}{R_c + \frac{T_w}{2}} \tag{36}$$

Substituting Equation 35 into Equation 36,

$$cos\theta = \frac{X}{R_c + \frac{T_w}{2}} = \frac{R_c + \frac{T_w}{2} - L_{proj-max}}{R_c + \frac{T_w}{2}} = 1 - \frac{L_{proj-max}}{R_c + \frac{T_w}{2}} \tag{37}$$

Rearranging to solve for $L_{proj\text{-}max}$, gives

$$cos\theta - 1 = -\frac{L_{proj-max}}{R_c + \frac{T_w}{2}} \tag{38}$$

$$L_{proj-max} = (1 - cos\theta)\left(R_c + \frac{T_w}{2}\right) \tag{39}$$

The maximum possible ratio of projected length to top-width is obtained by dividing both sides by T_w,

$$\frac{L_{proj-max}}{T_w} = \frac{1}{T_w}(1 - cos\theta)\left(R_c + \frac{T_w}{2}\right) \tag{40}$$

$$\frac{L_{proj-max}}{T_w} = (1 - cos\theta)\left(\frac{R_c}{T_w} + \frac{1}{2}\right) \blacksquare \tag{41}$$

Projected Slopes

The projection of a rock vane's geometry onto a cross-section perpendicular to the direction of flow is complicated by the curvature of the channel. Figure 62 shows the projection of a rock vane and associated coordinate system. The objective of the projection is to take every elevation, *z*, on the crest of the rock vane (the *y'* axis) and transfer it to a point on a cross-section

perpendicular to the direction of flow (the *y* axis). To accomplish this task, one must be able to determine the distance from the outer bank to each point along the crest of a rock vane.

For a rock vane, the elevation, *z*, of the vane at any point can be computed from the elevation of the water surface, z_0, the slope of the vane, $tan\phi$, and the distance from the waterline along the vane crest, *y*', by the expression

$$z = z_0 - y' tan\phi \quad for\ 0 \le y' \le L_c \tag{42}$$

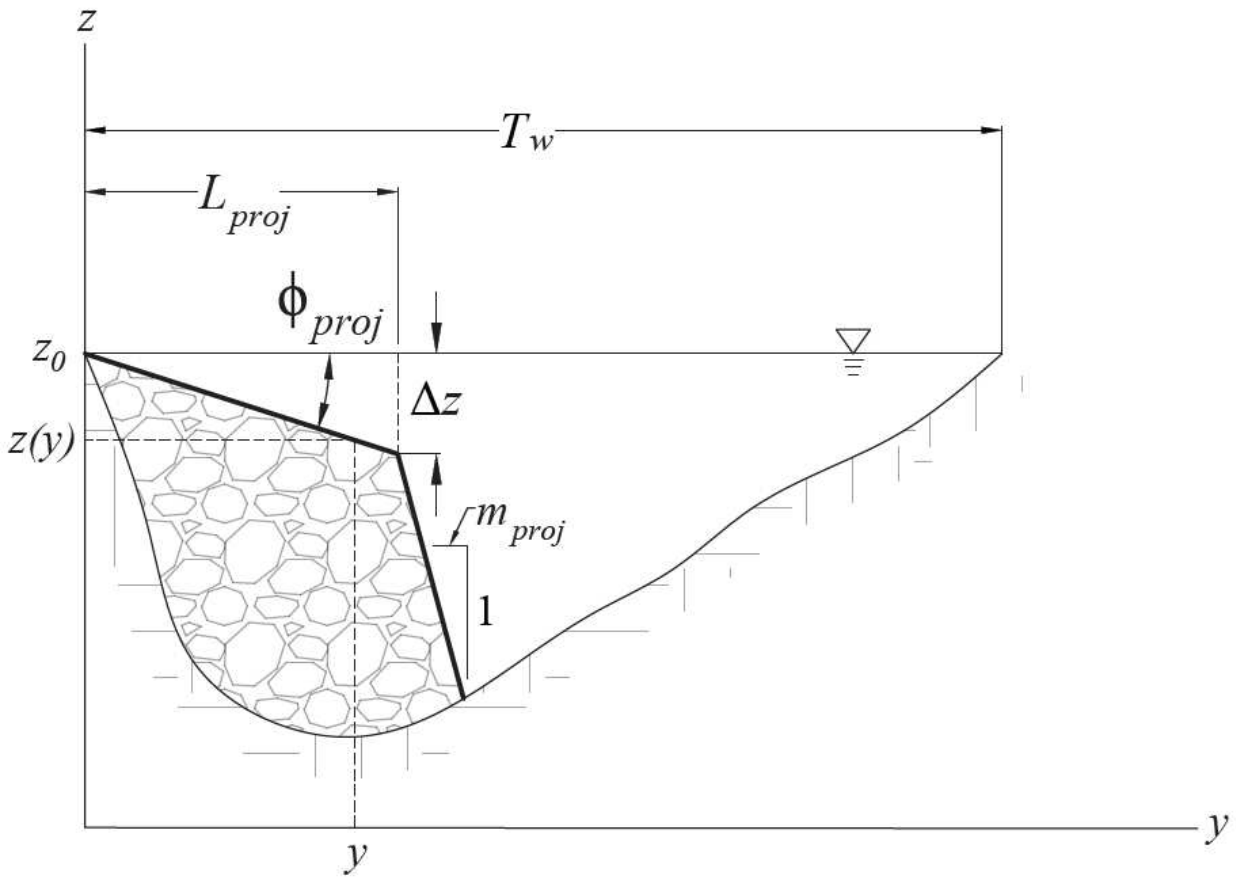

Figure 62. Projected view of a rock vane

The distance along the crest (*y'* axis) can be related to the distance from the outer bank (*y* axis) using Equation 32, as it is valid for any point on the rock vane, not just the tip of the crest. Substituting the variables *y* for L_{proj} and *y'* for L_c,

$$y' = \left(R_c + \frac{T_w}{2}\right) sin\theta - \sqrt{y^2 - 2y\left(R_c + \frac{T_w}{2}\right) + \left(R_c + \frac{T_w}{2}\right)^2 \sin^2\theta} \tag{43}$$

By substituting Equation 43 into Equation 42, the elevation of the vane crest can be computed at any point on the projected cross-section:

$$z = z_0 - \left[\left(R_c + \frac{T_w}{2}\right) sin\theta - \sqrt{y^2 - 2y\left(R_c + \frac{T_w}{2}\right) + \left(R_c + \frac{T_w}{2}\right)^2 \sin^2\theta}\right] tan\phi \tag{44}$$

$$for\ 0 \le y \le L_{proj}$$

Differentiating to obtain the slope of the crest at any point along the projected cross-section,

$$\frac{dz}{dy} = \left(\frac{y - \left(R_c + \frac{T_w}{2}\right)}{\sqrt{\left(R_c + \frac{T_w}{2}\right)^2 \sin^2\theta - 2y\left(R_c + \frac{T_w}{2}\right) + y^2}}\right) tan\phi \tag{45}$$

Because the slope is a function of *y*, the projected crest is not quite linear and its slope varies slightly along the *y* axis. However, the variation in slope is small and shall be neglected. The mean slope of the projected crest, denoted $tan(\phi_{proj})$, can simply be computed as the change in elevation divided by the projected length:

$$\tan\left(\phi_{proj}\right) = \frac{\Delta z}{L_{proj}} \quad \blacksquare \tag{46}$$

No general formula for the mean slope of the rock vane toe can be given, as the length of the toe depends on the cross-section of the channel. However, just like the projected crest slope, the projected toe slope is nearly constant. The instantaneous toe slope at the tip of a rock vane can be computed with the following procedure.

Substituting the toe slope, $1/m$ for the crest slope, $tan\phi$, in Equation 45 and evaluating it at $y = L_{proj}$,

$$\frac{dz}{dy} = \frac{1}{m}\left(\frac{L_{proj} - \left(R_c + \frac{T_w}{2}\right)}{\sqrt{\left(R_c + \frac{T_w}{2}\right)^2 \sin^2\theta - 2L_{proj}\left(R_c + \frac{T_w}{2}\right) + L_{proj}^2}}\right) \tag{47}$$

The projected toe slope of m_{proj} H:1V is expressed by $-1/m_{proj} = dz/dy$ so that,

$$m_{proj} = m\frac{\sqrt{\left(R_c + \frac{T_w}{2}\right)^2 \sin^2\theta - 2L_{proj}\left(R_c + \frac{T_w}{2}\right) + L_{proj}^2}}{\left(R_c + \frac{T_w}{2}\right) - L_{proj}} \tag{48}$$

The projected toe slope can also be expressed in terms of crest length,

$$m_{proj} = m\,\frac{\left(R_c + \frac{T_w}{2}\right)sin\theta - L_c}{\sqrt{L_c^2 - 2L_c\left(R_c + \frac{T_w}{2}\right)sin\theta + \left(R_c + \frac{T_w}{2}\right)^2}} \tag{49}$$

Equations 48 and 49 are both rather cumbersome. Considering the relatively small area blocked by the toe of a rock vane, not to mention the construction tolerances for riprap placement, a simpler formulation should be satisfactory for practical calculations. The effect of curvature can be neglected by taking the limit as R_c approaches infinity:

$$m_{proj} \approx \lim_{R_c \to \infty} m\,\frac{\left(R_c + \frac{T_w}{2}\right)sin\theta - L_c}{\sqrt{L_c^2 - 2L_c\left(R_c + \frac{T_w}{2}\right)sin\theta + \left(R_c + \frac{T_w}{2}\right)^2}} \tag{50}$$

Factoring the term $\left(R_c + \frac{T_w}{2}\right)$ out of the denominator, and moving the constant, m, out of the limit,

$$m_{proj} \approx m \lim_{R_c \to \infty} \frac{\left(R_c + \frac{T_w}{2}\right) sin\theta - L_c}{\left(R_c + \frac{T_w}{2}\right) \sqrt{\frac{L_c^2}{\left(R_c + \frac{T_w}{2}\right)^2} - \frac{2L_c sin\theta}{\left(R_c + \frac{T_w}{2}\right)} + 1}} \tag{51}$$

It is now clear that the term under the radical will approach one as R_c approaches infinity. The terming including L_c will therefore approach zero, leaving

$$m_{proj} \approx m \left[\lim_{R_c \to \infty} \frac{\left(R_c + \frac{T_w}{2}\right) sin\theta}{\left(R_c + \frac{T_w}{2}\right)} \right] = m * sin\theta \ \blacksquare \tag{52}$$

Equation 52, while an approximation, should be sufficient for practical applications.

Ratio of Projected Slope to Crest Slope

The ratio of the projected slope of a rock vane to the crest slope is of interest when considering the area of flow blocked by the rock vane. Rock vanes installed at small angles in tightly curved channels have projected slopes much steeper than their crest slopes, reducing the flow area blocked by the structures. A little bit of work on the equations previously derived can show that the ratio of projected slope to crest slope is a function of the ratios R_c/T_w, L_{proj}/T_w and the planform angle θ.

Starting from the definition of projected slope and recalling that $\Delta z = L_c tan\phi$, the ratio of the projected slope to crest slope can be evaluated as:

$$\frac{\tan(\phi_{proj})}{tan\phi} = \frac{\Delta z}{L_{proj}} \left(\frac{1}{tan\phi}\right) = \frac{\mathrm{L_c} tan\phi}{l_{proj} tan\phi} = \frac{L_c}{L_{proj}} \tag{53}$$

Substituting Equation 32 for L_c,

$$\frac{\tan(\phi_{proj})}{tan\phi} = \frac{\left(R_c + \frac{T_w}{2}\right) sin\theta - \sqrt{L_{proj}^2 - 2L_{proj}\left(R_c + \frac{T_w}{2}\right) + \left(R_c + \frac{T_w}{2}\right)^2 \sin^2\theta}}{L_{proj}} \tag{54}$$

Factoring out T_w and simplifying,

$$\frac{\tan(\phi_{proj})}{tan\phi} = \frac{T_w\left(\frac{R_c}{T_w}+\frac{1}{2}\right)sin\theta - T_w\sqrt{\left(\frac{L_{proj}}{T_w}\right)^2 - 2\frac{L_{proj}}{T_w}\left(\frac{R_c}{T_w}+\frac{1}{2}\right)+\left(\frac{R_c}{T_w}+\frac{1}{2}\right)^2\sin^2\theta}}{L_{proj}} \quad (55)$$

$$\frac{\tan(\phi_{proj})}{tan\phi} = \frac{T_w}{L_{proj}}\left(\frac{R_c}{T_w}+\frac{1}{2}\right)sin\theta - \sqrt{1-\frac{2T_w}{L_{proj}}\left(\frac{R_c}{T_w}+\frac{1}{2}\right)+\left(\frac{T_w}{L_{proj}}\right)^2\left(\frac{R_c}{T_w}+\frac{1}{2}\right)^2\sin^2\theta} \blacksquare (56)$$

APPENDIX B. PROCEDURE FOR CREATING 3D ROCK VANE AND BENDWAY WEIR MODELS

The procedure for creating the 3D models of bendway weirs and rock vanes used in the numerical model is based on Amanda Cox's 2015 method. The procedure has been modified to take advantage of new features in AutoCAD Civil3D to simplify the workflow.

Preliminary Steps

Before creating 3D models of each structure, an AutoCAD Civil3D file must be set up containing a surface with the channel topography used for the modelling. The coordinate system used for the surface in this study is the same as the coordinate system used for the physical model studies.

The waterline of the channel without structures installed should be located and an alignment created along the waterline that will be used to cut cross-sections. For ease of data extraction, the direction of the alignment should be such that the structures are always on the right side of the alignment. For the S-curve in the present study, the alignment in the upstream bend was created on the left bank of the channel with the alignment running in the downstream direction. The alignment for the downstream bend was created on the right bank with the alignment oriented in the upstream direction.

Finally, the centerline of each bendway weir or rock vane structure should be located in plan view based on the spacing criteria for the configuration.

Step 1: Extract Cross-Section

With the AutoCAD file set up to be working in plan view, cross-sections can be extracted along the centerline of each structure.

a. Create a sample line on the appropriate alignment (CREATESAMPLELINE), selecting the station as the point where the structure centerline intersects the edge of the water. Specify the left swath as zero and the right swath as any value longer than the structure crest length.

b. If the structure is not perpendicular to the edge of the water ($\theta \neq 90°$), use the grips on the end of the sample line to align it with the centerline of the structure. (The ROTATE command does not work on sample lines). It may be useful to draw a construction line (XLINE) along the centerline of the structure so the sample line remains longer than the structure crest length.

c. Create a section view for the sample line with the CREATESECTIONVIEW command. Select the desired sample line, then click “Create Section View” and place the section view at a convenient location in the drawing.

d. Export the cross-section data to Excel by selecting the cross-section in the section view, then right clicking and selecting "Edit Section…" Right click in the window and select "Copy All".

   NOTE: The Civil3D surface is so dense, 3 or 4 decimal places may be required for adequate display. To change the section precision in AutoCAD Civil 3D, open the Toolspace, go to the Settings tab, right click on Section, select Edit Feature Settings, and change the distance precision.

Step 2: Locate the Structure in Excel

a. Create a new structure design Excel file.

b. Paste the data from AutoCAD into cell A1 of the “Structure XS” sheet.

c. Columns A-E of the "Structure XS" sheet contain raw data from AutoCAD, columns H and I contain the coordinates of the points on the cross-section formatted as numbers, and columns K-M contain data formatted for export back to AutoCAD.

d. The "Structure Design" sheet shows the layout of a structure and contains calculations to determine the structure geometry and locate the structure in the channel.

   NOTE: Some of the formulas are specific to a particular configuration and will need to be modified to construct different configurations.

e. Once the appropriate values and formulas for a particular configuration has been entered into the "Structure Design" sheet, the values highlighted in green on the "Structure XS" sheet indicate the portion of the channel located under the structure.

f. Select the points under the structure in columns K-M of the "Structure XS" sheet and copy them.

Step 3: Import a PolyLine of the Channel under the Structure to Civil 3D

With the portion of the channel cross-section under the rock vane or bendway weir now located, the coordinates of the points under the structure can be transformed into the Civil3D file coordinate system and imported into the CAD file as a polyline.

a. Open a copy of VaneDesigns Excel File. Paste the copied data from Step 2f into the input column.

b. In Civil3D, draw a line starting from the intersection of the structure crest with the edge of water. The line should have a length equal to the crest length of the structure and should be in the same direction as the sample line used to create the cross-section in Step 1.

c. View the properties of the new line in AutoCAD. Copy the Start X, Start Y, and Angle values to the Start X, Start Y, and Phi columns in the VaneDesigns Spreadsheet. The coordinates in the Output columns of the VaneDesign spreadsheet are now ready for export back to AutoCAD (Figure 63).

Rotation and Transpose Calculation								
INPUT				OUTPUT				
x	y	z	x	y	z	Phi	Start X	Start Y
0	0	98.5262	27.3258	91.0342	98.5262	1.7167	27.3258	91.0342
0.1	0	98.4728	27.42576	91.0372	98.4728			
0.2	0	98.4012	27.52571	91.04019	98.4012			
0.3	0	98.345	27.62567	91.04319	98.345			
0.4	0	98.2824	27.72562	91.04618	98.2824			
0.5	0	98.2215	27.82558	91.04918	98.2215			
0.6	0	98.1602	27.92553	91.05217	98.1602			
0.7	0	98.1089	28.02549	91.05517	98.1089			

Figure 63. Example of coordinate transformation in Excel.

d. Run the DatatoCSV macro in the VaneDesign Spreadsheet. This will create a .csv file called "VaneXX.csv" located here: \\nasstore2.engr.colostate.edu\projects\hydra\aqua\Active Projects\BOR-ALBUQUERQUE\FLOW-3D Modeling\12 Seth Flow 3D Numerical Simulation\Structure Design

e. Open the csv file in notepad and add the text "3DPOLY" above the first line. Save and close the file.

f. Change the file extension from .csv to .scr with windows explorer.

g. In AutoCAD, run the SCRIPT command. Select the script file saved in step f and click OK to import it into AutoCAD. Object snapping may need to be disabled for this work properly; this can be accomplished by pressing F3.

Step 4: Drafting the Structure Civil 3D

a. Select the line created in Step 2b and set its Start Z and End Z coordinates to the crest elevation of the structure specified in the structure design Excel file in Step 2.
b. Offset the line created in Step a by 0.5 ft, twice on each side.
c. Create an arc with its start point at the end of the lower most line created by offsetting, its middle point at the end of the polyline imported in Step 3g, and its end at the end of the upper most line created by offsetting.
d. Move the arc to the elevation of the toe of the structure.
e. Draw a line from the highest point on the polyline import in step 3h to the end of the centerline of the structure crest. This line delineates the top of the structure.
f. Copy the line created in step e four times, using its lower point as the base point, and placing a copy at the end of each line created in step b.
g. Copy the polyline imported in step 3g, using its highest point as the base point and placing copies at the highest point on the outer two lines created in step f, those 1 ft on either side of the centerline.
h. Draw a line across the top of the structure.
i. Draw a line connecting the lower end points of the lines 0.5 ft on either side of the center line created in step f.
j. Delete the lines no longer needed.
k. In plan view, trim the arc and the outer polylines of the vane structure.

Step 5: Creating Points along the Structure

a. Using AutoCAD's "MEASURE" command, create points spaced 0.0625 ft along each line of the structure. Unfortunately, this command must be run separately for each

geometric element; however, the up arrow can be used to repeat the previous command and insert the previous spacing distance.

Step 6: Converting AutoCAD Points to Surface Points

a. Open the tool space (TOOLSPACE) and make sure the drawing contains no points. If it does, delete them before the next step.

b. Run the CREATEPTCONVERTADESKPTS command and select all of the points created in Step 5 to convert the AutoCAD points to surface points

c. In the Points Creation section of the Edit Point Settings dialog box, set the Prompt for Descriptions Property to "None". This prevents AutoCAD from manually prompting you for a description for every point (Figure 64).

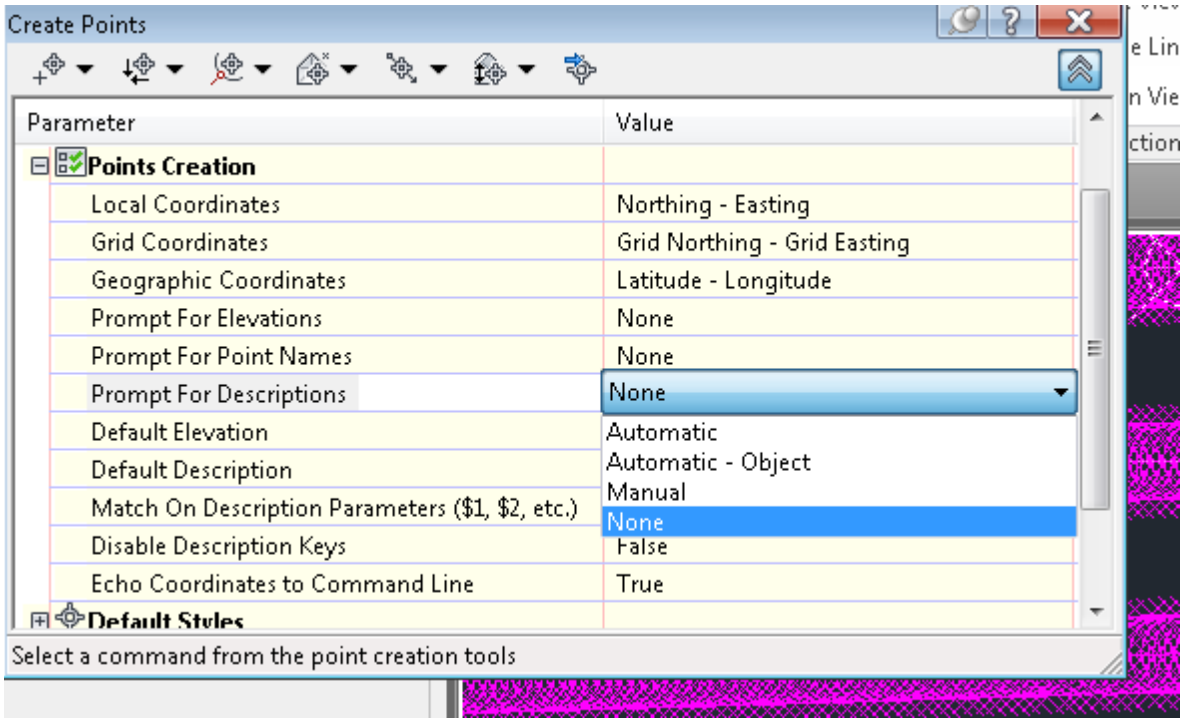

Figure 64. Window for turning off prompt for point description

Step 7: Creating a Surface from the AutoCAD Points

a. Under the "Prospector" tab of the "Toolspace", right click on "Surfaces" and select "Create Surface". Select "Elevation Banding 2D" as the surface style and click OK.

b. Expand the plus sign next to "Surfaces" in the "Prospector" tab of the "Toolspace"; expand the plus sign next to the new surface; and expand the plus sign next to "Definition".

c. Right click on "Point Groups", click "Add…" select the "_All Points" groups, and click OK. This create a new surface using all of the points created in Step 6 (Figure 65).

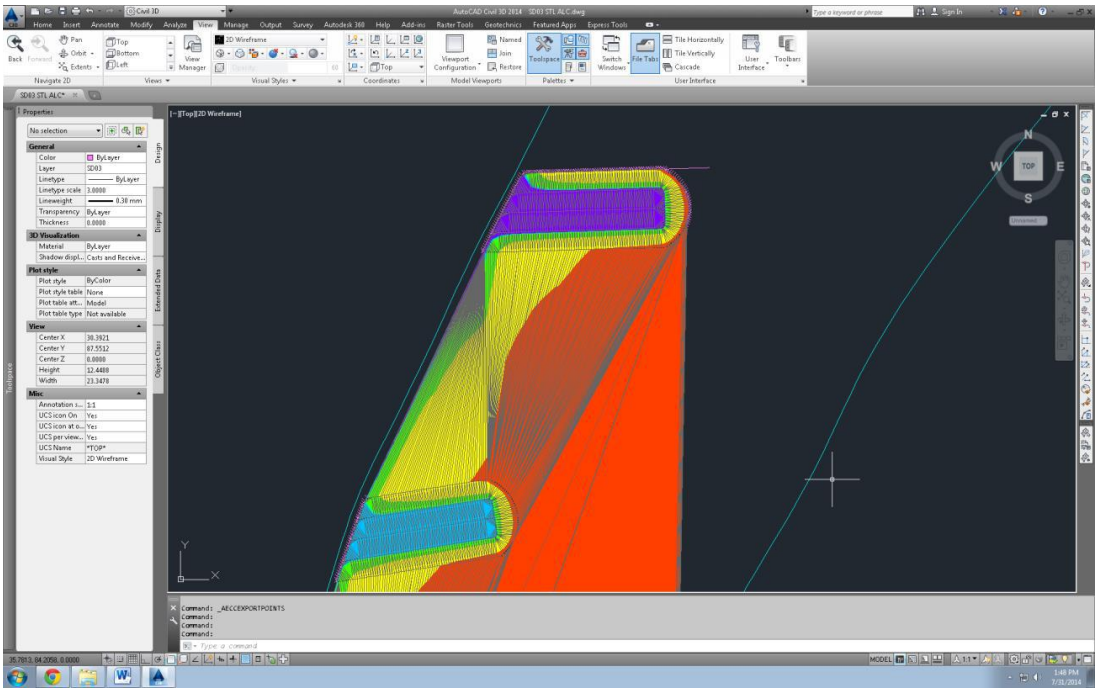

Figure 65. Plan view after surface creation (Step 7)

Step 8: Clean and Smooth the Surface

a. Under the "Modify" tab of AutoCAD, select "Surface". This will open a toolbar ribbon for surfaces at the top of the screen. Click on "Edit Surface" and select "Delete Line". Select the lines that should not be included in the structures and delete them (Figure 66).

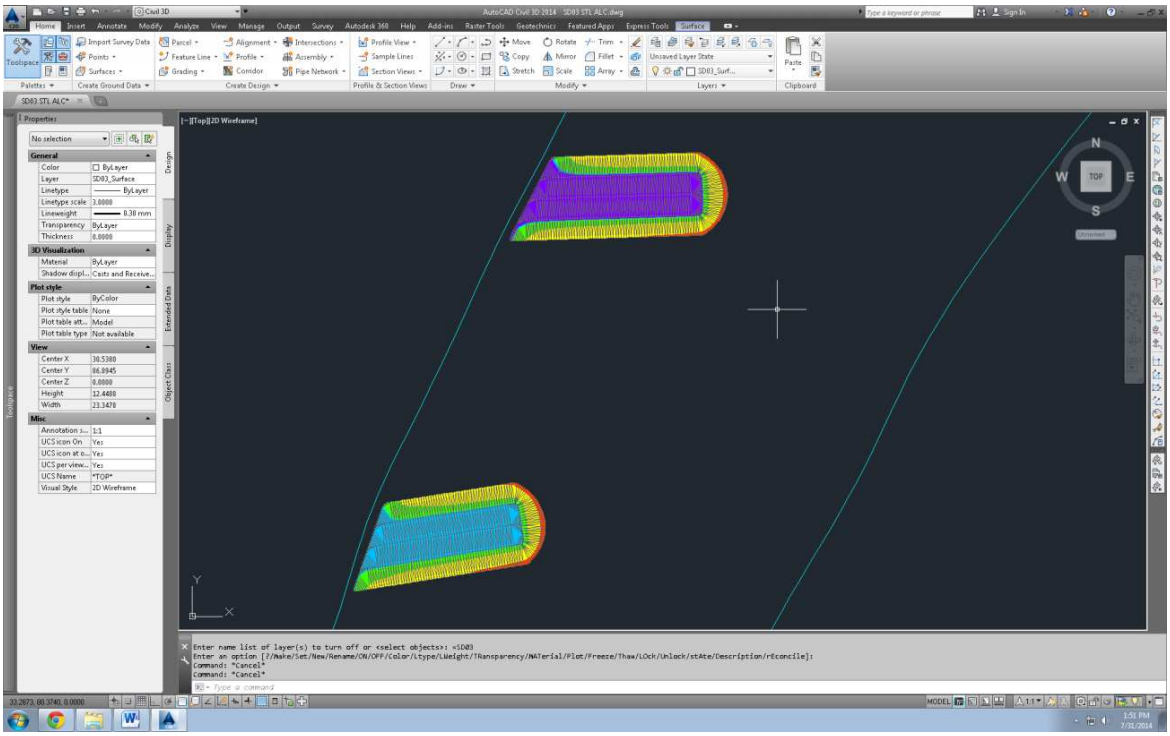

Figure 66. Plan view after deleting erroneous surface lines (Step 8a)

b. Once the extra lines are deleted, smooth the surface to create a grid of points at a spacing of 0.0625 ft (creates four segments of the top of a 3.0”-diameter rock) by clicking “Edit Surface” and select “Smooth Surface”. A “Smooth Surface” window will appear.

c. Select “Surface” for the output region (click the “…” at the far right of the input field and then type “S”).

d. Specify 0.0625 for both the Grid X and Grid Y spacing and click “OK” (Figure 67). The smooth surface should look like Figure 68.

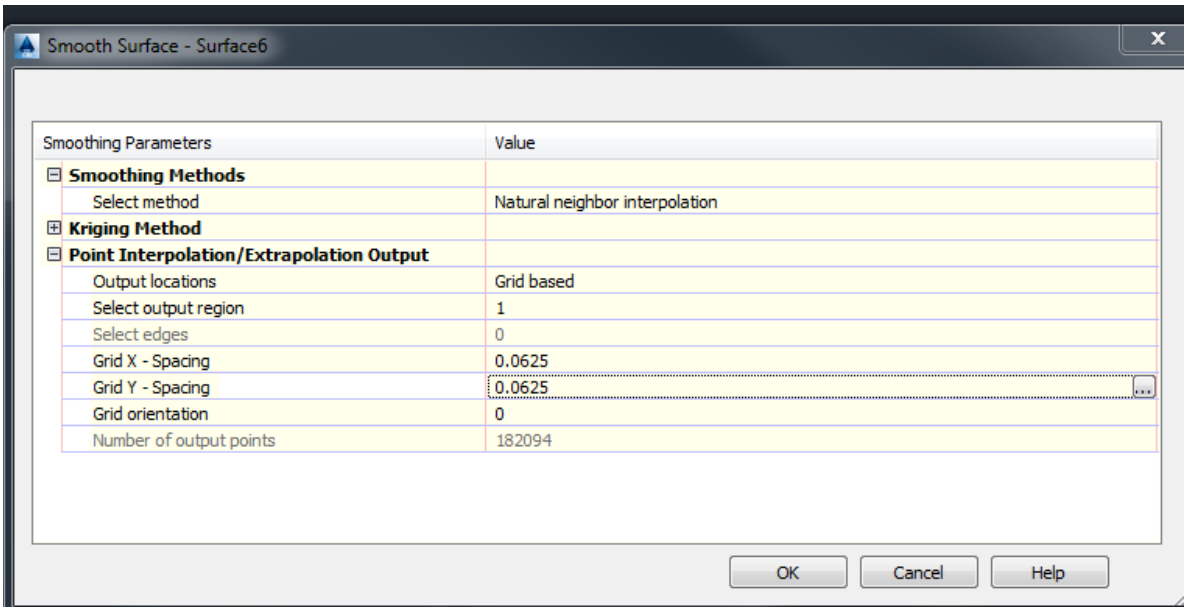

Figure 67. Smooth Surface inputs

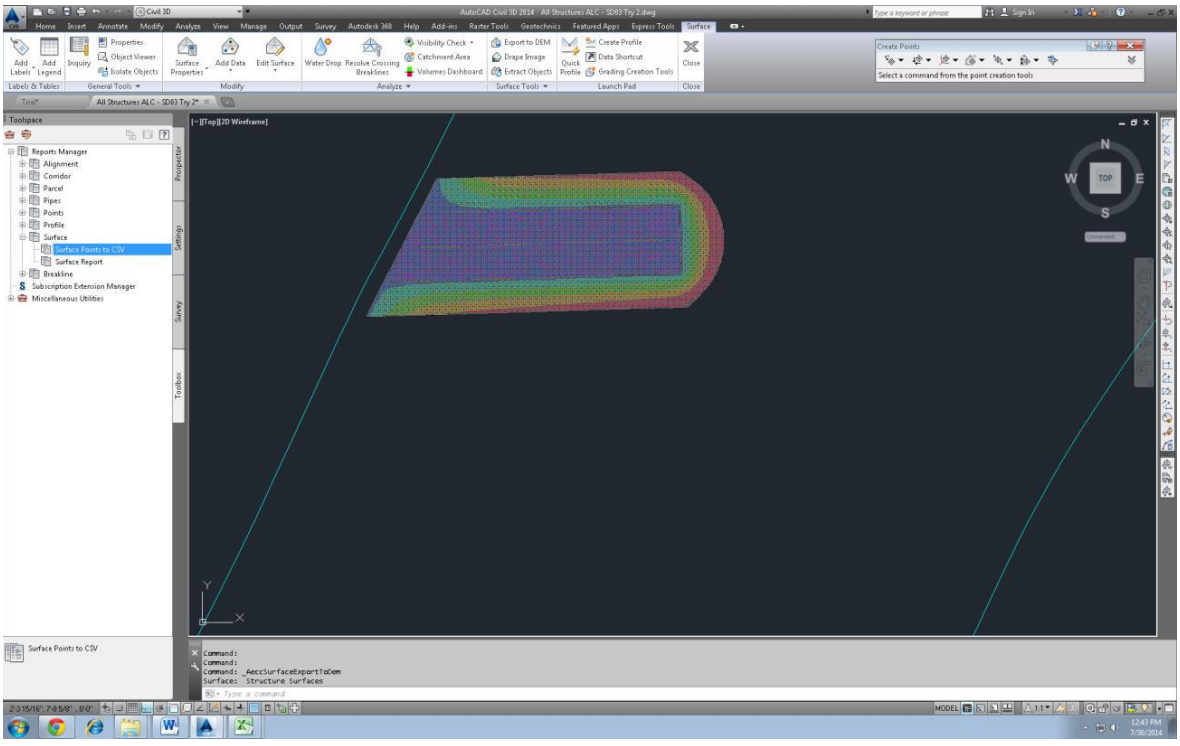

Figure 68. Plan view after smoothing the structure surface (Step 8d)

Step 9: Creating a Riprap Texture

The surface created in Step 8 is a 3D representation of the structures. However, to more realistically match structures constructed from rock riprap, a rough riprap texture must be added to the surface.

a. Select the "Toolbox" tab on the "Toolspace" window. Expand the plus sign next to "Reports Manager", expand the plus sign next to "Surface", and then click "Surface Points to CSV". Remove all check marks in the "Export to XML Report" window except the one next to the surface created in Step 7. Leave all other default settings the same. A .csv file should automatically open in Excel. Figure 69 shows an example of the "Export to XML Report".

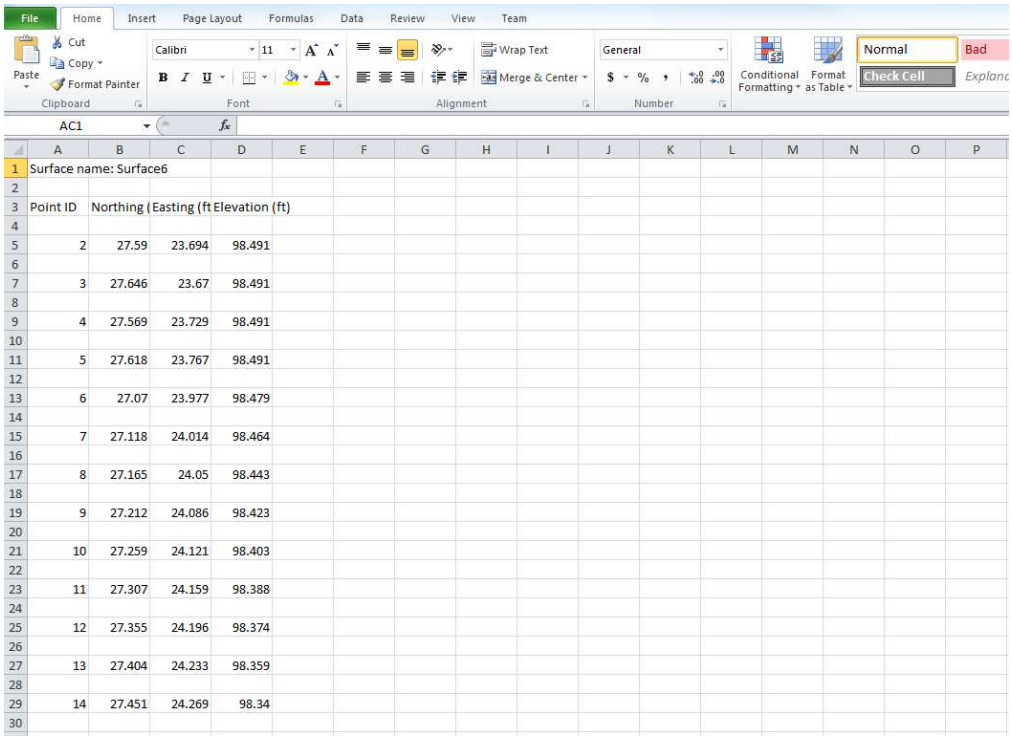

	A	B	C	D
1	Surface name: Surface6			
2				
3	Point ID	Northing (	Easting (ft	Elevation (ft)
4				
5	2	27.59	23.694	98.491
6				
7	3	27.646	23.67	98.491
8				
9	4	27.569	23.729	98.491
10				
11	5	27.618	23.767	98.491
12				
13	6	27.07	23.977	98.479
14				
15	7	27.118	24.014	98.464
16				
17	8	27.165	24.05	98.443
18				
19	9	27.212	24.086	98.423
20				
21	10	27.259	24.121	98.403
22				
23	11	27.307	24.159	98.388
24				
25	12	27.355	24.196	98.374
26				
27	13	27.404	24.233	98.359
28				
29	14	27.451	24.269	98.34
30				

Figure 69. Export to XML report open in Excel

b. Delete the header rows above the point data in the "Export to XML Report" file then copy and paste the elevation values in Column D of the "Export to XML Report" into

Column C of the preformatted Excel riprap surfaces macro. A copy of the macro file is located here: \\nasstore2.engr.colostate.edu\projects\hydra\aqua\Active Projects\BOR-ALBUQUERQUE\FLOW-3D Modeling\12 Seth Flow 3D Numerical Simulation\3D Structure AutoCad\Riprap Macro.xlsm

c. Click the duck icon to compute new elevations for the riprap surface (Figure 70). The elevation calculation macro uses a random number generator to determine the elevation changes to simulate irregular-shaped riprap with a median diameter of 0.25 ft.

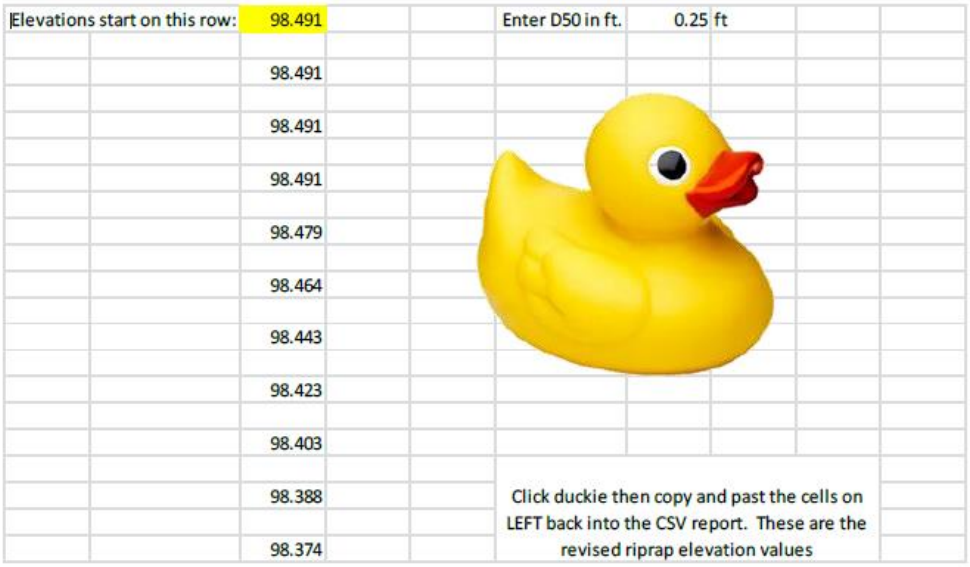

Figure 70. Riprap macro spreadsheet with the duck icon

d. Copy and paste the updated elevation cells from Column C to overwrite the original elevation values in Column D of the "Export to XML Report" file (Figure 71).

e. Delete the left column of point numbers and save the file using the name: "VaneXXriprap.csv". Close the file in Excel.

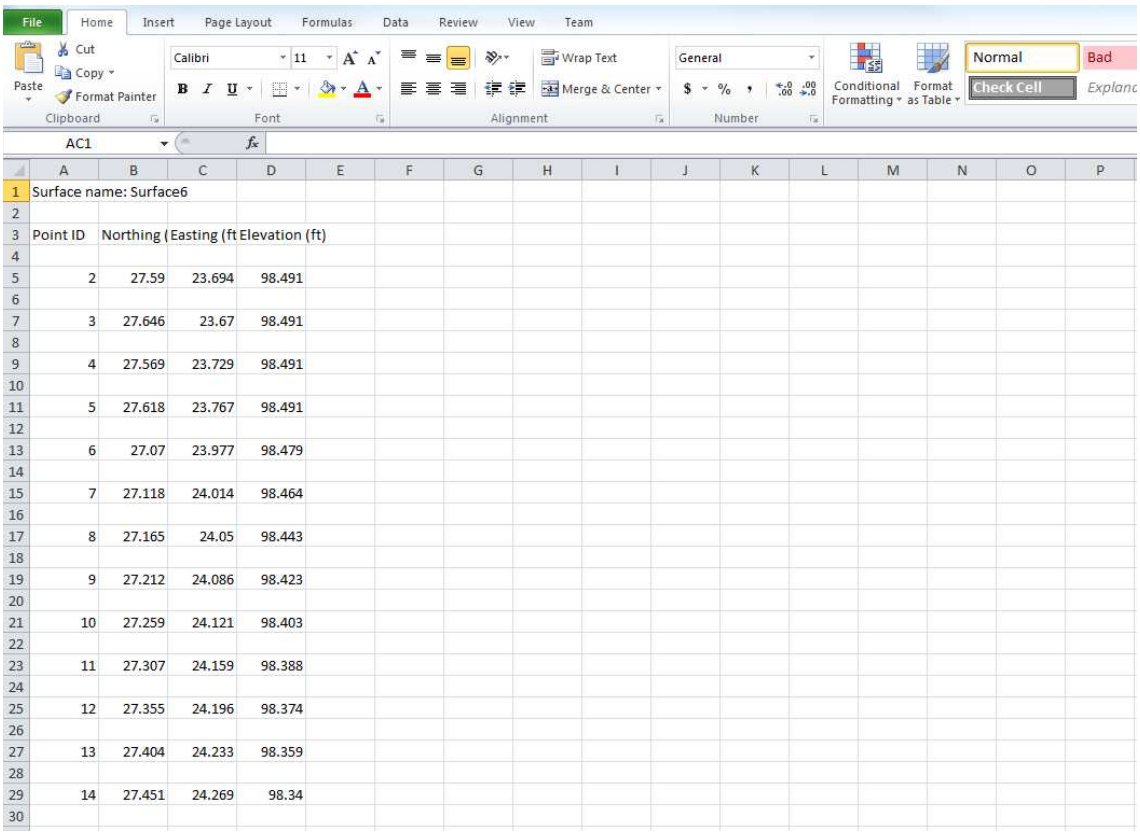

	A	B	C	D
1	Surface name: Surface6			
2				
3	Point ID	Northing (	Easting (ft	Elevation (ft)
4				
5	2	27.59	23.694	98.491
6				
7	3	27.646	23.67	98.491
8				
9	4	27.569	23.729	98.491
10				
11	5	27.618	23.767	98.491
12				
13	6	27.07	23.977	98.479
14				
15	7	27.118	24.014	98.464
16				
17	8	27.165	24.05	98.443
18				
19	9	27.212	24.086	98.423
20				
21	10	27.259	24.121	98.403
22				
23	11	27.307	24.159	98.388
24				
25	12	27.355	24.196	98.374
26				
27	13	27.404	24.233	98.359
28				
29	14	27.451	24.269	98.34
30				

Figure 71. Export to XML report after pasting in the values from the riprap macro

Step 10: Create a new Surface with Riprap Texture

a. Under the “Prospector” tab of the “Toolspace”, right click on “Surfaces” and select “Create Surface”. Select “Elevation Banding 2D” as the surface style and click OK.

b. Expand the plus sign next to “Surfaces” in the “Prospector” tab of the “Toolspace”; expand the plus sign next to the new surface; and expand the plus sign next to “Definition”.

c. Right click on “Point Files” and select “Add”. Select the “VaneXXriprap.csv” file created in Step 9 and select “NEZ (comma delimited)” for the point file format. Leave all other options set to the default option and select OK.

d. Remove surface lines that should not be in the three-dimensional structures. Under the “Modify” tab of AutoCAD, select “Surface”. This will open a toolbar ribbon for surfaces at the top of the screen. Click on “Edit Surface” and select “Delete Line”. Select each of the lines to be deleted and pressed “Enter”.

Step 11: Extract Solid Objects from the Surface

a. In the Modify Ribbon, click Surface, then, under the Extract from Surface drop-down, select Extract Solids from Surface.
b. Select the surface containing the structures with a riprap texture, set the depth to 3 ft (this is somewhat arbitrary), change the layer if desired, and then click OK. New solids should generate quickly.

Step 12: Transforming to the FLOW-3D Model Coordinate System

Up to this point, all work has been done in the coordinate system used to map the physical hydraulic model. The structures must now be transformed to align with the numerical model's coordinate system in FLOW-3D.

a. Select all of the structures and rotate them by -38.543° about the origin.
b. Select the structures again and move them 2.1916 ft in the x direction and 25.4035 in the y direction.

Step 13: Exporting to an STL File

a. Type in "EXPORT" to AutoCAD's command line. Specify the file type as .stl and select the location and file name of the exported file.
b. Select all of the structures, press ENTER, and the STL file will be created.

APPENDIX C. DEPTH-AVERAGED VELOCITY PLOTS

This appendix presents plots of steady state depth-averaged velocity for the tested configurations of rock vanes and bendway weirs.

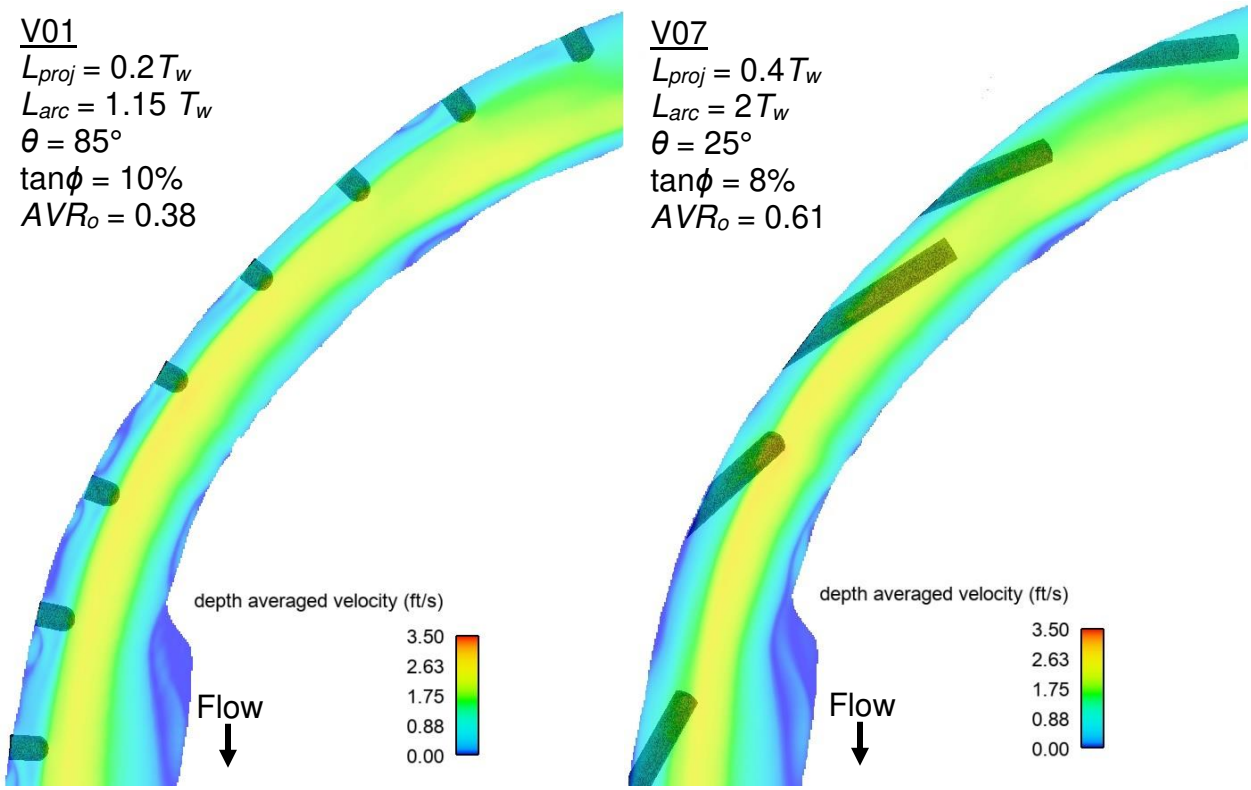

Figure 72. Steady state depth-averaged velocity for rock vane configurations V01 and V07

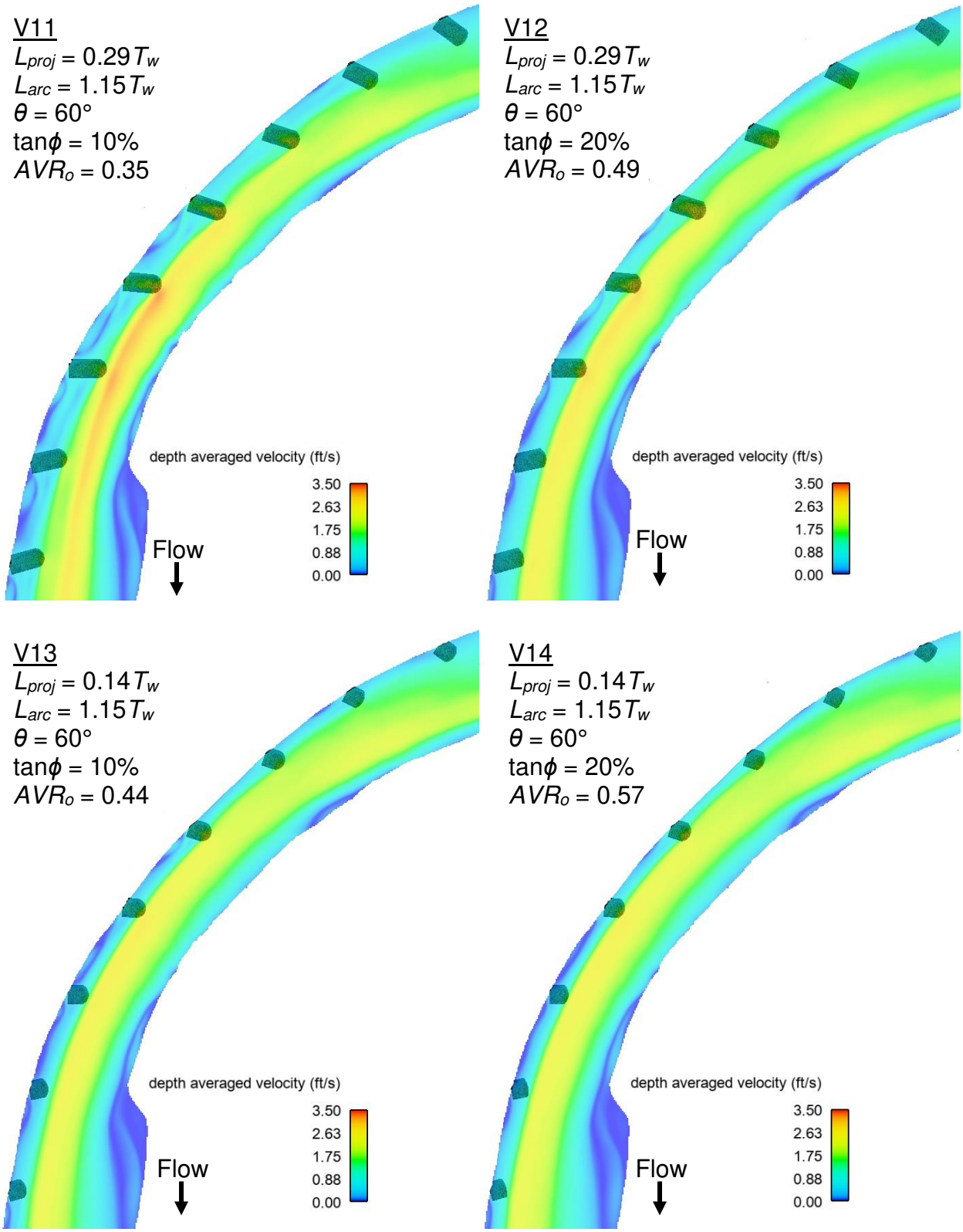

Figure 73. Steady state depth-averaged velocity for rock vane configurations V11-V14

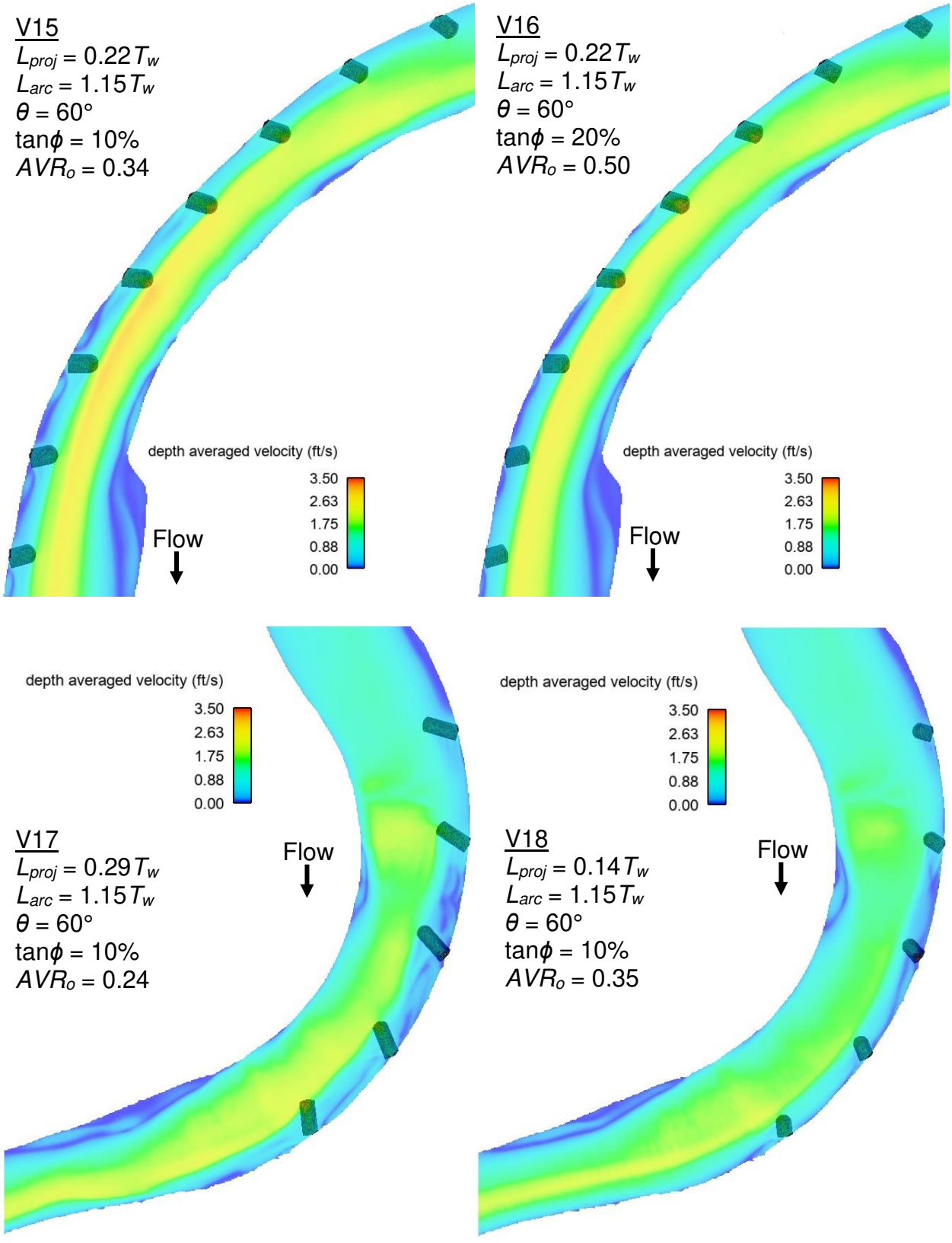

Figure 74. Steady state depth-averaged velocity for rock vane configurations V15-V18

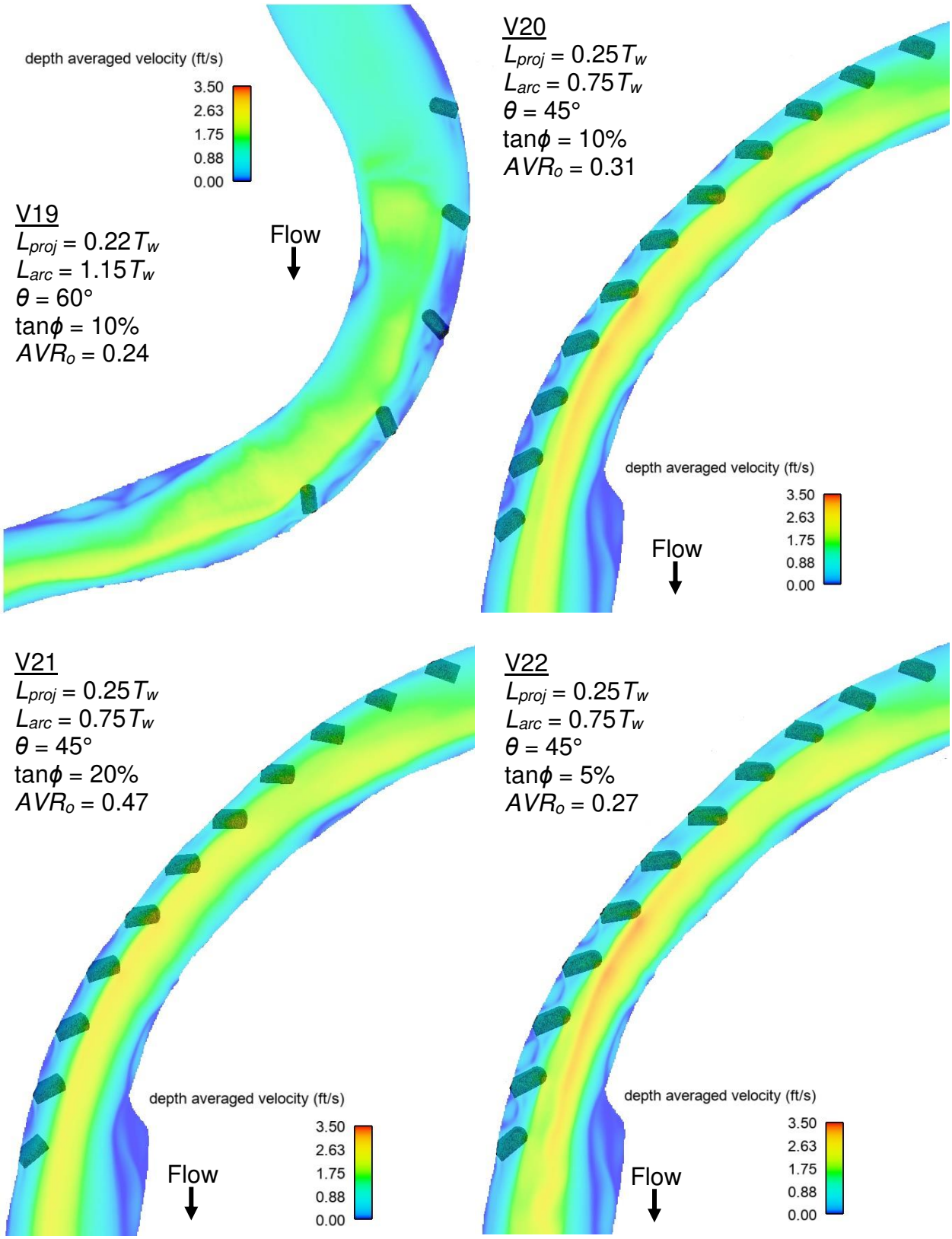

Figure 75. Steady state depth-averaged velocity for rock vane configurations V19-V22

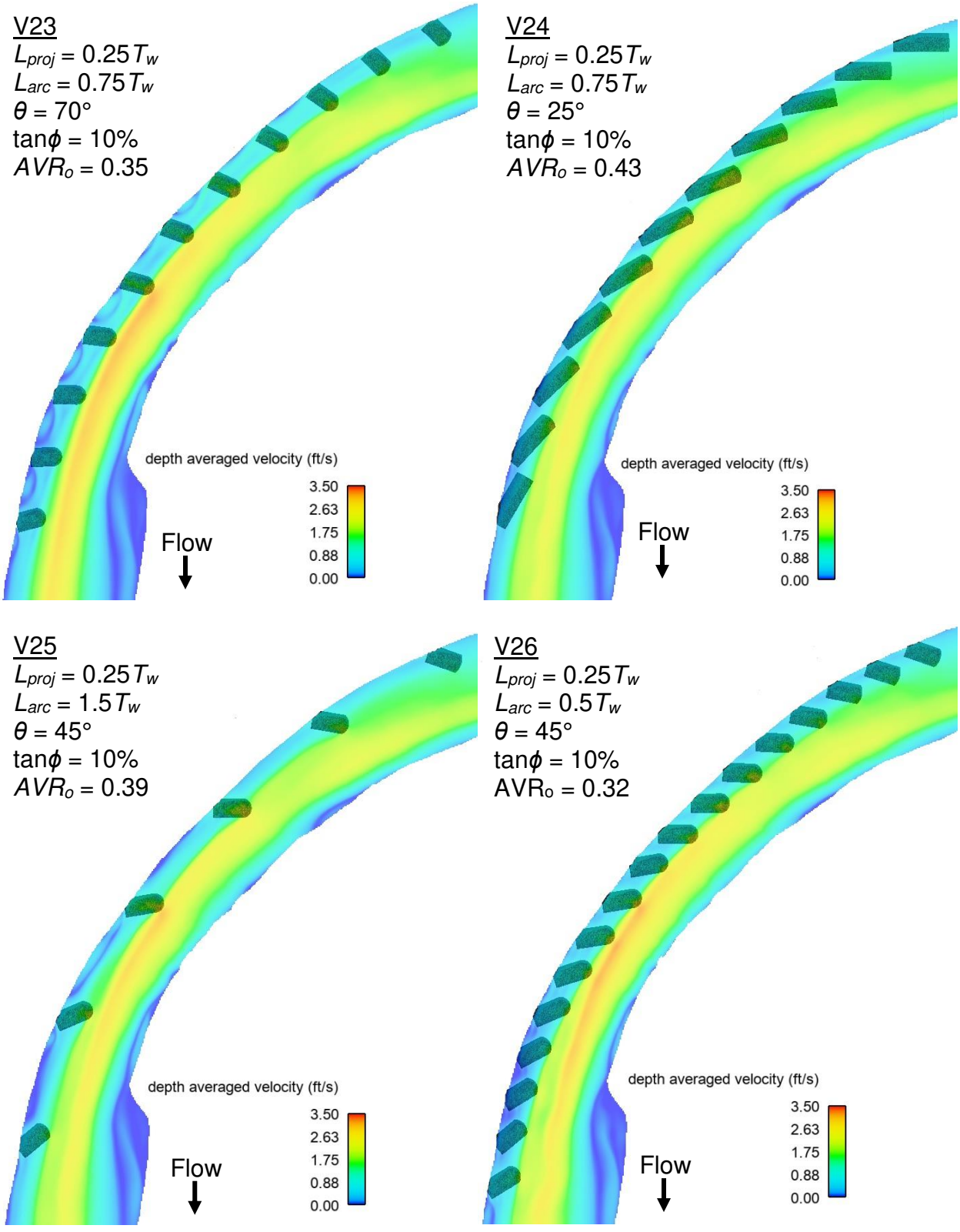

Figure 76. Steady state depth-averaged velocity for rock vane configurations V23-V26

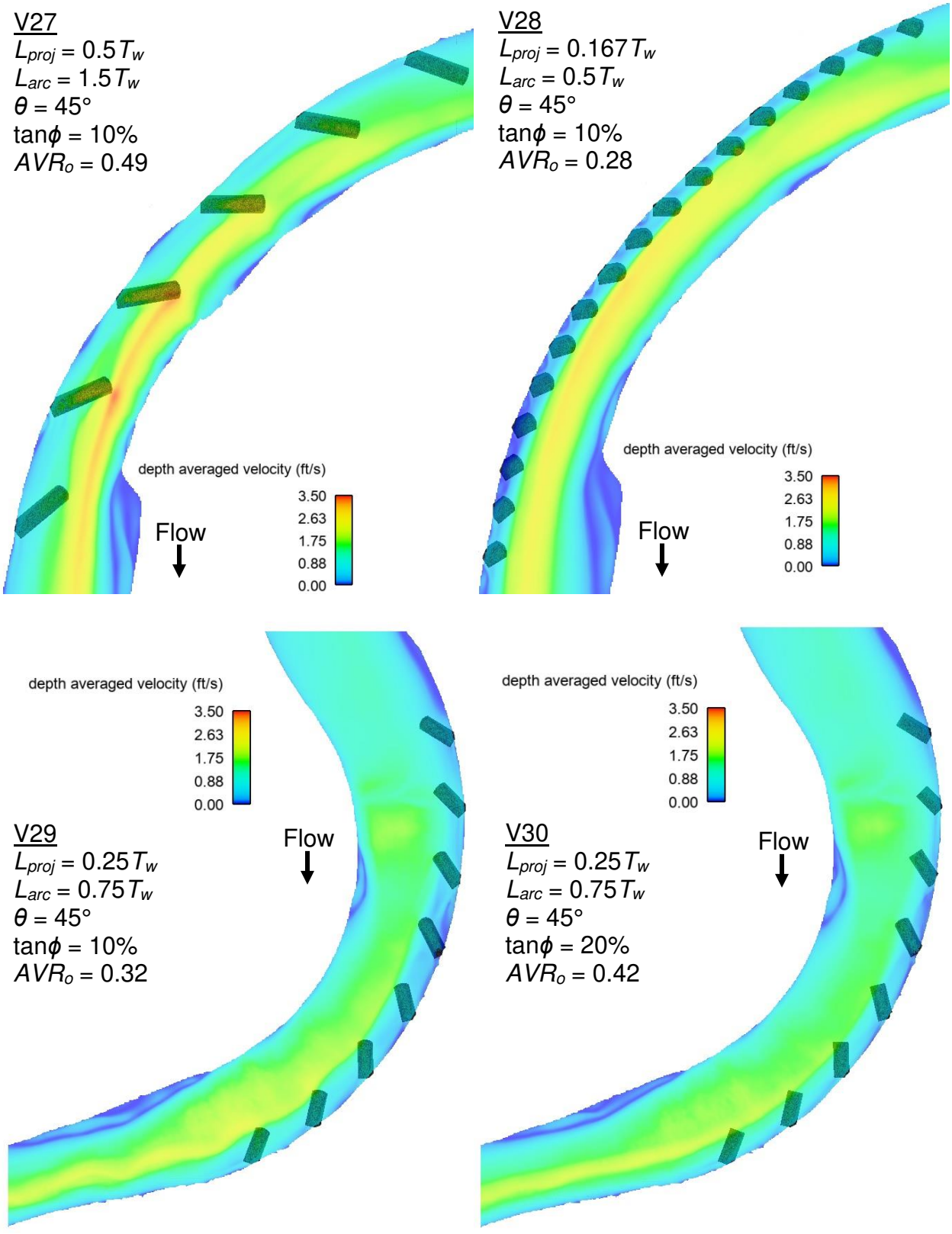

Figure 77. Steady state depth-averaged velocity for rock vane configurations V27-V30

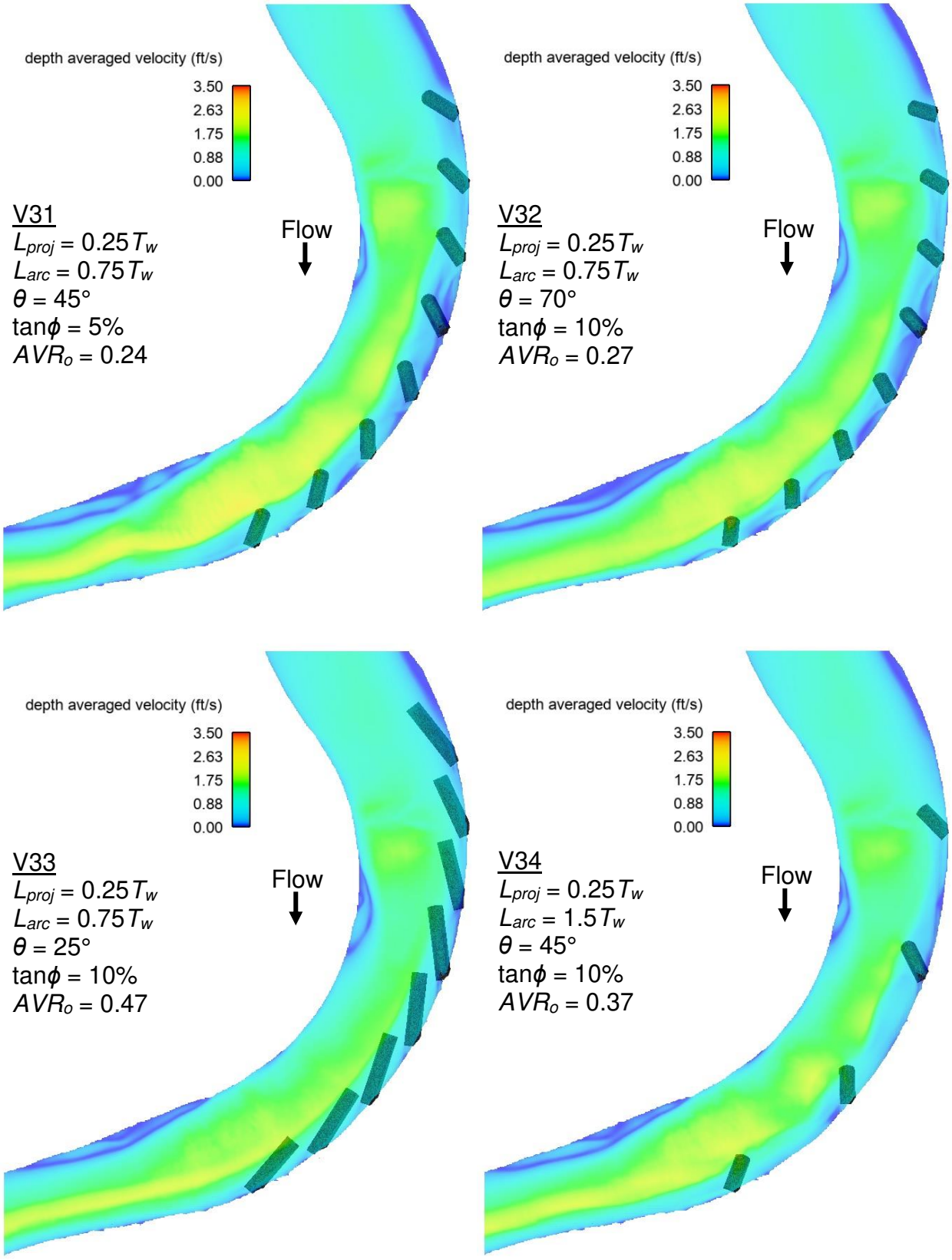

Figure 78. Steady state depth-averaged velocity for rock vane configurations V31-V34

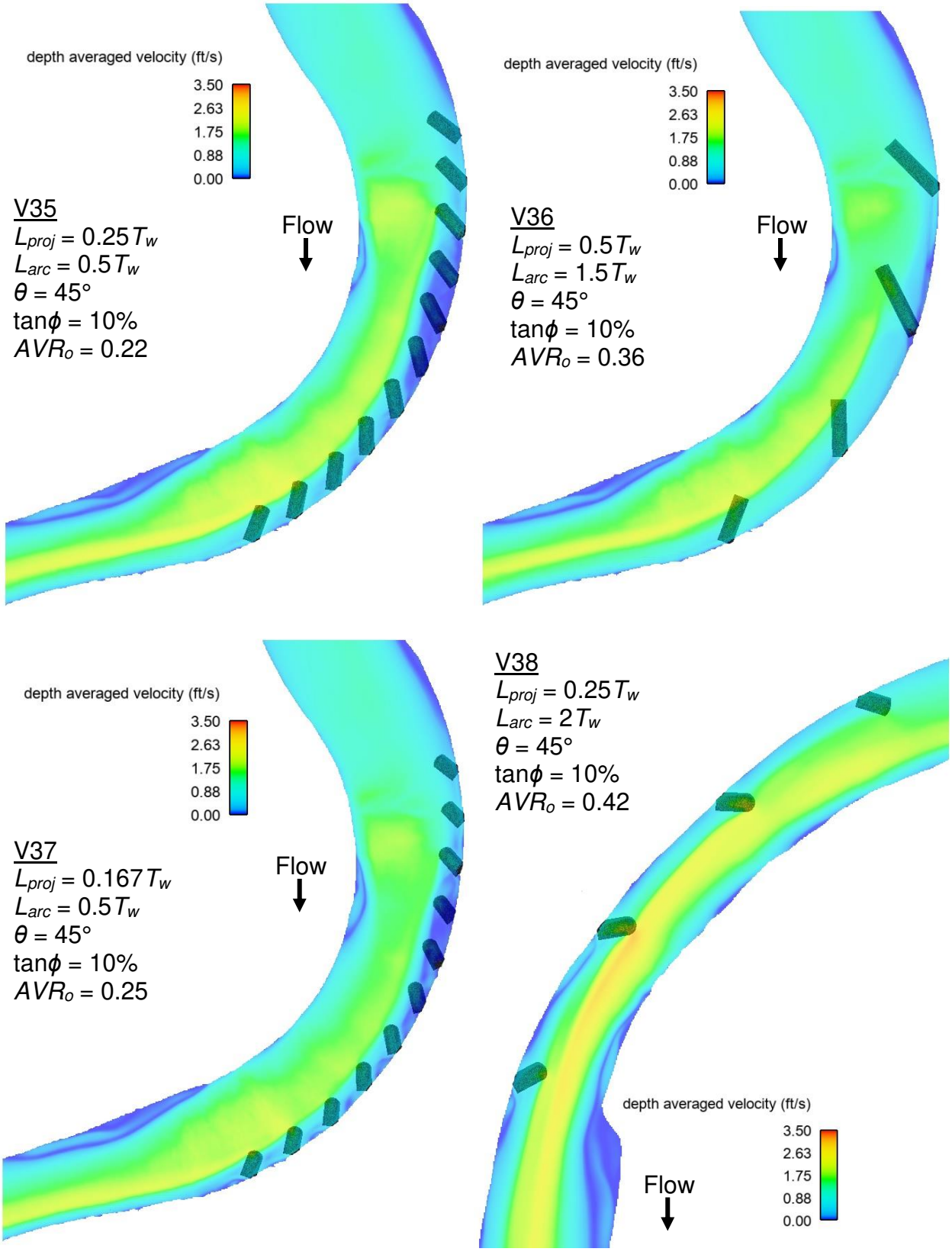

Figure 79. Steady state depth-averaged velocity for rock vane configurations V35-V38

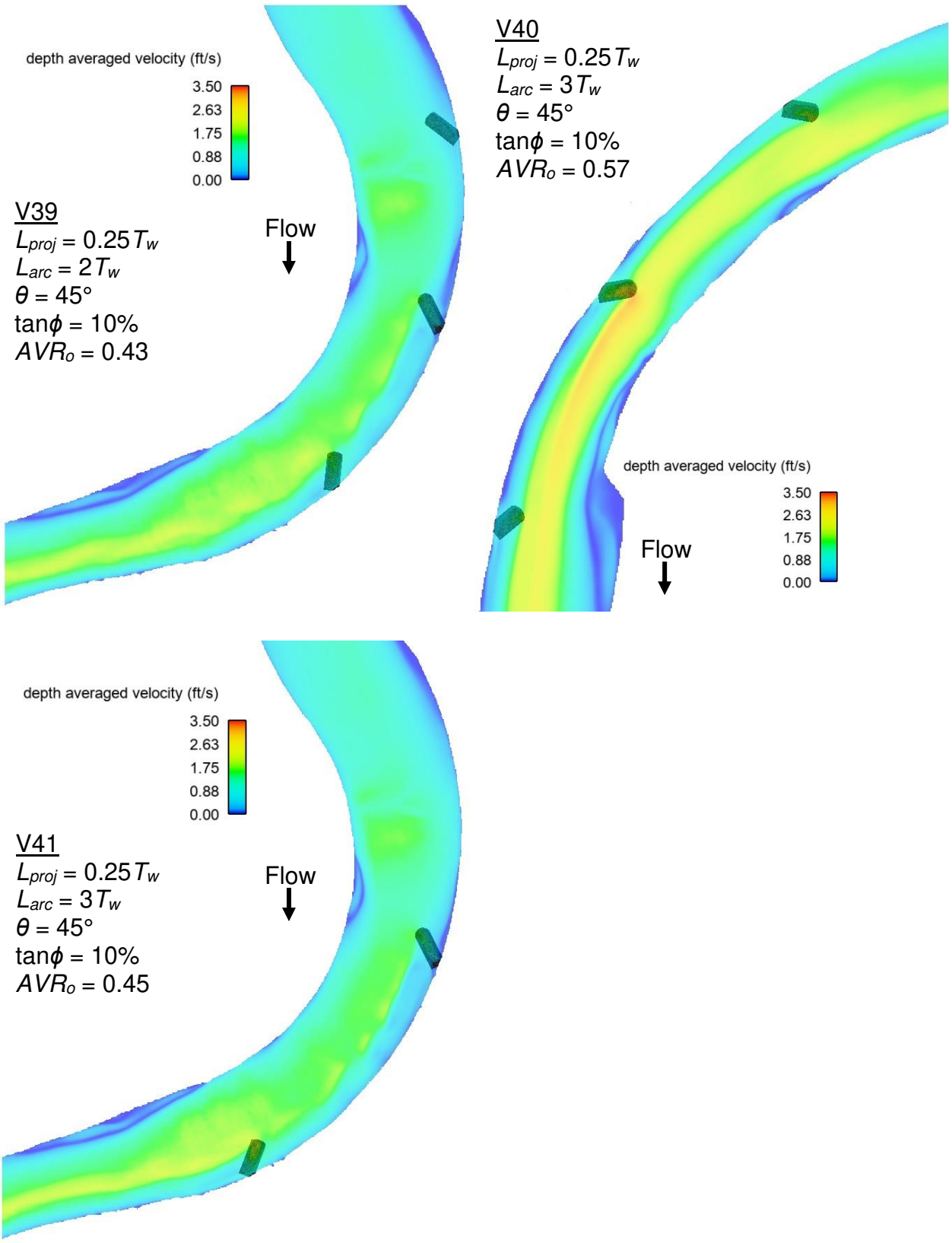

Figure 80. Steady state depth-averaged velocity for rock vane configurations V39-V41

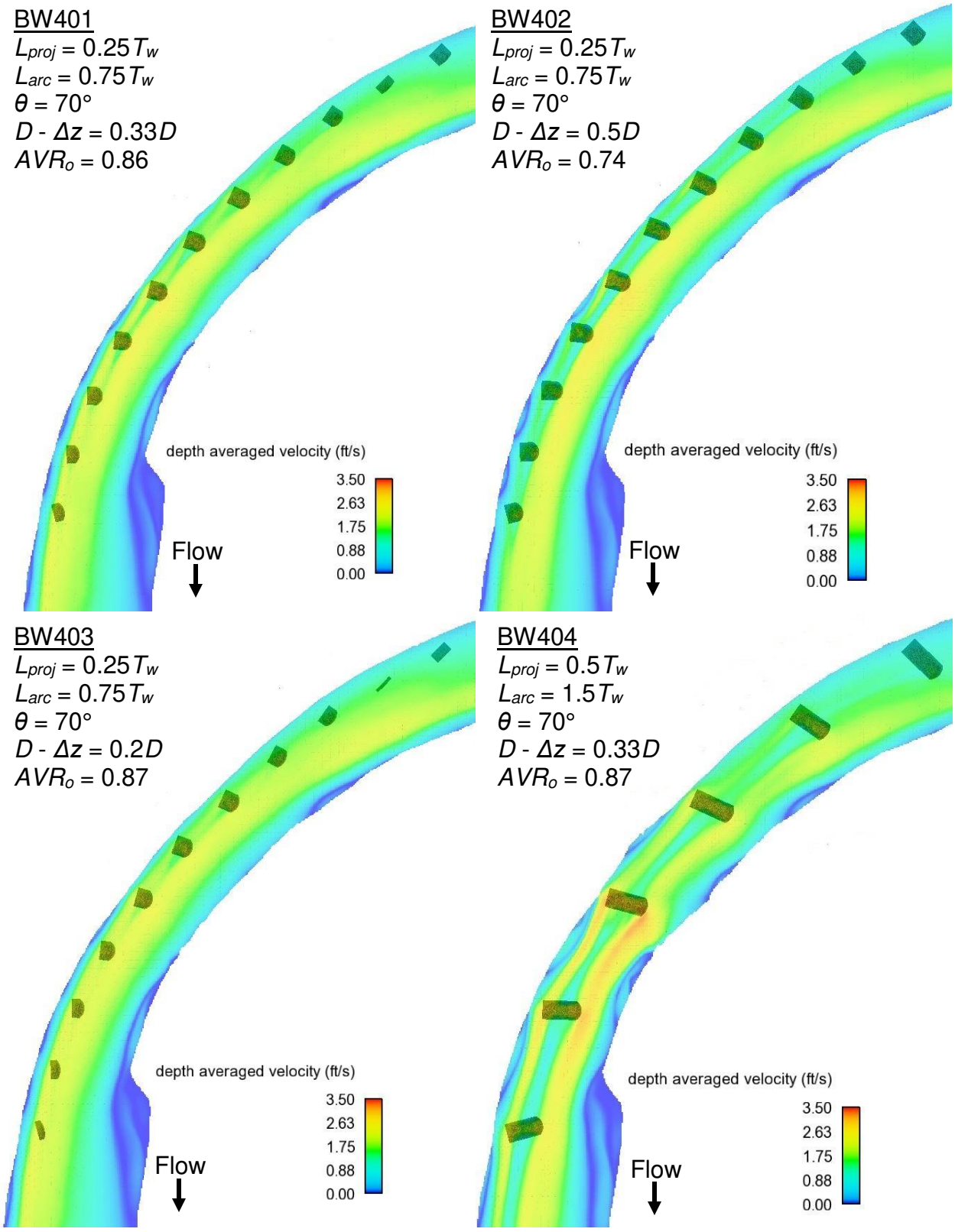

Figure 81. Steady state depth-averaged velocity for bendway weir configurations BW401-BW404

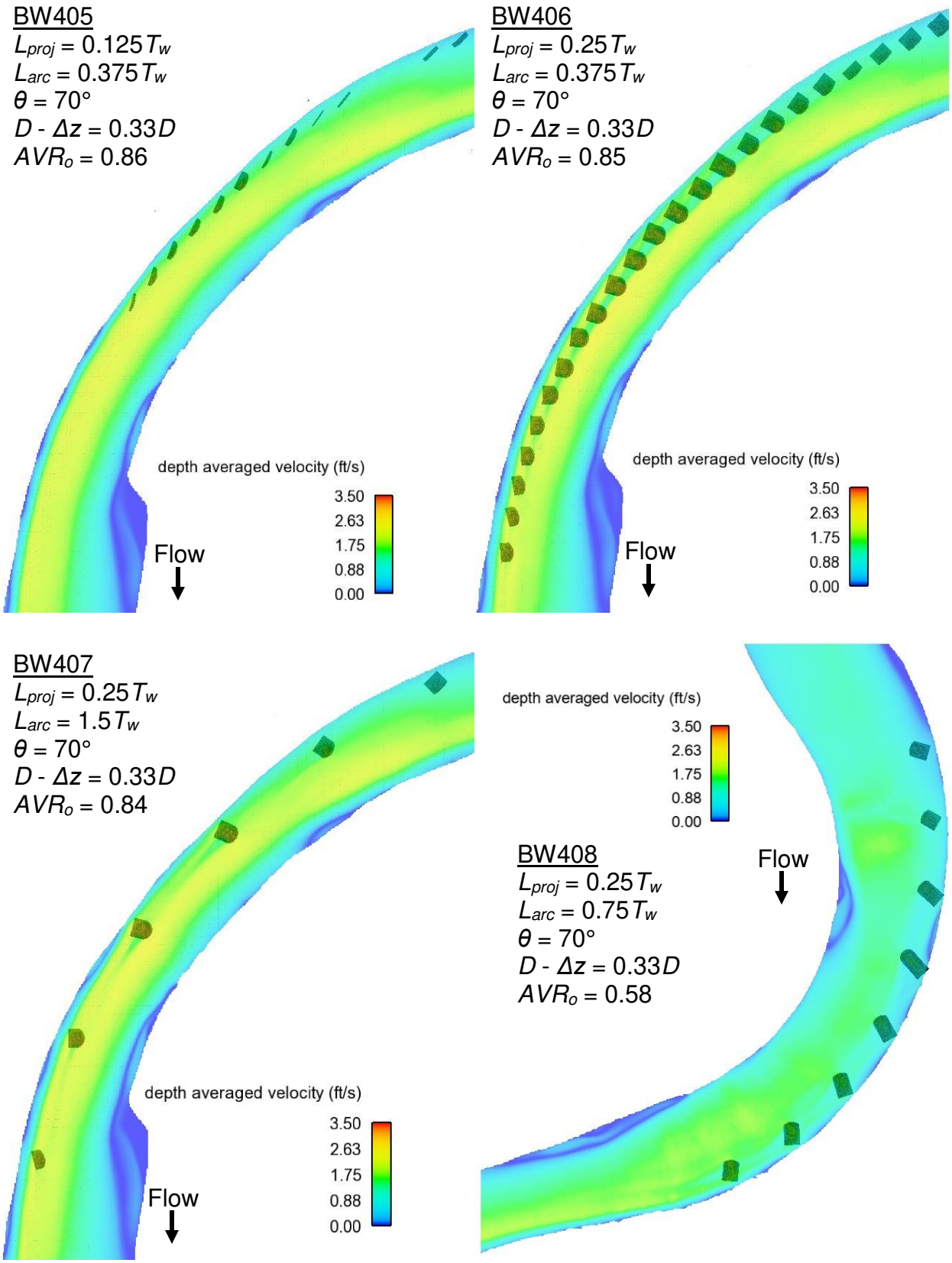

Figure 82. Steady state depth-averaged velocity for bendway weir configurations BW405-BW408

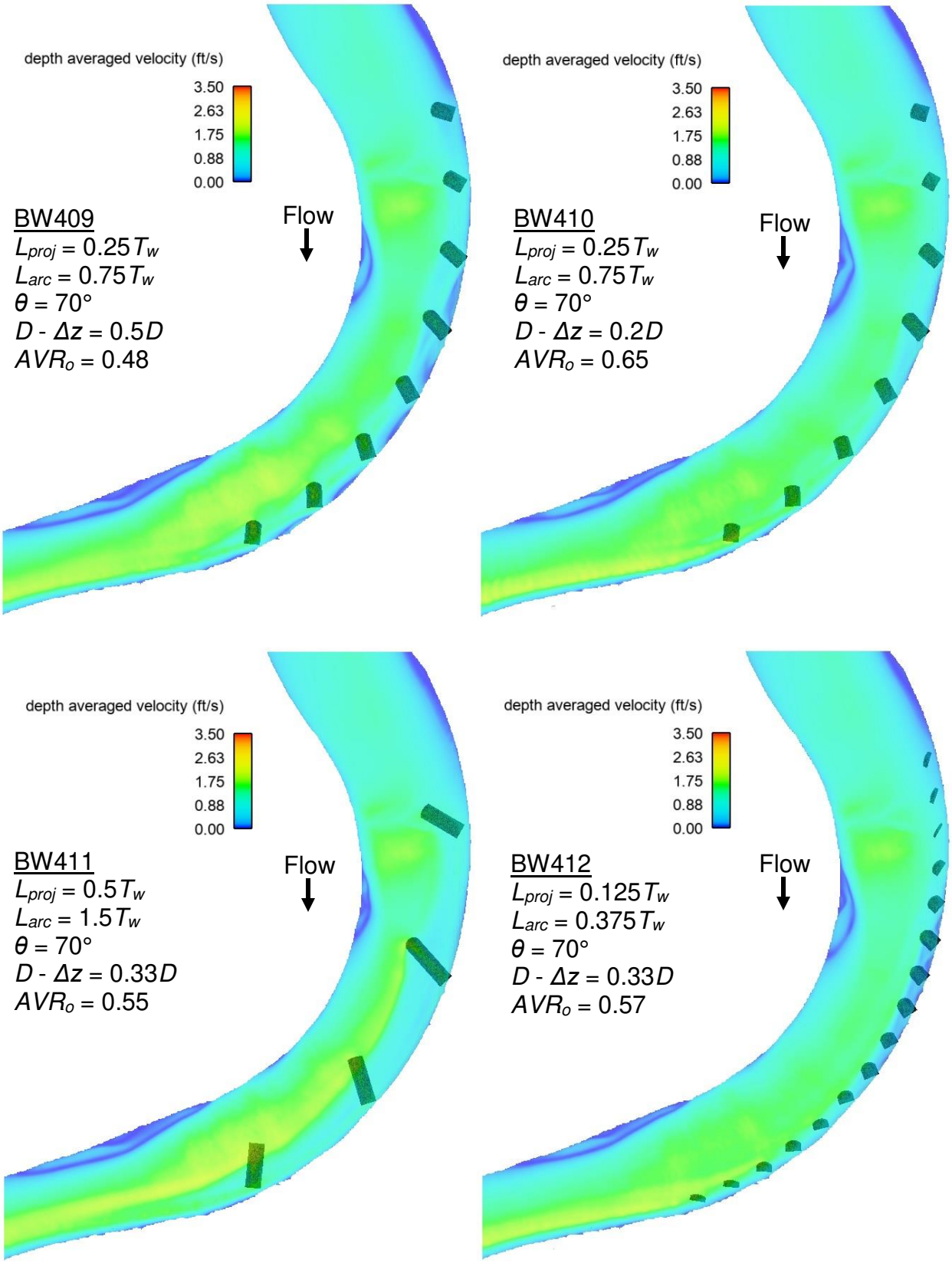

Figure 83. Steady state depth-averaged velocity for bendway weir configurations BW409-BW412

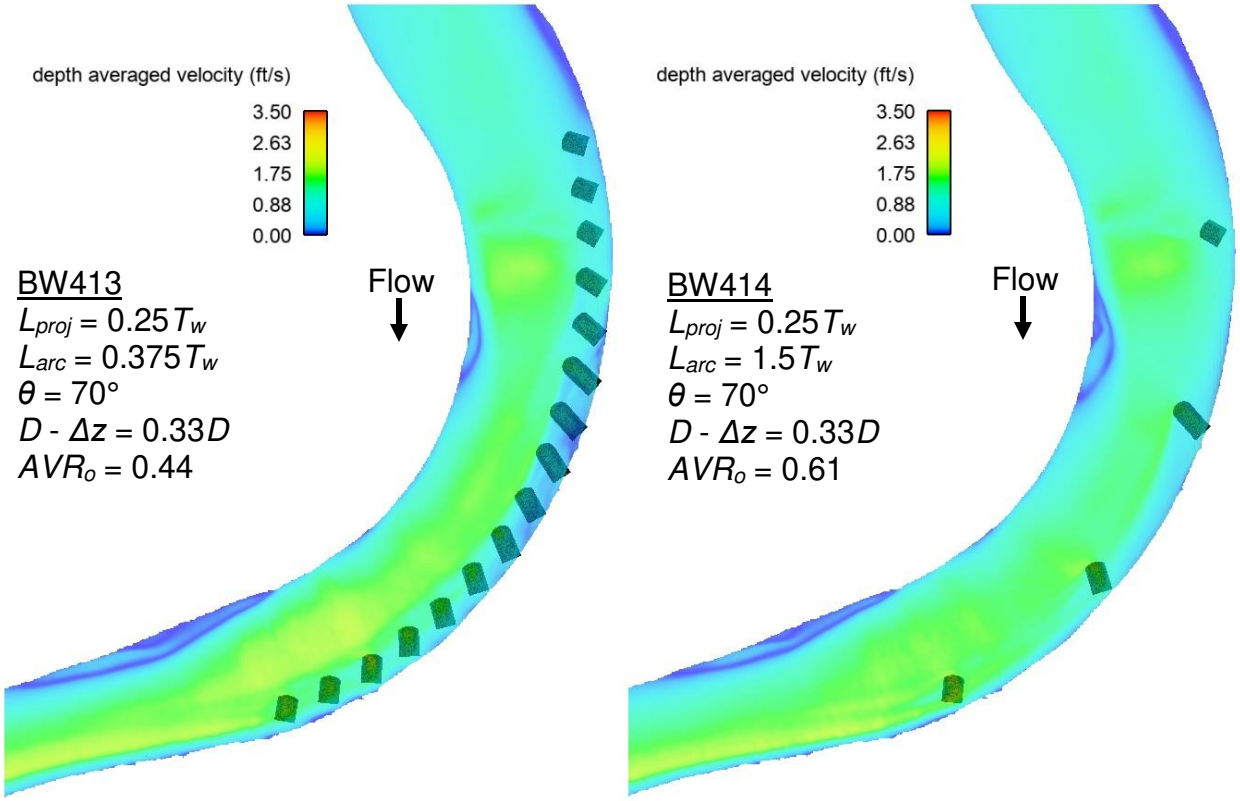

Figure 84. Steady state depth-averaged velocity for bendway weir configurations BW413 and BW414

APPENDIX D. ALTERNATIVE VELOCITY RATIO ANALYSIS

This appendix provides values from an alternative analysis method for computing the outer bank velocity ratio. The method used in this appendix differs from the Average Velocity Ratio along the outer bank described by Equation 11 (reproduced below) in that the velocity in the denominator is computed in the same region of the channel (along the outer bank) as the numerator.

$$AVR_o = \frac{V_{o-structures}}{V_{baseline}} \tag{11}$$

Where:

AVR_o = Average Velocity Ratio along the outer bank

$V_{o\text{-}structures}$ = Average velocity along the outer bank of the bend after the installation of structures

$V_{baseline}$ = Average velocity at the entrance of the bend before the installation of structures

The alternative method uses Equation 57 to compute the Bank Velocity Ratio (*BVR*), where $V_{o\text{-}baseline}$ is the average velocity along the outer bank of the bend before the installation of structures and is computed in the same portion of the flow domain used to compute $V_{o\text{-}structures}$.

$$BVR = \frac{V_{o-structures}}{V_{o-baseline}} \tag{57}$$

Results from Equation 57 are provided for the tested configurations of rock vanes (Table 25) and bendway weirs (Table 26).

Table 25. Bank Velocity Ratios for rock vane configurations

Configuration	Outer bank Velocity with Structures (ft/s) $V_{o\text{-}structures}$	Baseline Outer Bank Velocity (ft/s) $V_{o\text{-}baseline}$	Bank Velocity Ratio BVR	Bend
V01	0.56	1.31	0.43	DS
V07	0.90	1.31	0.69	DS
V11	0.52	1.31	0.40	DS
V12	0.73	1.31	0.56	DS
V13	0.66	1.31	0.51	DS
V14	0.85	1.31	0.65	DS
V15	0.51	1.31	0.39	DS
V16	0.74	1.31	0.57	DS
V17	0.35	1.12	0.32	US
V18	0.51	1.12	0.46	US
V19	0.36	1.12	0.32	US
V20	0.46	1.31	0.35	DS
V21	0.70	1.31	0.53	DS
V22	0.41	1.31	0.31	DS
V23	0.52	1.31	0.40	DS
V24	0.65	1.31	0.49	DS
V25	0.58	1.31	0.44	DS
V26	0.47	1.31	0.36	DS
V27	0.73	1.31	0.56	DS
V28	0.42	1.31	0.32	DS
V29	0.47	1.12	0.42	US
V30	0.61	1.12	0.55	US
V31	0.35	1.12	0.31	US
V32	0.39	1.12	0.35	US
V33	0.68	1.12	0.61	US
V34	0.54	1.12	0.48	US
V35	0.32	1.12	0.29	US
V36	0.53	1.12	0.47	US
V37	0.37	1.12	0.33	US
V38	0.62	1.31	0.47	DS
V39	0.53	1.12	0.56	US
V40	0.85	1.31	0.65	DS
V41	0.65	1.12	0.58	US
Maximum	-	-	0.69	-
Minimum	-	-	0.29	-
Average	-	-	0.46	-

.

Table 26. Bank Velocity Ratios for bendway weir configurations

Configuration	Outer bank Velocity with Structures (ft/s) $V_{o\text{-}structures}$	Baseline Outer Bank Velocity (ft/s) $V_{o\text{-}baseline}$	Bank Velocity Ratio BVR	Bend
BW401	1.28	1.31	0.98	DS
BW402	1.10	1.31	0.84	DS
BW403	1.29	1.31	0.99	DS
BW404	1.29	1.31	0.99	DS
BW405	1.28	1.31	0.98	DS
BW406	1.27	1.31	0.97	DS
BW407	1.25	1.31	0.95	DS
BW408	0.84	1.12	0.75	US
BW409	0.70	1.12	0.62	US
BW410	0.95	1.12	0.85	US
BW411	0.80	1.12	0.72	US
BW412	0.83	1.12	0.74	US
BW413	0.64	1.12	0.57	US
BW414	0.89	1.12	0.80	US
Maximum	-	-	0.99	-
Minimum	-	-	0.57	-
Average	-	-	0.84	-

APPENDIX E. CONSTRAINTS ON ROCK VANES AT SMALL PLANFORM ANGLES

The installation of rock vanes at small planform angles magnifies the effect of channel curvature. Curvature effects result in geometric design constraints that are negligible at larger angles but become very pronounced as the angle decreases. For the ratios of R_c/T_w typical of river bends, curvature effects become very important for planform angles less than about 45°. This appendix describes the resulting implications for projected length and projected area.

Projected Length Equations

Equation 27 from Appendix A (reproduced below) simplifies to $L_{proj} = L_c sin\theta$ for $\theta =$ 90° or for R_c approaching infinity. This section examines the limitations of the simplified form.

$$L_{proj} = R_c + \frac{T_w}{2} - \sqrt{L_c^2 + \left(R_c + \frac{T_w}{2}\right)^2 - 2L_c\left(R_c + \frac{T_w}{2}\right) sin\theta} \tag{27}$$

By dividing Equation 27 by L_c and performing some algebraic manipulations, it is possible to express the ratio of projected length to crest length as a function of rock vane planform angle (θ) and the dimensionless term $\frac{T_w}{L_{proj}}\left(\frac{R_c}{T_w} + \frac{1}{2}\right)$:

$$\frac{L_{proj}}{L_c} = \frac{1}{\frac{T_w}{L_{proj}}\left(\frac{R_c}{T_w} + \frac{1}{2}\right) - \sqrt{1 - 2\frac{T_w}{L_{proj}}\left(\frac{R_c}{T_w} + \frac{1}{2}\right) + \left(\frac{T_w}{L_{proj}}\right)^2\left(\frac{R_c}{T_w} + \frac{1}{2}\right)^2 \sin^2\theta}} \tag{58}$$

Using the simplified relationship, the ratio of projected length to crest length is only a function of planform angle:

$$\frac{L_{proj}}{L_c} = sin\theta \tag{59}$$

Plotting Equation 58 for selected values of $\frac{T_w}{L_{proj}}\left(\frac{R_c}{T_w}+\frac{1}{2}\right)$ in Figure 85 along with Equation 59 illustrates the differences in the equations.

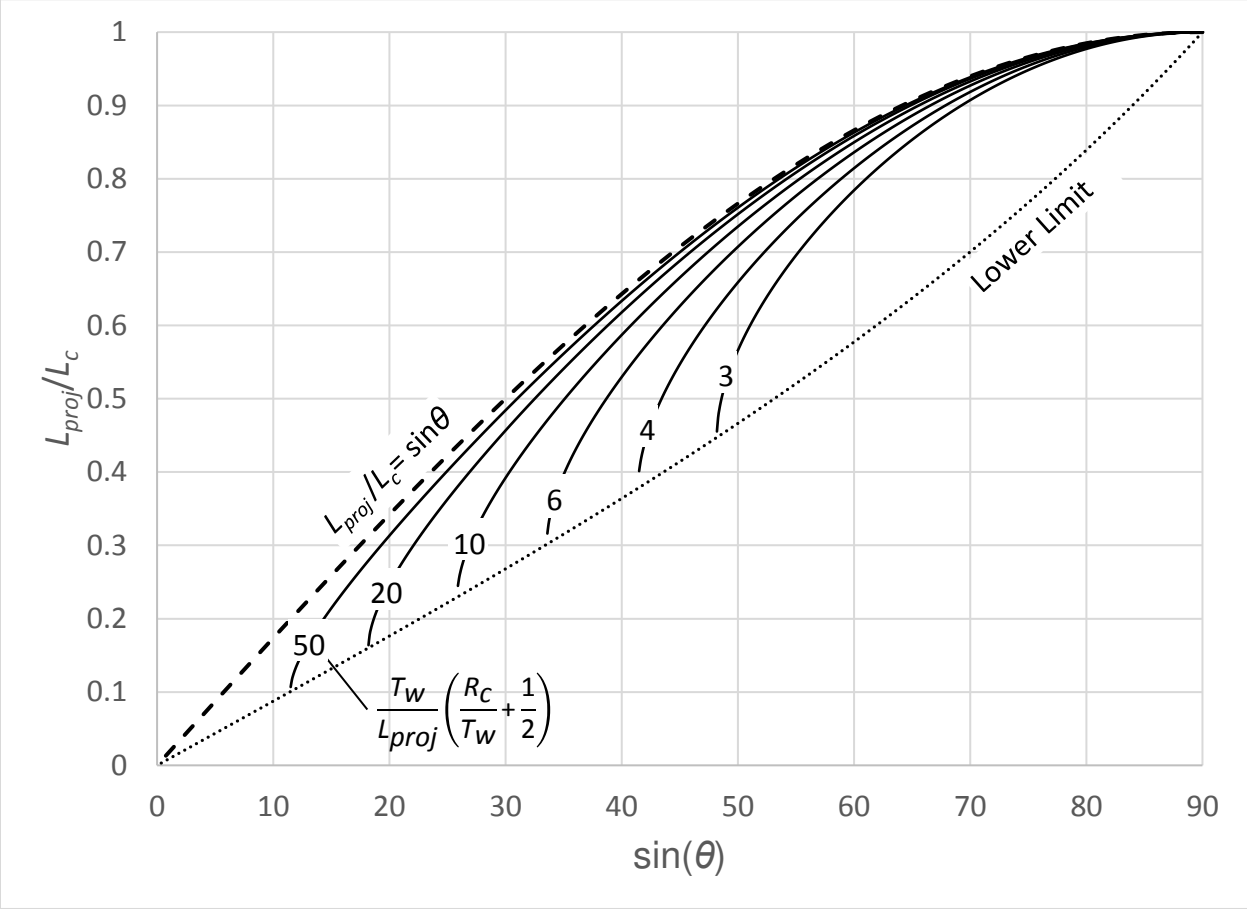

Figure 85. Comparison of the ratio of projected length (L_{proj}) to crest length (L_c) using Equation 58 for selected values of T_w/L_{proj} (R_c/T_w + 1/2) (solid lines) and Equation 59 (dashed line)

The following observations are made from Figure 85:

- Equation 59 is equivalent to evaluating Equation 58 for $R_c = \infty$ (i.e. a straight channel).
- Longer rock vanes (larger values of L_{proj}/T_w) and tighter bends (smaller values of R_c/T_w) increase the difference between the two equations.

- For realistic rock vanes (T_w/L_{proj} = 3) in very tight river bends (R_c/T_w = 1) Equation 59 provides a very good approximation (less than 5% difference) for the projected length of rock vanes for θ > 60°.
- For all rock vane installations with T_w/L_{proj} (R_c/T_w + 1/2) > 10, Equation 59 can be used to approximate the projected length with errors of less than 10%, as long as θ > 45°.

Maximum Projected Length

As derived in Appendix A, the maximum ratio of projected length to channel top-width for a rock vane of given planform angle in a channel of given curvature can be expressed as:

$$\frac{L_{proj-max}}{T_w} = (1 - cos\theta)\left(\frac{R_c}{T_w} + \frac{1}{2}\right) \quad (41)$$

The projected length becomes constrained as the channel curvature becomes tighter and the angle of the structures decreases. Figure 86 plots Equation 41 for selected values of R_c/T_w. Considering the case of a channel with R_c/T_w = 3, the planform angle must be greater than 20° to achieve a projected length of $0.25T_w$. For smaller angles, a projected length of $0.25T_w$ will not physically fit in the channel because of its curvature. Designers of rock vane structures must be aware of such constraints when evaluating rock vanes installed at small angles and verify the rock vane design is physically compatible with the channel in which it will be installed.

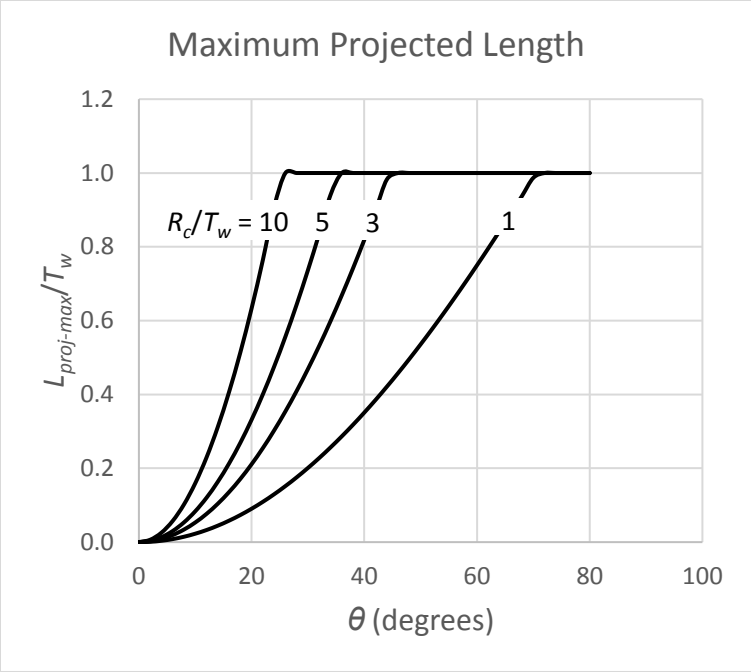

Figure 86. Maximum rock vane projected length for selected values of R_c/T_w

Projected Crest Slope and Projected Area

Constructing a rock vane with a given projected length requires a longer crest as the planform angle decreases. As a result, for a rock vane with a given projected length and crest slope, a smaller planform angle will result in a larger tip submergence and steeper projected sloped. The steeper projected slope in turn results in a decreased projected area. Equation 56, as derived in Appendix A, describes the relationship between projected slope, crest slope, projected length, curvature, and planform angle:

$$\frac{\tan(\phi_{proj})}{tan\phi} = \frac{T_w}{L_{proj}}\left(\frac{R_c}{T_w}+\frac{1}{2}\right) sin\theta - \sqrt{1-\frac{2T_w}{L_{proj}}\left(\frac{R_c}{T_w}+\frac{1}{2}\right)+\left(\frac{T_w}{L_{proj}}\right)^2\left(\frac{R_c}{T_w}+\frac{1}{2}\right)^2 \sin^2\theta} \quad (56)$$

Plotting Equation 56 for selected values of R_c/T_w and L_{proj}/T_w in Figure 87 and Figure 88 shows how projected slope increases rapidly as the planform angle approaches zero. Because the area of flow blockage decreases as projected slope increases, extremely steep projected slopes

block only a small portion of the flow area. The designer must be aware of this fact and pay careful attention to the projected area of any rock vane installed at a planform angle less than 45° to verify that it will provide the desired hydraulic effect.

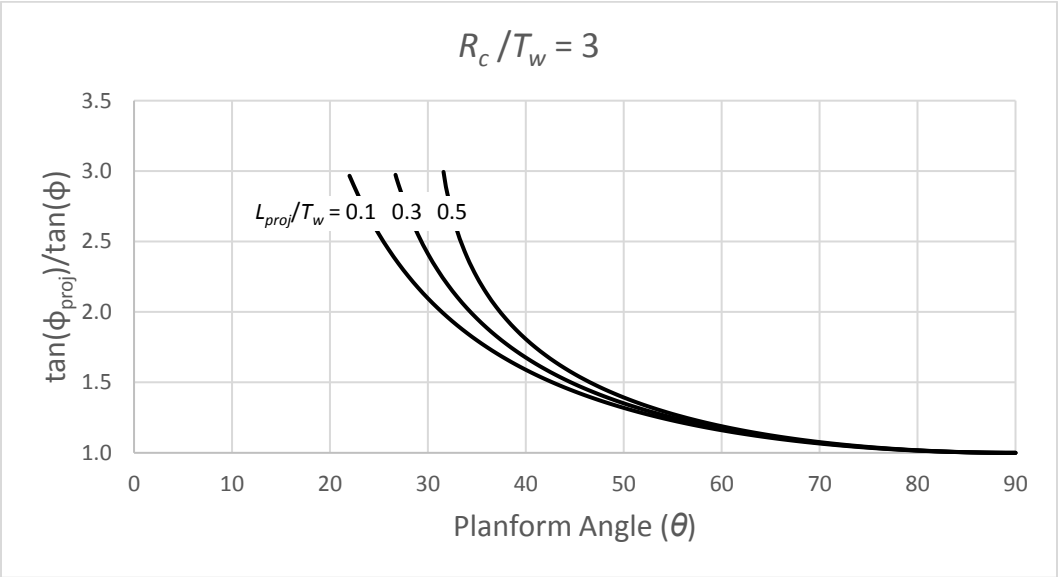

Figure 87. Ratio of project slope to crest slope for $R_c/T_w = 3$

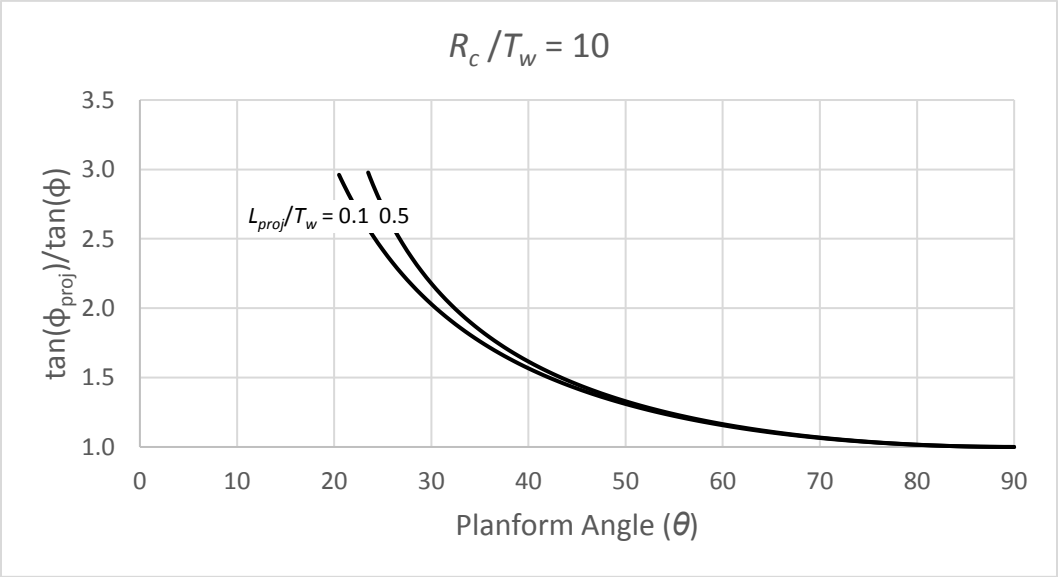

Figure 88. Ratio of project slope to crest slope for $R_c/T_w = 10$